

**Guidelines for Natural Hazard Risk Analysis on
Public Conservation Lands and Waters**

**Part 4: A commentary on analysing landslide risk to
point and linear sites**

SJ de Vilder

Cl Massey

**GNS Science Consultancy Report 2024/38
September 2024**



DISCLAIMER

This report has been prepared by the Institute of Geological and Nuclear Sciences Limited (GNS Science) exclusively under contract to the Department of Conservation (DOC). GNS Science accepts no responsibility for any use of or reliance on any contents of this report by any person other than DOC and shall not be liable to any person other than DOC, on any ground, for any loss, damage or expense arising from such use or reliance. However, in the event that, notwithstanding this statement of disclaimer, GNS Science is at law held to have a duty of care to a third party, liability to that third party shall be limited and excluded on the same terms as liability to DOC is excluded and limited under the contract with DOC. Any party using or relying on this report will be regarded as having accepted the terms of this disclaimer.

Use of Data:

Date that GNS Science can use associated data: June 2024

BIBLIOGRAPHIC REFERENCE

de Vilder SJ, Massey CI. 2024. Guidelines for natural hazard risk analysis on public conservation lands and waters – Part 4: a commentary on analysing landslide risk to point and linear sites. Lower Hutt (NZ): GNS Science. 81 p. Consultancy Report 2024/38.

CONTENTS

EXECUTIVE SUMMARY.....	V
1.0 AIM OF COMMENTARY	1
1.1 Report Background.....	1
1.2 Purpose of Report	1
1.3 Scope of Report.....	1
1.3.1 Preliminary Screening Tool	1
1.3.2 Basic-Level Analysis	1
1.3.3 Advanced-Level Analysis	1
1.4 Department of Conservation Expert Panel.....	1
1.5 Terminology.....	1
2.0 METHOD OUTLINE OF LANDSLIDE QUANTITATIVE RISK ANALYSIS	2
2.1 Landslide Risk and Risk Management.....	2
2.2 Landslide Quantitative Risk Analysis	2
2.3 Risk Analysis and Uncertainty	2
2.3.1 Subjective Probability	2
2.4 Risk Metrics.....	2
2.5 Risk Comparators.....	2
3.0 SPATIAL SCALE AND EXTENT OF ANALYSIS	3
4.0 DATA COMPILATION / DESKTOP STUDY	4
4.1 Data Sources.....	4
4.2 Pre-Disposing Factors	4
4.2.1 Conceptual Geomorphic Model.....	4
4.2.2 Pre-Disposing Factors	6
4.2.3 Topographic Analysis	7
4.2.4 Engineering Geomorphological and Engineering Geological Mapping.....	8
4.2.5 Landslide Mapping Guide.....	12
4.3 Landslide Inventory	14
4.4 Triggering Factors	16
4.4.1 Rainfall Triggers	16
4.4.2 Climate Change.....	17
4.4.3 Earthquake Triggers.....	18
4.4.4 Volcanic Triggers.....	26
5.0 FIELD STUDY	27
6.0 DATA ANALYSIS.....	29
6.1 Landslide Source Susceptibility	29
6.2 Landslide Size	30
6.2.1 Topographic Controls on Landslide Size	30
6.2.2 Area to Volume Scaling Relationships	31
6.3 Landslide Frequency	34

6.3.1	Earthquake-Induced Landsliding: Compiling Magnitude-Frequency Relationships for Different Levels of Earthquake Shaking for Advanced-Level Analysis.....	36
6.4	Landslide Impact Area	39
6.4.1	Landslide Runout	39
6.4.2	Empirical Landslide Runout Datasets	41
6.4.3	Debris Flow Runout Estimation	47
6.4.4	Example Calculation Route of $P_{(T:L)}$	51
6.4.5	Slippage.....	54
7.0	CONSEQUENCE ANALYSIS	55
7.1	Elements at Risk.....	55
7.2	Exposure	55
7.3	Vulnerability	55
7.3.1	Vulnerability for Persons (Physical Vulnerability).....	56
7.3.2	Vulnerability for Property	57
7.3.3	Vulnerability for Persons in Property	59
7.3.4	Vulnerability for People in Vehicles	60
8.0	RISK ESTIMATION	62
8.1	Local Personal Risk	62
8.1.1	Example Risk Calculation of Local Personal Risk.....	62
8.2	Risk Per Trip.....	63
8.2.1	Example Basic Analysis Calculation Route.....	63
8.3	Annual Individual Fatality Trip.....	68
8.4	Multiple Fatality Risk.....	68
8.5	Asset Impact.....	70
8.6	Risk-Sensitivity Analysis	70
9.0	RISK MITIGATION	71
10.0	REPORTING REQUIREMENTS	72
10.1	Peer-Review Requirements	72
11.0	ACKNOWLEDGEMENTS	73
12.0	REFERENCES	73

FIGURES

Figure 4.1	Example conceptual models.....	5
Figure 4.2	The effect that using different digital elevation model resolutions has on 3D rockfall runout simulations	8
Figure 4.3	Block diagram of an idealised complex rotational earth slide and earth flow showing typical landslide features	12
Figure 4.4	Examples of factors that reduce the strength of rock mass and increase the stresses acting upon it over time.....	18
Figure 4.5	Peak ground acceleration hazard map for 100-year return period.	19

Figure 4.6	Peak ground acceleration hazard map for 250-year return period.	20
Figure 4.7	Peak ground acceleration hazard map for 500-year return period.	21
Figure 4.8	Peak ground acceleration hazard map for 1000-year return period.	22
Figure 4.9	Example peak ground acceleration hazard curve displaying the annual exceedance probability in any one year for Cape Kidnappers, Hawke’s Bay.	26
Figure 6.1	Histograms of the occurrence of landslide for local slope relief categories	31
Figure 6.2	Landslide source areas and volumes	32
Figure 6.3	Explanation of the graphical presentation of a landslide size frequency model.....	35
Figure 6.4	Landslide area-probability distributions and power-law scaling for medium to large landslides induced by the 1968 M_w 7.6 Inangahua earthquake, 1929 M_w 7.8 Murchison earthquake and for nominally complete landslide inventories for the 1976 M_w 7.6 Guatemala, M_w 6.6 1994 Northridge and 2008 M_w 7.9 Wenchuan earthquakes.....	37
Figure 6.5	The cumulative number of landslides \geq a given volume per km^2 per PGA Band for slopes $\geq 30^\circ$	39
Figure 6.6	Fahrböschung correlated to landslide volume	41
Figure 6.7	Calculation of the probability of runout exceedance based on the scatter in the empirical data.....	42
Figure 6.8	Empirical relationship between $\Delta H/L$ ratio and volume of dry (i.e. earthquake-induced) debris avalanches ($<100,000 \text{ m}^3$) and rock avalanches ($>100,000 \text{ m}^3$).....	43
Figure 6.9	H/L ratio versus volume for rainfall-induced debris avalanches from international case studies	44
Figure 6.10	H/L ratio versus volume for rainfall-induced debris flows in New Zealand and Hong Kong.....	45
Figure 6.11	H/L ratio versus volume for fill slope failures in Wellington and Hong Kong.....	46
Figure 6.12	Debris flows induced by rain in Eastbourne, Wellington, in November 2006.....	47
Figure 6.13	Example from Cougar Creek, Alberta, Canada, of the different sections of a fan receiving sediment during the last ~ 3200 years.....	48
Figure 6.14	Oblique aerial view of debris-flow fans in the Makarora valley	49
Figure 6.15	Example of fan delineation based on topographic contours.	49
Figure 6.16	Schematic representation of how the order of a stream is defined in the River Environment Classification by the Ministry for the Environment.....	51
Figure 6.17	Schematic of the input data and variables required to calculate $P_{(T:L)}$	53
Figure 6.18	Schematic of a slide.	54
Figure 7.1	Damage ratio versus debris height for falling debris: debris flows, combining both the literature and New Zealand (NHC Toka Tū Ake) datasets, $N = 168$, for all building types	57
Figure 7.2	Damage ratio versus the kinetic energy for falling debris: rockfalls, combining both the literature and New Zealand (NHC Toka Tū Ake) datasets, $n = 41$, for all building types.....	58
Figure 7.3	Human vulnerability to landslides over a range of common landslide inundation depths	59
Figure 7.4	Example event-tree model for road-user risk assessment for rockfalls on Wakefield Avenue, Christchurch	60

TABLES

Table 4.1	Factors that may predispose a slope to landslides (including shallow slides, rockfalls and deep-seated slides) on natural slopes	6
Table 4.2	Morphology layer descriptions	9
Table 4.3	Interpreted materials layer descriptions	10
Table 4.4	Genesis layer descriptions	11
Table 4.5	Landslide features and criteria for remote sensing and field recognition	13
Table 4.6	Input datasets for the creation of a landslide inventory	15
Table 4.7	Landslide and Environmental Criteria often observed at different levels of ground shaking – peak ground acceleration and the New Zealand Modified Mercalli intensity scale	23
Table 5.1	Questions to be addressed in slope stability and landslide investigations for a given site	28
Table 6.1	Compilation of scaling relationships between landslide area and volume from Massey et al. (2020a)	33
Table 6.2	Details of the power-law trends fitted to the cumulative number of landslides \geq a given volume per km ² per PGA Band	38
Table 6.3	Techniques to analyse landslide runoff	40
Table 6.4	Summary of the Melton Ratio and catchment length used to estimate the dominant hazard type at each fan	50
Table 6.5	Example calculation route and input data required to calculate the $P_{(S:H)}$ at the cliff bottom and F-angle extent.	52
Table 7.1	Summary of Hong Kong vulnerability ranges for persons and recommended values for loss of life for landsliding in similar situations	56
Table 7.2	Vulnerability values for different elements at risk and size of impact block as determined by expert judgement	56
Table 7.3	Damage functions and statistics for falling debris: all data for debris flows and debris avalanches	58
Table 7.4	Damage functions and statistics for falling debris: all data for rockfalls	59
Table 7.5	Effective diameters perpendicular to the main trajectory of debris and the assumed vulnerability of road users per travel mode	61
Table 7.6	Vulnerabilities of road users in collision with / trying to avoid boulders on the road ahead	61
Table 8.1	Example calculation route and input data required to calculate local personal risk for the cliff toe.	62
Table 8.2	Calculation route for annual frequency of non-event-induced landslides.	63
Table 8.3	Calculation route for spatial probability of impact $P_{(T:L)}$	65
Table 8.4	Estimate of the size and number of most likely and maximum credible landslides that could occur during a 1-in-500-year earthquake event	66
Table 8.5	Calculation route for spatial probability of impact.	67
Table 8.6	Worked example to calculate an F/N pair for multiple fatality risk.	69
Table 8.7	Input parameters used in the Port Hills rockfall model for each assessment and the impact of their variance on average risk	70

EXECUTIVE SUMMARY

This report presents a commentary on the Part 3 guideline report. The guideline report provides a methodology for quantitative risk analysis (QRA) from landslide hazards at point sites (such as at huts and car parks) and linear sites (such as track and roads) within public conservation lands and waters (Department of Conservation [DOC] land). The methodology quantitatively assesses life-safety risk to visitor and workers, as well as impact to assets on public conservation lands and waters and is based on the AGS (2007a–d) and the JTC-1 guidelines (Fell et al. 2008b). These have been modified where appropriate to provide guidance specific to a New Zealand context and for analysing the risk to point sites (e.g. huts and viewing areas) and linear sites (e.g. tracks and roads) from landslide hazards present within the public conservation lands and waters.

The guideline outlines two levels of analysis: basic and advanced. The basic level of analysis represents an initial estimation of the landslide risk that workers or visitors are exposed to and the potential impact to assets using simple and limited input datasets and data analysis. The advanced level of analysis involves greater time and resources dedicated toward data collection, input datasets, data analysis and peer review of the risk calculation process. The guideline outlines for the various spatial scales, resolution and type of data inputs and subsequent data analysis required.

The purpose of the commentary report is to provide additional background, relevant references and data sources, comments and guidance relevant to the Part 2 preliminary screening analysis (de Vilder and Massey 2024a) and Part 3 guideline report (de Vilder and Massey 2024b) and risk-analysis framework in general (as outlined in the Part 1 report [de Vilder et al. 2024]). This commentary report is a live document (maintained by DOC) and represents the most up-to-date and current scientific information on landslide hazard and risk analysis.

This page left intentionally blank.

1.0 AIM OF COMMENTARY

1.1 Report Background

No additional comment.

1.2 Purpose of Report

In preparing the quantitative landslide risk-analysis guideline report (Part 3), the intention has been to limit the length of the document in so far as possible as to provide a clear and concise set of recommended requirements and principles. The purpose of the commentary report is to provide additional background, relevant references and data sources, comments and guidance relevant to the Part 2 preliminary screening analysis and Part 3 guideline report and risk-analysis framework in general (as outlined in the Part 1 report). This commentary report is a live document (maintained by the Department of Conservation [DOC]) and represents the most up-to-date and current scientific information on landslide hazard and risk analysis. This commentary report is to be updated regularly, on a 2–5-year basis, to incorporate new scientific, engineering geology and engineering knowledge.

1.3 Scope of Report

No additional comment.

1.3.1 Preliminary Screening Tool

No additional comment.

1.3.2 Basic-Level Analysis

No additional comment.

1.3.3 Advanced-Level Analysis

No additional comment.

1.4 Department of Conservation Expert Panel

No additional comment.

1.5 Terminology

No additional comment.

2.0 METHOD OUTLINE OF LANDSLIDE QUANTITATIVE RISK ANALYSIS

2.1 Landslide Risk and Risk Management

No additional comment.

2.2 Landslide Quantitative Risk Analysis

No additional comment.

2.3 Risk Analysis and Uncertainty

Uncertainty is an inherent component of risk analysis. It can be separated into two categories:

- **Aleatory uncertainty** (or randomness), where the outcome is inherently unpredictable. Aleatory uncertainty cannot be reduced by further study as it expresses the inherent variability of a phenomenon (Lee and Jones 2014).
- **Epistemic uncertainty** (or lack of knowledge), where uncertainty is associated with the level of understanding of a problem. Epistemic uncertainty can be reduced through time as more data are collected and research is completed in order to better understand and model the processes occurring but can never be eliminated (Lee and Jones 2014).

As perfect knowledge is not achievable, it is convenient to assume a degree of randomness (i.e. aleatory uncertainty) when modelling natural processes. Therefore, in risk analysis, what can be practicably done within the scope of the risk analysis should be done to reduce epistemic uncertainty.

2.3.1 Subjective Probability

If there is a lack of historical records and/or trigger events, such as earthquakes and rain, for a study area, the consultant will have to rely on subjective probability or a 'degree of belief'. As AGS (2007a) states:

"The consultant will have to make the best estimates of susceptibility, landslide size, and landslide frequency from limited site data, using experience and broad knowledge of an area or other areas of similar slope form and geology."

However, we emphasise that such issues still exist in qualitative risk analysis (Ho et al. 2000). Vick (2002) discusses the role of evidence and logical inference to subjective probability and engineering judgement. Although the assessed probability will be a subjective judgement, it should be based on evidence (Moon and Wilson 2004). However, there are issues with the use of 'degree of belief' methods. Lee and Jones (2014) and Roberds (1990) contain further discussion about these potential problems.

2.4 Risk Metrics

No additional comment.

2.5 Risk Comparators

No additional comment.

3.0 SPATIAL SCALE AND EXTENT OF ANALYSIS

No additional comment.

4.0 DATA COMPILATION / DESKTOP STUDY

No additional comment.

4.1 Data Sources

No additional comment.

4.2 Pre-Disposing Factors

4.2.1 Conceptual Geomorphic Model

A conceptual geomorphic model usually provides the basis for landslide hazard analysis. It provides a description of all the different possible landslide types that could occur in a study area and their association with specific triggering events or environmental factors. For example, a geomorphic model may identify that debris flows occur within a gully, within particular geological terrains (Figure 4.1). They are routinely used to define hazard zones.

The conceptual geomorphic model is developed as the pre-disposing landslide 'susceptibility' factors, triggering events and landslide inventory datasets are compiled. It is validated and verified via field investigations and/or peer review, and it should be routinely reviewed and updated if new information becomes available. Developing a sound conceptual geomorphic model of the study area and landslide hazards present, including how the slope formed and behaved in the past, will give an understanding of how it will behave in the future. As Moon and Wilson (2004) state:

"The ability to build up such a model comes from the knowledge of the slope and its surrounds, knowledge of similar slopes in similar environments and a range of skills and knowledges bases that result from training and experience."

The model acts as a check on the subsequent susceptibility, magnitude-frequency analysis and runout assessment to ensure that the outputs of the analysis could occur in reality, is tailored to landslide type and covers all possible landslide sizes. A conceptual geomorphic model can comprise, but is not limited to:

1. Annotated photographs.
2. Simple schematics of landslide types.
3. Complex or simple site-specific geomorphic schematic figures.
4. An engineering geomorphological map.

The geomorphic conceptual model should be used to identify factors such as the morphological, geological, hydrological and land-use factors that combine to make certain slopes more susceptible to landslides, and particular landslide types, than others. As such, the geomorphic conceptual model is a necessary and important input to understand the spatial locations of landslides (Fell et al. 2008b) and landslide susceptibility modelling. A good understanding of slope failure mechanisms (as outlined in the conceptual landslide hazard model) is crucial for correctly identifying which pre-disposing factors may influence slope stability and the types of landslide produced.

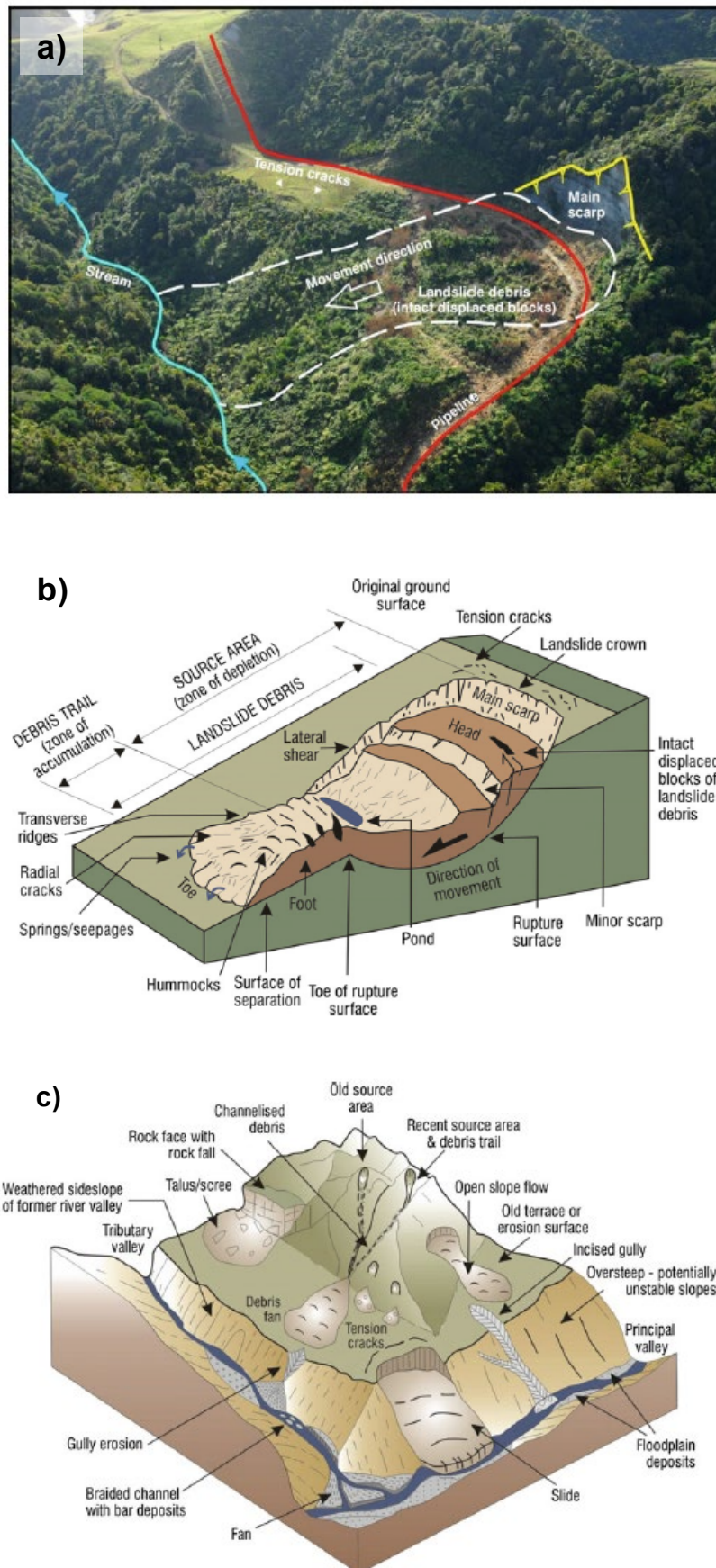


Figure 4.1 Example conceptual models. (a) Annotated aerial photograph of the Waikorora Bluff slide, Taranaki, New Zealand. (b) Block diagram of complex rotational earth slide and earth flow displaying typical landslide features (adapted from Cruden and Varnes [1996]). (c) Block diagram displaying the interacting natural hazard features in a landscape. All figures sources from Massey et al. (2018a).

4.2.2 Pre-Disposing Factors

A range of pre-disposing inputs for landslides on natural slopes can be identified and mapped (Table 4.1). The selected variables must be relevant to explaining the occurrence of landslides in the study area. An important component of this is the engineering geomorphological map, which forms the basis of understanding pre-disposing factors and landslide occurrence. Comprehensive reviews of pre-disposing factors relevant for landslide susceptibility mapping include Corominas et al. (2014), Reichenbach et al. (2018) and van Westen et al. (2008).

Sources of error and uncertainty surrounding the compilation of pre-disposing factors include:

1. Poor quality input datasets from which pre-disposing factors are derived. This is characterised by either high uncertainty in the input data (e.g. material properties) or a mismatch in scale between the resolution of the pre-disposing factor data and the landslide sizes in a study area. For example, slope angle information from a 20 m² grid resolution DSM is unsuitable to be used to understand landslide processes that may occur in a 10 m² area.
2. Inclusion of irrelevant variables, where these variables are not relevant to the landslide and slope processes operating within the study area (Reichenbach et al. 2018).
3. Inappropriate selection and/or scale of mapping unit. Mapping units often consist of grid cells, unique conditions or slope units. Grid cells are the most popular due to their simplicity to be processed and analysed; however, grid cells are not landslides, therefore the size of the grid cell must be matched to that of the landslide type being analysed (Reichenbach et al. 2018).

Table 4.1 Factors that may predispose a slope to landslides (including shallow slides, rockfalls and deep-seated slides) on natural slopes (AGS 2007c; van Westen et al. 2008; Corominas et al. 2014).

Pre-Disposing Factor Type	Example Variables	Potential Data Sources
Topography	<ul style="list-style-type: none"> • Slope angle, aspect, curvature • Local slope relief • Flow direction and accumulation • Drainage density 	<ul style="list-style-type: none"> • Digital Surface or Elevation Models (DSM/DEM)
Geology	<ul style="list-style-type: none"> • Rock type • Weathering • Discontinuities • Rock block sizes • Geological Strength Index (GSI) • Faults/folds 	<ul style="list-style-type: none"> • Geology maps • Other reports and studies • Field mapping • Ground investigations • Geophysical investigations
Soil	<ul style="list-style-type: none"> • Soil type and depth • Geotechnical properties • Hydrological properties 	<ul style="list-style-type: none"> • Other reports and studies • Field mapping • Ground investigations • Geophysical investigations • Soil maps
Geomorphology	<ul style="list-style-type: none"> • Physiographic units • Surface mapping units • Geomorphological units (sub-units) 	<ul style="list-style-type: none"> • DSM/DEM • Satellite / aerial / ground imagery • Field mapping • Ground investigations • Geophysical investigations

Pre-Disposing Factor Type	Example Variables	Potential Data Sources
Land use	<ul style="list-style-type: none"> • Land-use classes • Land-use changes • Vegetation characteristics • Infrastructure 	<ul style="list-style-type: none"> • DSM/DEM • Satellite / aerial / ground imagery • Field mapping • Archival data • Land Cover Database (LCDB; Manaaki Whenua Landcare Research) • Land-use and land-cover survey (LUCAS; European Commission)
Hydrology	<ul style="list-style-type: none"> • Water table • Soil moisture • Stream network • Groundwater 	<ul style="list-style-type: none"> • DSM/DEM • Satellite / aerial / ground imagery • Field mapping • Ground investigations • Geophysical investigations

4.2.3 Topographic Analysis

A topographic model represents the topography of the study area and rasterised models can be categorised into:

1. **Digital Elevation Model (DEM)**, which represents the bare ground surface without features such as vegetation; or
2. **Digital Surface Model (DSM)**, which represents the ground surface including all features such as vegetation, buildings, etc.

A topographic model forms the basis for correct analysis of geomorphic processes, landslide mapping and volume estimates, landslide susceptibility modelling and landslide runout and rockfall trajectory modelling. As such, errors in a base model, or using a base model that is at a lower resolution than required for the study scope and level of analysis, will result in the error/uncertainty being propagated throughout the whole risk analysis. Figure 4.2 shows that landslide trajectories and the area impacted change depending on the quality of the topographic model. The trajectories and area impacted are important for understanding the consequence to elements at risk. DEMs are preferred to DSMs to negate the effect of vegetation in the topographic model.

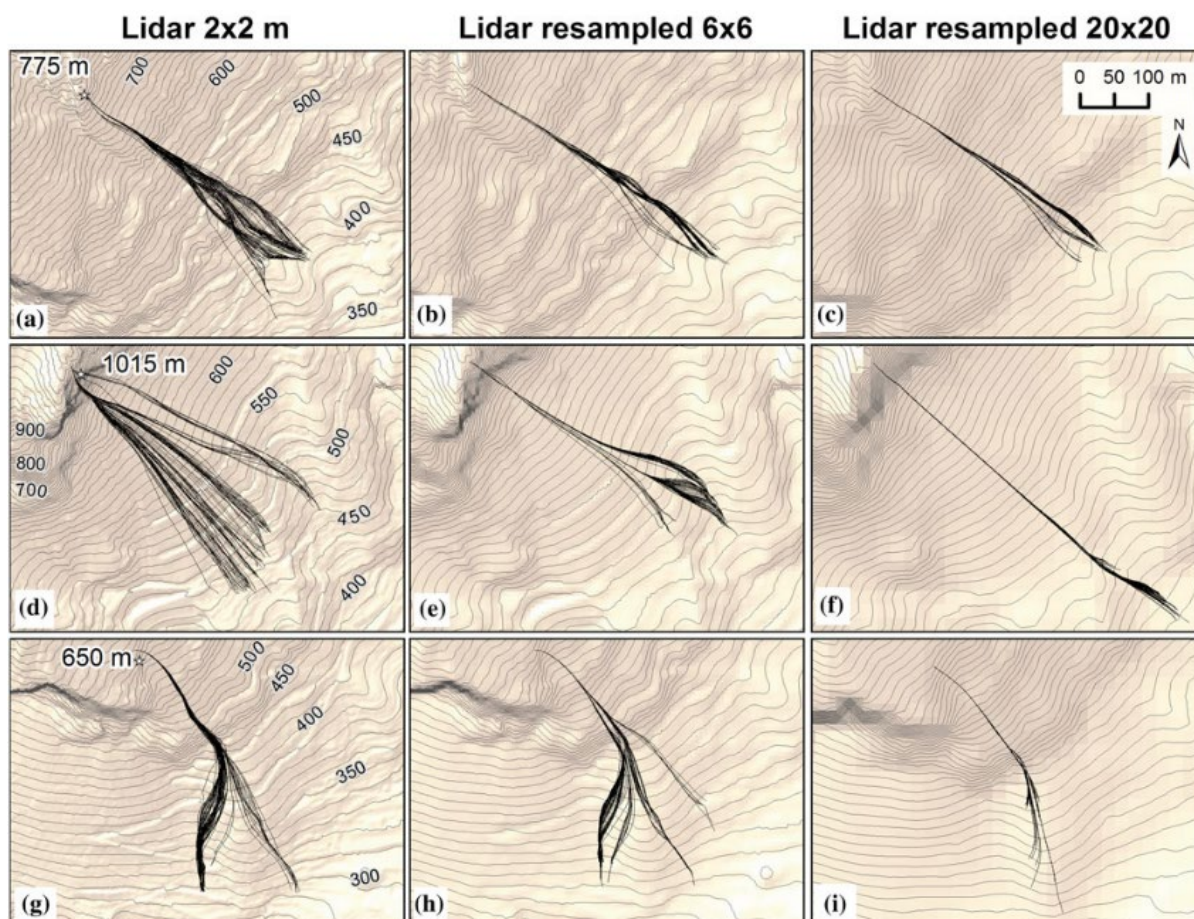


Figure 4.2 The effect that using different digital elevation model (DEM) resolutions has on 3D rockfall runoff simulations: 2 m (a, d, g), 6 m (b, e, h) and 20 m (c, f, i). Lower resolution DEMs were obtained by resampling full resolution ones. For each case, 100 rockfall blocks were simulated from point-like (one cell) sources, with the elevation of this point source given in metres in the top right-hand sections of boxes (a), (d) and (g) (Crosta et al. 2015).

4.2.4 Engineering Geomorphological and Engineering Geological Mapping

Engineering geomorphological and engineering geological mapping are performed by assessing landforms (geomorphology), interpreting their origin and characterising the mechanical properties of the materials. The level of detail of mapping should scale appropriately with the basic level versus advanced level of analysis, as well as with the spatial scale of analysis.

For point site analyses carried out at a site-specific scale, detailed mapping of geomorphic and geological features can be undertaken. We recommend that a similar methodology, at an appropriate scale, be used for both point and linear sites. The methodology for linear sites is outlined below. For advanced-level analyses of point sites, the mapping should, if appropriate, be conducted or transformed into a GIS format. For basic-level analyses, hand-drawn maps and sketches adopting an appropriately scaled base map will suffice.





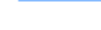








For linear site analyses carried out a regional to local spatial scale, using the methodology outlined in Townsend et al. (2012) and Townsend et al. (2020) is recommended. The description of the methodology is taken directly from Townsend et al. (2020).

For advanced-level analysis where GIS mapping is warranted, GIS layers should be produced as part of the map.

Townsend et al. (2020) shows an example of GIS mapping, which comprises a polyline layer (*morphology*) and two polygon layers (*interpreted materials* and their *genesis*). These layers can be produced by analysing and digitising directly from aerial photographs and topographic models. These layers should later be verified in the field. Categories outlined in Tables 4.2–4.4 have been expanded to include descriptions of features and material included in other risk-analysis reports for DOC (see Massey et al. [2019a] for more information). The amount of detail required should be based on the level and scale of the analyses, but whatever is produced should be documented and described in the form of tables similar to Tables 4.2–4.4.









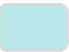
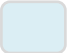
The *morphology* layer should be a polyline shapefile containing linear features such as drainage lines, landslide scarps, cliffs and significant breaks in slope, which are directly observable from the images and/or digital topographic models. Categories are described in Table 4.2.

Table 4.2 Morphology layer descriptions (Townsend et al. 2020).

Description	Symbology	Appearance
Cliff		Steep to vertical rock faces, typically natural bluffs formed by coastal erosion processes.
Ephemeral drainage line (well-defined)		Streams and gullies with a well-defined watercourse; these may be permanent watercourses in some cases.
Ephemeral drainage line (poorly defined)		Streams and gullies with a poorly defined watercourse.
Stream		Permanent small watercourses.
River		Permanent large watercourses.
Lineation (lineament)		Linear feature resembling a fault or discontinuity in the landscape.
Tension crack		Visible crack located on a slope or at the top of a slope, often at a similar location to a change in slope.
Rounded concave change in slope		Smooth change from steep topography above to gentle topography below.
Rounded convex change in slope		Smooth change from gentle topography above to steep topography below.
Sharp ridge line		Steep or sharp ridge lines, sometimes with rock outcrop.
Rounded ridge line		Smoothly rounded ridge lines with little or no rock outcrop.
Sharp concave break in slope		Sharp change from steep topography above to gentle topography below.
Sharp convex break in slope		Sharp change from gentle topography above to steep topography below.



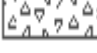
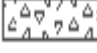
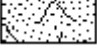
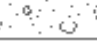


The interpreted materials GIS layer should contain geological information about the substrate or regolith. Categories are described in Table 4.3. In areas where there has been over-printing, or where it is difficult to distinguish between two substrate types, the interpreted material can be described as a mix, for example, mixed colluvium/moraine.

Table 4.3 Interpreted materials layer descriptions (Townsend et al. 2020).

Type	Symbology	Appearance
Rock at/near surface		Intact rock visible at the surface or overlain by 1–2 m of soil, colluvium, etc.
Talus		Generally boulders of loose rock, mainly at bases of steep cliffs, but including pebbles to sand. These deposits lack the large (> c. 2 m), coherent masses of intact bedrock, which show up as very high contrast areas on photos. Talus is differentiated from colluvium mainly by its coarser texture, steeper slope and position at/near the bases of rock bluffs. It is usually difficult to interpret unless the ground is bare, in which case it will most likely be mapped as colluvium. Talus is mapped at the coast on a geomorphic criterion of convex 'talus cones' (or part thereof) filling in shallow depressions below arcuate, convex breaks in slope, similar in appearance to landslide head scarps.
Colluvium		Sheets of colluvium form relatively smooth surfaces in valley bottoms and in broad depressions on rock. The resulting landscape surface is mainly fine-textured and quite smooth, typically well-vegetated. Colluvium accumulates in depositional areas, such as steep valleys and gullies, and on gentle faces below ridges composed of rock. Most hill surfaces have a thin covering of colluvium, sometimes mixed with thin loess deposits. It can grade from/into talus and can be several metres thick, especially in gullies and fossil gullies. Any material forming debris fans and landslide deposits is mapped as colluvium.
Loess		Silt and fine sand, commonly weathering to stiff clay. Commonly forms thin (<1 m) cap over rock at higher elevations (generally included in rock at/near surface mapping unit), especially where the surface is natural. In farmed areas, terracettes may develop where stock have repeatedly walked, forming narrow steps and short risers. Loess can also form featureless mantling deposits, especially on ridge crests where there is little drainage catchment or run-off.
Alluvium		Deposits range from gravel to silt and peat, forming featureless flat ground or terraces. Some outcrops of alluvium forming low terraces are mapped adjacent to smaller streams and many merge with colluvial hill slope deposits. Some large fans adjacent to and merging with the coastal plain are interpreted to be underlain by alluvium.
Sand and gravel		Flat coastal ground is interpreted as beach deposits composed of sand and gravel.
Boulders		Boulder beds commonly form narrow strips of beach below coastal bluffs and are likely to be talus deposits partly reworked by wave action.
Fill		Areas modified by anthropogenic activities can contain fill, which are materials placed by human activity and that can vary in both extent and depth. Within the public conservation lands and waters, this is most likely associated with roads and tracks. Anthropogenic fill typically consists of a range of materials and clast sizes from boulders to gravel, with intermixed soil.
Moraine		A mound, ridge or other topographically distinct accumulation of unsorted, unstratified glacial drift, predominantly till, deposited primarily by the direct action of glacier ice in a variety of landforms.
Water body		A water body, such a lake, river, pond, glacier, etc.

The *genesis* layer should identify the geomorphological processes that occur, and/or have occurred in the past, within the study area and have formed the materials interpreted as being at/near the ground surface. Many of these processes produce material of a particular type (captured in the *interpreted materials* layer), which can also have a distinct morphology (captured in the *morphology* layer). For example, the debris from a landslide (a geomorphic erosion process) is called colluvium (material type) and is often associated with ‘rough’ and/or ‘hummocky’ ground. The ‘genesis’ layer, therefore, is trying to capture the processes that generate the observed materials, i.e. the products derived from the processes. Some of these products, such as colluvium, can be linked to a landslide scar (source area and debris trail), which can be observed directly in the aerial photographs. However, some processes are more difficult to identify from the surface morphology, topographic position and materials. The *genesis* layer therefore requires the most ‘interpretation’ to generate when compared to the other layers and so takes the most time and is also the least accurate. Categories for the *genesis* layer are outlined in Table 4.4.

Table 4.4 Genesis layer descriptions (Townsend et al. 2020).

Type	Symbology	Appearance
Cut slope		Include mappable areas of excavated ground, which are usually underlain by rock; in a few cases, they may also include alluvium and/or colluvium.
Fill body		Interpreted as being formed mainly of fill materials, but they may also contain colluvium, alluvium and/or rock.
Rockfall (many scattered boulders)		Local piles of talus and high concentrations (one every 2–10 m) of boulders, primarily below rock cliffs.
Rockfall (few scattered boulders)		Low concentration (one every 10–50 m) of scattered boulders. Mapped in a few places.
Fans		Typically rounded or conical lobes at the bases of narrow (side) valleys composed of remobilised silt (loess) and rock (colluvium and debris flow deposits). The source is usually obvious, with colluvium in catchment. Surface texture can be hummocky, but more often smooth; gentler than slopes covered with colluvium.
Landslides		Includes landslide source area and debris, which should be mapped separately. Steep, hummocky ground, commonly with ponds and localised areas of poor drainage. Runout area (debris train) may merge with colluvium/debris fan (possibly from secondary debris flows off the toe). Deposits typically consist of shattered mixtures of cobbles and boulders to clay- and silt-sized clasts. Usually initiated in loess or colluvium, occasionally rock. Categorised into: <ul style="list-style-type: none"> Recent: head scarp usually distinguishable from debris. Scarp area mapped as underlying material, debris mapped as colluvium. Relict: hummocky ground, but may be blanketed with loess (older); head scarp degraded/eroded; mapped as colluvium.
Swamp/wetland		Flat, waterlogged ground, usually underlain by peat, with minor alluvial gravels and silt. Swamps commonly have a lower albedo than surrounding areas and typically richer vegetation.
Gully erosion		Erosion of small channels with steep sides in unconsolidated materials by concentrated but intermittent flow of water usually during and immediately following heavy rains or ice/snow melt.

4.2.5 Landslide Mapping Guide

Landslides have geomorphic features that make them identifiable as mass movement landforms. Landslides can be mapped as part of the geomorphological mapping and inform the landslide inventory generation. Typical landslide features and their internationally recognised names are shown in Figure 4.3, which are unchanged from Varnes' (1978) classification, apart from the addition of some minor features (landslide pond, hummocky ground, springs and seeps). These latter features are important, as their recognition makes it possible to identify landslides from aerial and ground inspections. Important landslide features, their significance and some simple ways to recognise them are summarised in Figure 4.3 and Table 4.5.

The level of detail of mapping of the different features within a landslide, outlined in Table 4.5, should scale with the types of analysis, from less detailed for a basic-level analysis to more detailed for an advanced-level analysis. In addition, the level of detail will also vary with the spatial scale of analysis, with regional-scale analysis of linear sites resulting in lesser detailed landslide mapping. For regional- to local-scale analysis, this may essentially consist of mapping the source area, landslide debris and any tension cracks. More detailed mapping of landslide features may apply for particular larger landslides identified in high hazard and risk areas. For point sites at a site-specific scale, detailed mapping of features within a landslide may be appropriate for basic-level analysis and is required for advanced-level analysis.

For rockfalls, mapping of rockfall scars, debris trails and boulder and talus deposits is important for both basic-level and advanced-level analysis. For advanced-level analysis, more detailed mapping of geologic structure, tension cracks and boulder geometry may be appropriate.

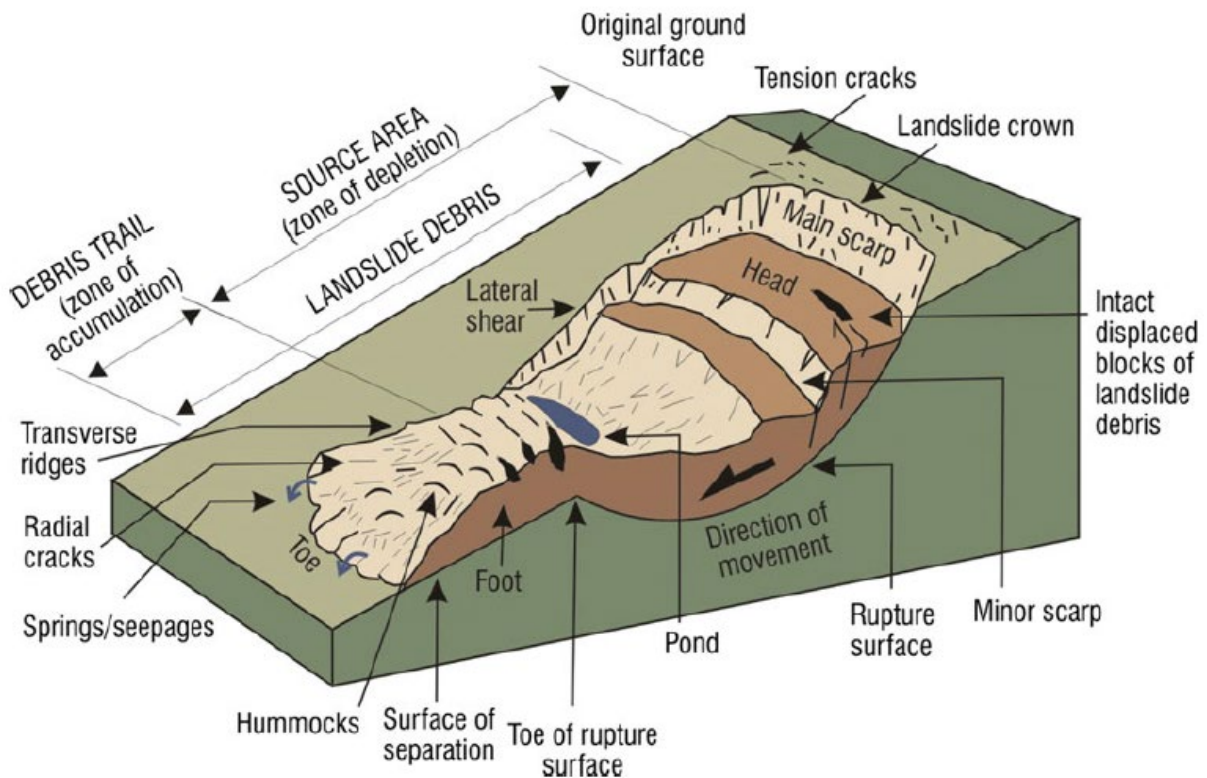


Figure 4.3 Block diagram of an idealised complex rotational earth slide and earth flow showing typical landslide features (adapted from Varnes [1978]).

Table 4.5 Landslide features and criteria for remote sensing and field recognition.

Landslide Features	Description of Features
Active Landslides (and Recently Active or Dormant Landslides)	
Landslide scar	Includes the source area and debris trail.
Source area	The area at the head of the landslide (zone of depletion) where the landslide mass (debris) is derived from.
Landslide debris	Material (rock, soil, vegetation) displaced from the source area and transported down-slope by gravity.
Main scarp	The main scarp is the steep slope in undisturbed ground at the head of the slide (head scarp) – the visible part of the failure surface. Minor (secondary) scarps may be present within the displaced material of the landslide mass.
Tension cracks	Often located upslope of the landslide main scarp and tend to be aligned in an arc; can be continuous or discontinuous but are essentially linear. These indicate horizontal (pull-apart) movement but may also show vertical and shear movement.
Hummocky ground	Ground surface irregular, often formed of low-amplitude hummocks, resulting from differential (compressional and shear) deformations within the displaced material – a feature of many landslides (active and inactive).
Ponds (un-drained)	Ponds formed in depressions, which are often un-drained, are present within the displaced material of many landslides, especially at the slide head; they may be filled by seepage from springs or by rainfall.
Springs, seepages	Give rise to areas of swampy or boggy ground; seepage water may accumulate in ponds.
Trees with curved trunks or leaning backwards	Wind, snow loading, steep topography and ground movement can all give rise to non-vertical tree trunks, so care is required in their interpretation and additional supporting evidence of landslide movement is required.
Disruption of natural drainage	May be seen directly or inferred from seepages. Also, where landslide debris may have totally/partially blocked a drainage line or where the drainage line has been forced to alter its course.
Cracking of structures and paved surfaces and dislocation of drainage structures	These can also be related to local settlement of fill and foundations so additional supporting evidence is required, e.g. presence of source areas / landslide debris, tension cracks, trees leaning backwards.
Relict Landslides (Inactive Old Landslides with Little Potential for Re-Activation)	
Relict landslides typically have eroded, rounded and subdued features, with no sharp features or bare scarps visible. The main scarp is generally eroded and well-vegetated. The displaced landslide mass often has ponds and hummocky, irregular ground. Generally no cracks or indications of movement are visible. Trees and established vegetation show no evidence of tilting, non-vertical trunks or disturbance.	

4.3 Landslide Inventory

A landslide inventory is a record of landslides that have occurred within or adjacent to a study area. The landslide inventory can be compiled at multiple scales. For regional- and local-scale analyses of linear sites, the landslide inventory will likely contain more landslides and take longer to create than an inventory for a site-specific analysis of a point site. The landslides can be distinguished by classification, geometry and activity (Corominas et al. 2015). A landslide inventory is a core component of landslide hazard analysis. Landslide inventories form the most important input into landslide susceptibility maps (van Westen et al. 2008; Van den Eeckhaut and Hervás 2012) by outlining the spatial location of previous landslides.

Landslide inventories, where possible, require multi-temporal input data over and adjacent to the study area in order to understand where and when landslides occur. Creation of landslide inventories can be undertaken using multiple techniques (Table 4.6) depending on the basic level or advanced level of analysis.

For the preliminary hazard and exposure analysis and the basic level of risk analysis, landslides should be mapped as either polygons or points, regardless of scale. If polygons are mapped, then separating source areas from debris trails is important. If this cannot be done, then points could be used to show the source area and lines used to show the assessed length of the landslide debris trail. This should be done for slopes within the study area boundary and on slopes adjacent to it. The extent of mapping will depend on the study area boundary and the type of sites, linear or point.

For the advanced level of analysis, the same approach as the basic level should be carried out but with more attention given to mapping the landslides as polygons, separating source from debris trail. The resolution of any mapping will depend on the availability of data, its resolution and resources/experience to complete the work. For landslides included in an inventory, it is useful to record the type of landslide, an estimate of its volume and the nature of the source material, the date it occurred or an estimate of its age if possible, and the state of activity (e.g. active, dormant, relict). Comprehensive reviews of landslide inventory mapping, including sources of error and uncertainty, are provided by Corominas et al. (2014), Guzzetti et al. (2012) and van Westen et al. (2008).

Table 4.6 Input datasets for the creation of a landslide inventory (AGS 2007c; Fell et al. 2008b; van Westen et al. 2008; Guzzetti et al. 2012; Corominas et al. 2014).

Input Datasets		Description
Field Mapping of Landslides		Field observations of landslides and validation of other techniques. This includes mapping landslide and rockfall scars and talus deposits at the base of slopes.
Remote Sensing Techniques	Aerial photographs and high-resolution satellite imagery	Manual visual interpretation and mapping of landslides from imagery.
		Semi-automatic mapping methods of landslides from imagery.
	Multi-spectral imagery	Manual visual classification methods for mapping landslides.
		Semi-automatic classification methods of landslides from imagery.
	Digital elevation data (e.g. airborne LiDAR, terrestrial LiDAR, aerial photogrammetry)	Visual interpretation and analysis of surface morphology and change-detection analysis.
InSAR	Surface deformation analysis.	
Archival Information	Past landslide events (e.g. newspaper archives, interviews, road maintenance organisations)	Historical information on location, timing, size, impacted area and triggering mechanism.
	Damage data (e.g. insurance claims)	Historical information on economic losses and population affected with dates, location and characterisation.

Sources of error and uncertainty surrounding landslide inventories include:

1. Incomplete datasets of previous landslide events in an area due to a lack of (quality) input datasets (van Westen and Soeters 2006; van Westen et al. 2008; Guzzetti et al. 2012).
2. A lack of separation between the source and depositional areas of a landslide. A lack of separation will result in an incorrect susceptibility analysis, as the attributes of depositional areas are assigned the same importance as source areas.
3. Consultant inexperience, resulting in errors in landslide identification, mapping or mis-characterisation of landslide type.

Good data on historical or pre-historical landslide frequency are often difficult to find or generate, and often frequency information is limited to the recent historical past. In turn this constrains the range of event probabilities that can be reliably considered. For example, if historical records are limited to 30 years, then the probability of single events will be limited to a basic 1-in-30-year probability (about 0.03, though this may be modified by the probability of trigger events during that period) for a population of similar landslides in similar geology and geomorphology.

4.4 Triggering Factors

Landslides can occur in response to a trigger, such as an earthquake, heavy rainfall or snowmelt event, or in the apparent absence of a discernible trigger. It is important to understand the magnitude and frequency of such trigger (and non-trigger) events in order to understand the associated landslide hazard, including the number of landslides generated, their spatial distribution and size. The (potential) triggers of landslides and type of landslide generated by such triggers (e.g. debris flows in heavy rainfall events) in the study area need to be identified.

The magnitude-frequency of a triggering event (such as an earthquake) needs to be quantified to understand how events of varying magnitudes can produce different landslide distributions and how often these events occur. At many sites, such information will not be available, therefore the relative frequency and associated impacts (the number and size of landslides produced) will need to be estimated based on expert judgement, as outlined in the Part 3 report.

For advanced-level analysis, where appropriate, this involves compiling inventories of landslide-inducing events (compare with Guzzetti et al. [2012]). When generating landslide inventories, effort should be made to understand the occurrence of a landslide with respect to a potential trigger. However, this information is often not available for a study area due to the need for (and associated lack of) multi-temporal datasets (van Westen et al. 2008; Guzzetti et al. 2012), and therefore event inventories from other areas can be used, with caution, if they share similar pre-disposing factors consistent with the conceptual geomorphic model. An open source repository of earthquake-induced landslide (EIL) datasets from around the world is available at <https://www.sciencebase.gov/catalog/item/583f4114e4b04fc80e3c4a1a>, with Tanyaş et al. (2017) providing more information about the datasets.

New Zealand examples of EIL inventories, including magnitude-frequency analysis, from the Kaikōura, Murchison and Inangahua earthquakes is provided in Section 6.3.1.

Sources of error and uncertainty surrounding the characterisation of triggering factors include:

1. Incomplete landslide event inventories, due to insufficient multi-temporal datasets from which to generate landslide inventories for a particular trigger and magnitude, as well as no record of a triggering event of given magnitude occurring within the time-frame of the datasets (Guzzetti et al. 2012).
2. Incomplete knowledge of magnitude-frequency characteristics of trigger events.
3. Changing environmental conditions, resulting in a change in trigger frequency. This is particularly pertinent for climate-change scenarios, where changes in rainfall and storm characteristics will influence landslide-inducing events (AGS 2007d; Corominas et al. 2014; Lee and Jones 2014; Gariano and Guzzetti 2016).
4. Depletion of source material, for example, colluvium deposits in gullies or other changes in susceptibility conditions.

4.4.1 Rainfall Triggers

As set out in Section 4.4 of the Part 3 report, at the preliminary screening tool and basic levels of analysis, it is unlikely that landslide occurrence and severity (numbers of landslides produced and their volumes) will be able to be linked to the rain amount and duration that triggered them. Therefore, the number and size of landslides that could be triggered at a site by rain events will need to be estimated from historical records. This may be as simple as mapping the landslide distribution and their size (adopting volume classes) and estimating the period over which they are thought to have occurred.

For advanced-level analysis, it is recommended to estimate the magnitude and frequency of rainfall events and associated landsliding:

1. Using the National Institute of Water & Atmospheric Research (NIWA)'s National Climate Database (CliFlo) and council rainfall databases, analyse the magnitude and frequency of past rainfall events from nearby and appropriate meteorological stations.
2. Using NIWA's High Intensity Rainfall Design System (HIRDS¹) database, determine the annual re-occurrence interval of varying intensity-duration rainfall events (e.g. a series of bands of increasing intensity-duration rainfall events).
3. Estimate the number and magnitude (volume) of landslides that might be triggered within each rainfall intensity-duration band based on the landslide inventory.
4. For larger individual landslides, the longer-term rainfall patterns (i.e. seasonal cycles) that drive pore-water pressure fluctuations and lead to landslide displacement.

The linkage between rainfall and landslide occurrence and severity for some study areas may not be possible to establish. In such instances, it may be best to use the mapped distribution of rainfall-induced landslides at or adjacent to the site, coupled with any historical information about past landslide events, to estimate the frequency of landslides of a given volume occurring. Section 6.3 contains more information on determination of landslide magnitude–frequency data for different triggering events. Alternatively, or in addition, data from similar terrain may be used.

4.4.2 Climate Change

Theoretically, climate changes have the potential to impact the frequency and intensity of landslides. Landslides occur when the stress acting on a slope is greater than the strength of the slope (Figure 4.4), and climatic processes can affect both the strength and the stresses. For example, rainfall can increase the stress on a slope or decrease the strength of a slope. Additionally, cycles such as wetting and drying, heating and cooling and tidal cycles, will reduce the strength of a slope over time until a landslide occurs without an obvious trigger.

For example, under climate-change scenarios:

- Rainfall-induced landslides and their associated impacts are expected to increase both due to overall increase in rainfall for some parts of Aotearoa New Zealand but also more extreme storm activity (Crozier 2010).
- Increases in rockfalls and rock avalanches in alpine areas may increase with summer heat waves and associated changes in permafrost (e.g. Ravelle et al. 2017).
- Increased wildfire activity may result in more burned slopes with no vegetation and increased likelihood of debris flows following rainfall (e.g. Kean et al. 2019).
- Increases in sea level and changes in marine and storm activity may also result in greater coastal erosion and landsliding (e.g. Jakob 2022).

NIWA's HIRDS database provides future projections of rainfall for different return periods and event durations based on historical rainfall and climate-change scenarios (Representative Concentration Pathways). More information on climate-change scenarios can be found on the NIWA² and Ministry for the Environment³ websites.

1 <https://niwa.co.nz/climate-and-weather/high-intensity-rainfall-design-system-hirds>

2 <https://niwa.co.nz/climate-and-weather/climate-change-scenarios-new-zealand>

3 <https://environment.govt.nz/publications/climate-change-projections-for-new-zealand/>

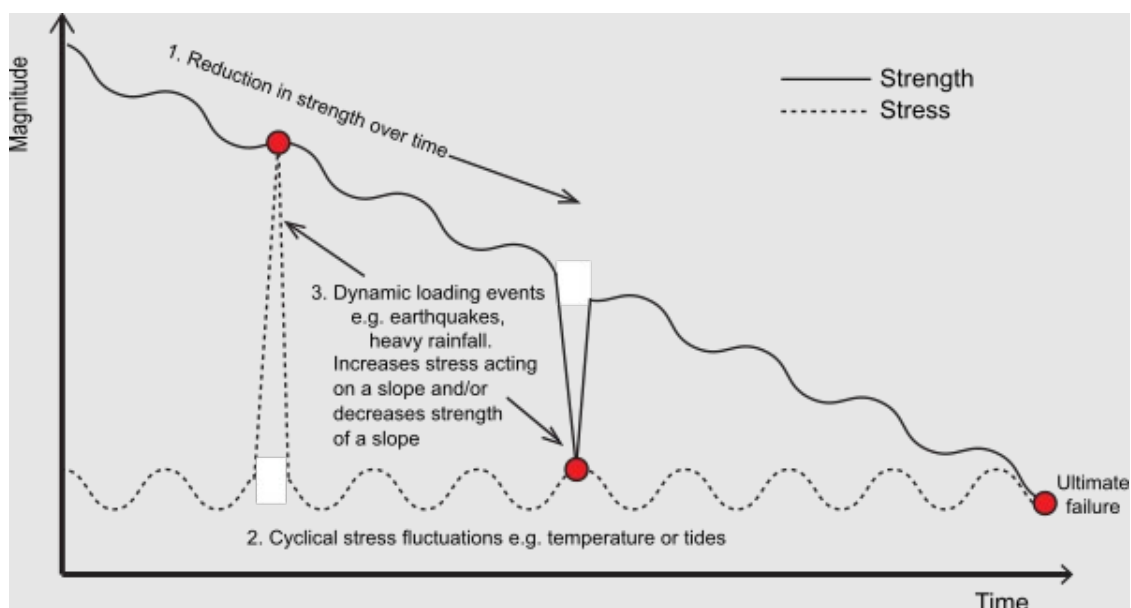


Figure 4.4 Examples of factors that reduce the strength of rock mass and increase the stresses acting upon it over time (the x axis). The red dots represent when failure conditions are met and landslides can occur. The gradual reduction in rock-mass strength is driven by environmental processes (e.g. weathering). Dynamic-loading events can both increase the stress acting on a slope or decrease the strength of the slope, which allows failure to occur (modified from Gunzburger et al. [2005]).

4.4.3 Earthquake Triggers

4.4.3.1 Peak Ground Acceleration Maps

PGA hazard maps for different return periods can be used to determine the potential for EIL to occur in a study area, along with the intensity of the landsliding that could occur during an earthquake event. Examples of PGA for different return periods for site class B conditions from the previous version of the National Seismic Hazard Model (NSHM; Stirling et al. 2012) are provided in Figures 4.5–4.8.

4.4.3.2 Earthquake-Induced Landslides

Using the PGA hazard maps in Figures 4.5–4.8, maps of EIL probability have been produced for all of New Zealand (cf. Massey et al. [2021]), which calculate the probability of a landslide occurring for a given level of ground shaking based off a set of physiographic and geological variables. These EIL probability maps can be used to determine the potential for EIL to occur in a study area, along with the intensity of landsliding that could occur during an earthquake event. The EIL probability maps are available on request to DOC as *.kmz* files.

For the preliminary screening and basic levels of analysis, use the method given in Section 4.4.2 of the Part 3 report, along with the earthquake-induced thresholds for landsliding given in Table 4.7, to determine whether EIL are likely to affect the study area. Analysis of past landsliding triggered during earthquake events of varying magnitude and levels of ground shaking have revealed that widespread soil/rock falls and avalanches are typically only triggered for earthquakes with associated ground shaking typically greater than Modified Mercalli (MM) intensity of MM >5 and peak ground accelerations (PGA) of ≥ 0.2 g (Dowrick et al. 2008; Hancox et al. 2014, 2016; Massey et al. 2018b). The intensity of the ground shaking varies with earthquake magnitude and depth; therefore, earthquake magnitude alone is not a good measure of ground shaking intensity. For large slides, longer duration shaking at low frequencies may be important rather than high PGA. Landslide and other environmental criteria often observed at different levels of ground shaking are shown in Table 4.7.

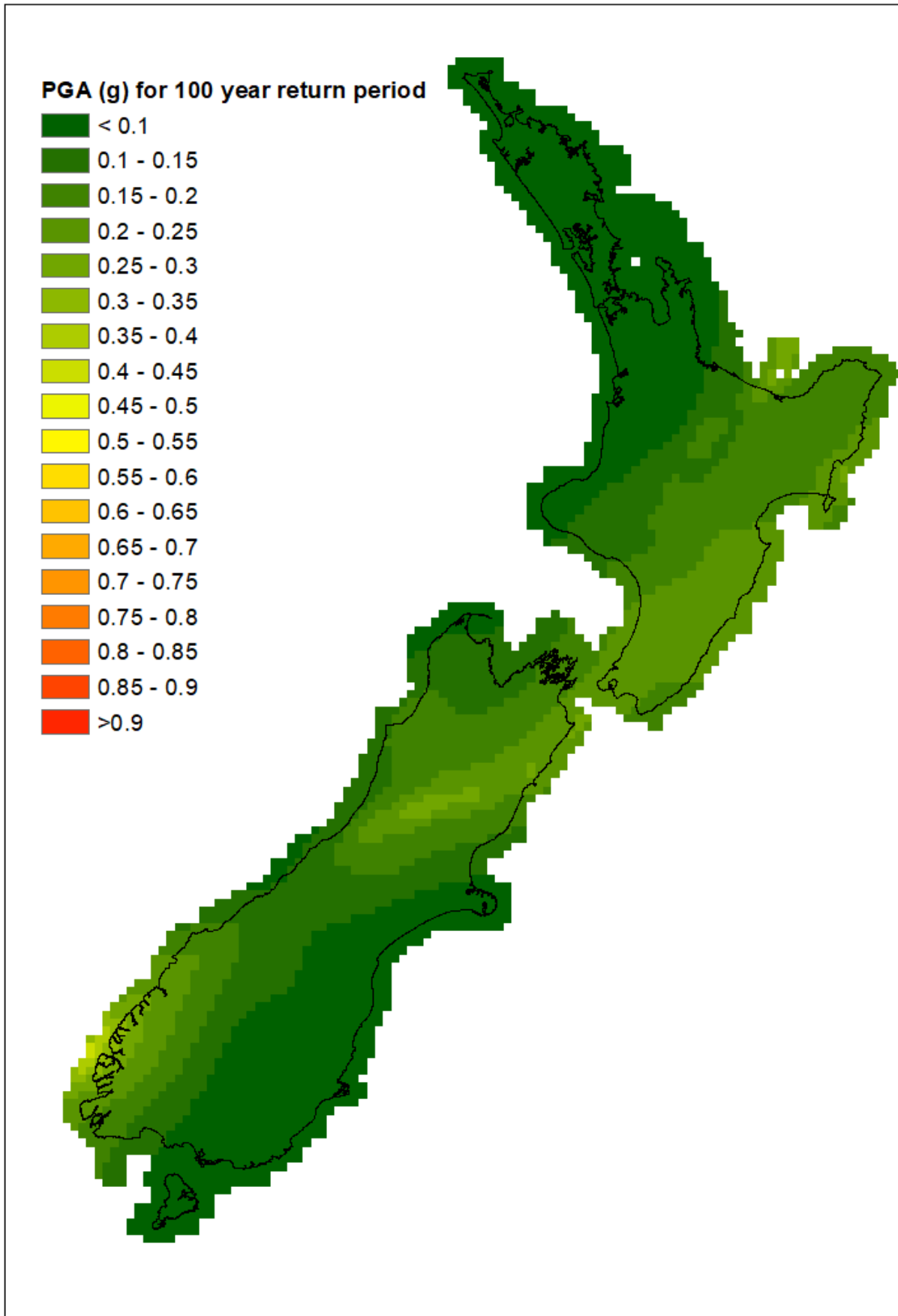


Figure 4.5 Peak ground acceleration hazard map for 100-year return period.

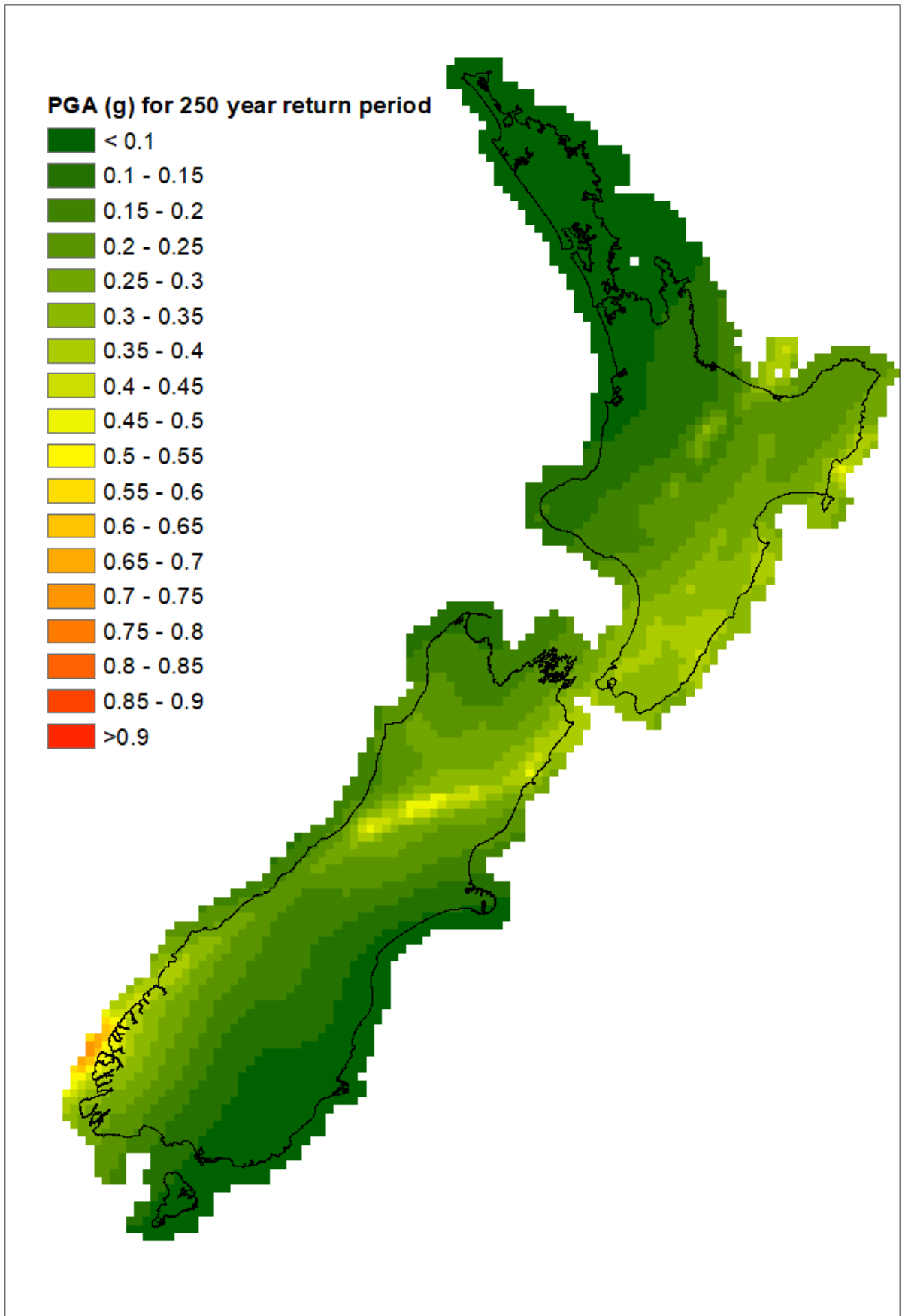


Figure 4.6 Peak ground acceleration hazard map for 250-year return period.

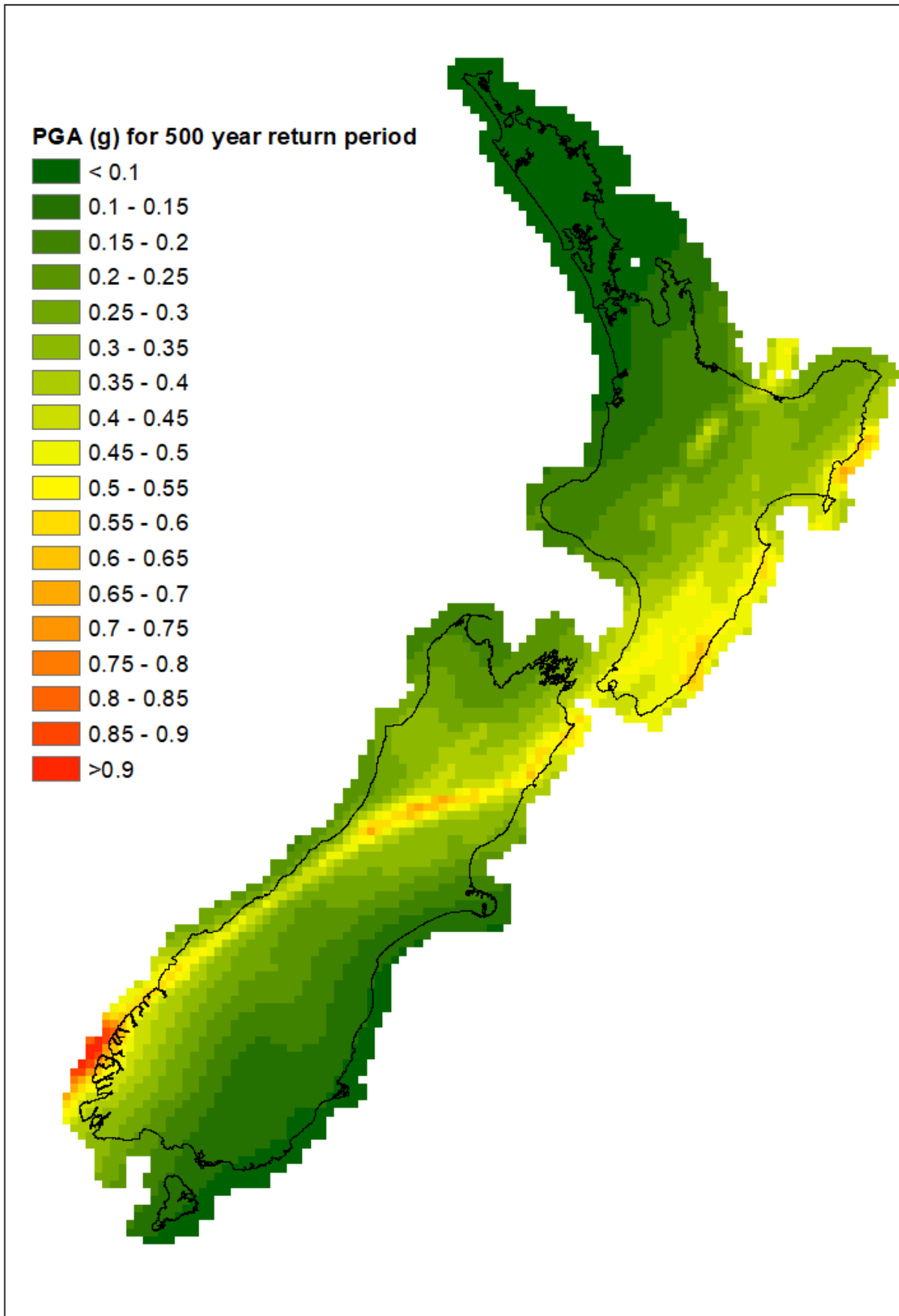


Figure 4.7 Peak ground acceleration hazard map for 500-year return period.

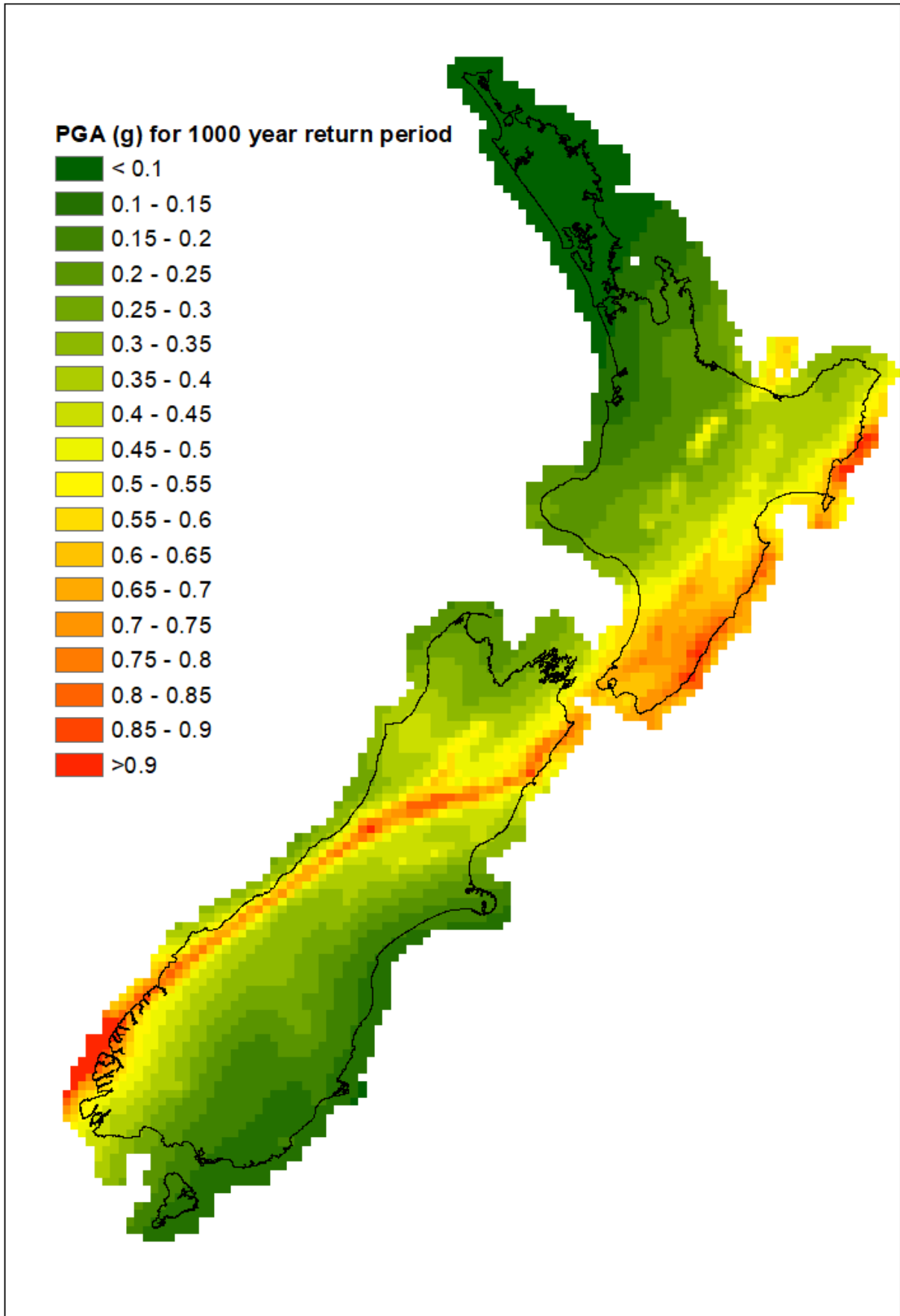


Figure 4.8 Peak ground acceleration hazard map for 1000-year return period.

Table 4.7 Landslide and Environmental Criteria often observed at different levels of ground shaking – peak ground acceleration (PGA) and the New Zealand Modified Mercalli intensity scale (MM) – modified from Hancox et al. (2002) and adopting the PGA to MMI relationship of Moratalla et al. (2021).

MODIFIED MERCALLI (MM) INTENSITY SCALE Landslide and Environmental Criteria
<p>PGA: <0.1 g (MM >5–6)</p> <ul style="list-style-type: none"> • Trees and bushes shake or are heard to rustle. Loose material dislodged on some slopes, e.g. existing slides, talus and scree slope. • A few very small (<1000 m³) soil and regolith slides and avalanches and occasional soil/rock falls from steep banks and cuts. • A few minor cases of liquefaction (sand boils) in highly susceptible alluvial and estuarine deposits.
<p>PGA: 0.1–0.2 g (MM 6–7)</p> <ul style="list-style-type: none"> • Water made turbid by stirred-up mud. • A few very small (<1000 m³) disrupted soil slides, avalanches and falls of sand and gravel banks, and rock falls and avalanches from steep slopes and cuttings common. • Fine cracking on some slopes and ridge crests. • A few small to moderate (1000–100,000 m³) slides and avalanches in soil and regolith, and falls of soil/rock falls from steep slopes (>30°) and on coastal cliffs, gorges, road cuts/excavations, etc. • Small discontinuous areas of minor shallow sliding/cracking and mobilisation of scree slopes in places. Minor small failures in road cuts and in more susceptible materials. • A few instances of liquefaction (small water and sand ejections) in alluvium.
<p>PGA: ≥0.2–0.5 g (MM 7–8)</p> <ul style="list-style-type: none"> • Cracks appear on steep slopes and in wet ground. • A few pre-existing landslides could re-activate, causing new cracks to form. • Significant landsliding likely in susceptible areas. • Small to moderate (1000–100,000 m³) slides widespread; many soil/rock falls on steep slopes (terrace edges, gorges, cliffs, cuts, etc). • Significant areas of shallow regolith landsliding and re-activation of scree slopes. • A few large (100,000–1,000,000 m³) landslides from coastal cliffs and possibly large to very large (>1,000,000 m³) rock slides and avalanches from steep mountain slopes. • Larger landslides in narrow valleys may form small temporary landslide-dammed lakes. • Roads damaged and blocked by small to moderate failures of cuts and slumping of road-edge fills. • Evidence of soil liquefaction common, with small sand boils and water ejections in alluvium and localised lateral spreading (fissuring, sand and water ejections) and settlements along banks of rivers, lakes, canals, etc.

MODIFIED MERCALLI (MM) INTENSITY SCALE

Landslide and Environmental Criteria

PGA: ≥ 0.5 – 1.1 g (MM 8–9)

- Landsliding widespread and damaging in susceptible terrain, particularly on slopes steeper than 20° . Cracking on flat and sloping ground.
- Extensive areas of shallow regolith failures and many rock falls and disrupted rock and soil slides on moderate and steep slopes (20 – 35° or greater), cliffs, escarpments, gorges and man-made cuts.
- Many small to large (1000 – $1,000,000$ m³) failures of regolith and bedrock, and some very large landslides ($>1,000,000$ m³) on steep, susceptible slopes.
- Very large failures on coastal cliffs and low-angle bedding planes in Tertiary rocks. Large rock/debris avalanches on steep mountain slopes in well-jointed greywacke and granitic rocks. Landslide-dammed lakes formed by large landslides in narrow valleys.
- Some pre-existing landslides will re-activate, causing new cracks to form. The debris from some may break down to form avalanches.
- Damage to road and rail infrastructure widespread, with moderate to large failures of road cuts and slumping of road-edge fills. Small to large cut slope failures and rock falls in open mines and quarries.
- Liquefaction effects widespread with numerous sand boils and water ejections on alluvial plains, and extensive, potentially damaging, lateral spreading (fissuring and sand ejections) along banks of rivers, lakes, canals, etc. Spreading and settlements of river stop banks likely.

PGA: >1.1 g (MM >9)

- Landsliding is very widespread in susceptible terrain (3).
- Similar effects to MM 8–9, but more intensive and severe, with very large rock masses displaced on steep mountain slopes and coastal cliffs. Landslide-dammed lakes formed. Many moderate to large failures of road and rail cuts and slumping of road-edge fills and embankments may cause great damage and closure of roads and railway lines.
- Many pre-existing landslides will re-activate, causing new cracks to form. The debris from some may break down to form avalanches.
- Liquefaction effects (as for MM 8–9) widespread and severe. Lateral spreading and slumping may cause rents over large areas, causing extensive damage, particularly along river banks, and affecting bridges, wharfs, port facilities and road and rail embankments on swampy, alluvial or estuarine areas.

NOTES:

1. 'Some' or 'a few' indicates that threshold for an effect or response has just been reached at that intensity. At less than MM 5 shaking, landslide effects are insignificant in New Zealand and are therefore not included in this scale.
2. Intensity is principally a measure of building damage. Environmental damage (response criteria) also occurs, mainly on susceptible slopes and in certain materials; hence, the effects described above may not occur in all places but can be used to reflect the average or predominant level of damage (or MM intensity) in a given area.
3. Environmental response criteria have not been suggested for $>MM$ 9 because the environmental effects at high levels of shaking would be similar to those at MM 8–9, but possibly more widespread and severe.

The information in Table 4.7 can be used as a guide to understand and estimate the intensity and magnitude landsliding potentially generated from ground shaking. It should be noted that the dynamic response of a slope during an earthquake comprises a complex interaction between seismic waves and the hill-slope (e.g. Sepúlveda et al. 2005). The response of a slope to an earthquake is thought to be controlled by: (1) the nature of the earthquake source, (2) wave propagation path effects and (3) local site conditions and their effects on amplifying or de-amplifying shaking (Kramer 1996; Sepúlveda et al. 2005; Kaiser et al. 2014; Massey et al. 2017).

For co-seismic landslide studies, the response of a slope to an earthquake is typically assessed using metrics that describe both the: (1) amplification effects and (2) amounts of permanent displacement. Amplification effects are usually described as a ratio between the measured/modelled peak ground acceleration (PGA), peak ground velocity (PGV), Arias Intensity or spectral acceleration in the free field, compared to those measured or modelled at: (i) the slope crest, (ii) various locations in the slope and (iii) along the slide surface of an assumed sliding mass (e.g. Makdisi and Seed 1979; Ashford and Sitar 2002; Bray and Travasarou 2007; Athanasopoulos-Zekkos and Seed 2013). Estimates of the amount of permanent slope displacement can be made using multiple techniques (a good summary is provided by Jibson [2011]), ranging from Newmark (1965) rigid-block to decoupled and fully coupled procedures incorporating seismic site-response assessments (e.g. Wartman et al. 2003; Bray and Travasarou 2007; Strenk and Wartman 2011; Rizzitano et al. 2010; Gischig et al. 2015) in both two and three dimensions.

In most cases, such a detailed assessment of slope response to earthquake shaking is not warranted. Therefore, for the advanced-level analysis, it is recommended that the number of landslides of a given volume generated at different levels of earthquake ground shaking, from low to high, are estimated for the site. To do this, the peak ground acceleration (PGA), the preferred metric of earthquake shaking, is routinely used in landslide stability analyses, and PGA hazard maps are available for New Zealand. PGA hazard curves are routinely used in New Zealand to determine the likelihood of a given level of shaking occurring at a site; an example is provided in Figure 4.9. The process is set out NZS 1170.5:2004 (Structural Design Actions – Part 5: Earthquake Design Actions – New Zealand), which uses the National Seismic Hazard Model (NSHM) to generate probabilistic estimates of earthquake shaking in the form of peak ground acceleration (PGA) hazard curves (Stirling et al. 2012). PGA hazard curves should be generated by suitably qualified earthquake engineers/scientists.

The frequency (number) and volume of landslides likely to be generated at different magnitudes of ground shaking intensity can then be estimated. This is typically done using forecasts derived from empirical relationships between the area affected by landslides, or the number and volume of landslides, and the level of earthquake magnitude and ground shaking intensity, associated with past earthquakes (e.g. Keefer 1984; Parker et al. 2015; Massey et al. 2017; Fan et al. 2019). An example of the number and volume of the landslides generated in New Zealand at different bands of PGA by the Kaikōura, Murchison and Inangahua earthquakes is given in Section 6.3.1.

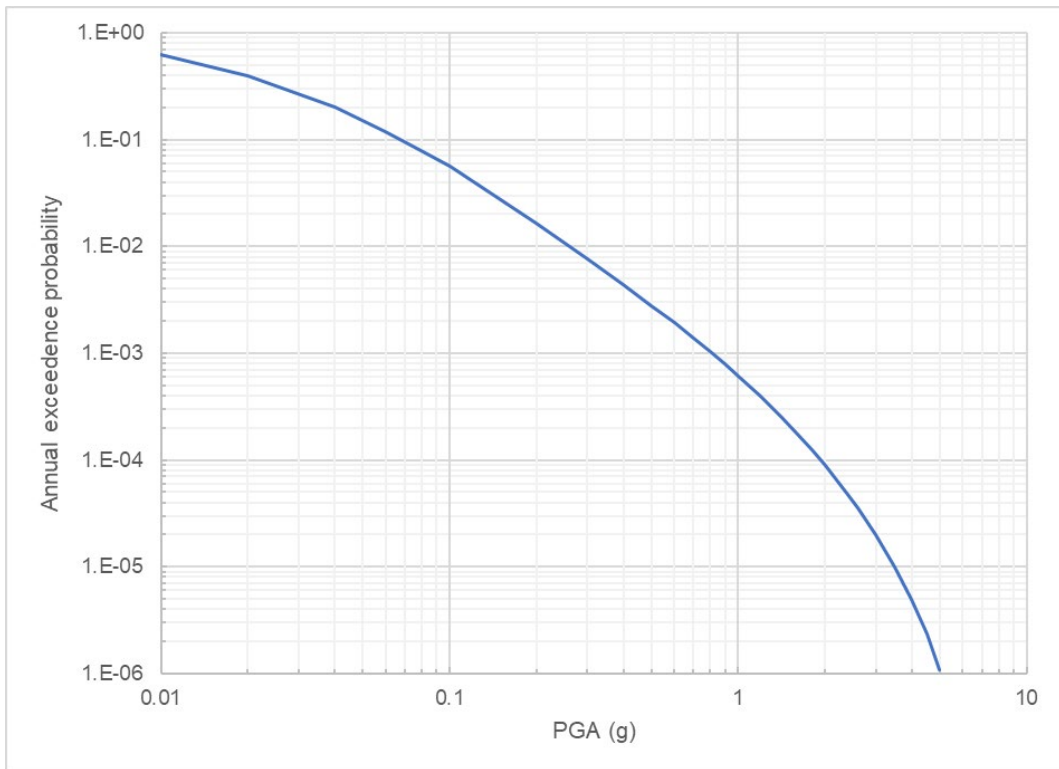


Figure 4.9 Example peak ground acceleration (PGA) hazard curve displaying the annual exceedance probability in any one year for Cape Kidnappers, Hawke's Bay.

4.4.4 Volcanic Triggers

No additional comment.

5.0 FIELD STUDY

The methods used, and associated level of detail and time for fieldwork, should take into account (adapted from AS 1726:2007) the:

1. Type of analysis: basic or advanced level.
2. Spatial scale of analysis, from regional to site-specific, with reference to the study area boundary and type of site (point or linear being analysed).
3. Objectives of the investigation.
4. Site conditions.
5. Health, safety and environmental considerations.

Fieldwork should typically include the following:

1. Mapping of, or field-truthing of previously mapped, topography, geology, geomorphology and other relevant natural hazard features.
2. Loggings of outcrops (e.g. slope cuttings or other exposures). Material descriptions should be in accordance with the NZGS (2005) field description of soil and rock guidelines.
3. Indirect methods, such as terrestrial laser scanning and photogrammetry.

Additional analysis may be needed for advanced analysis at point sites, such as geophysical surveys, collection of samples for testing and any subsurface works. Depending on the level (basic or advanced) and spatial scale of analysis, the questions outlined in Table 5.1 may be useful prompts in determining areas for fieldwork investigations required to estimate the risk from landslide hazards to a site, including site-walkovers, mapping, sampling and surveying.

Table 5.1 Questions to be addressed in slope stability and landslide investigations for a given site (Fell et al. 2000).

Question	Sub-Question
1. Topography?	1.1 In the landslide source and along the potential runout path 1.2 Effect and timing of natural and human activity on the topography 1.3 Changes over time
2. Geological Setting?	2.1 Regional stratigraphy, structure, history (e.g. glaciation, sea-level submergence and emergence) 2.2 Local stratigraphy, slope processes, structure/discontinuities, history 2.3 Geomorphology of slope and adjacent areas
3. Hydrogeology?	3.1 Regional and local groundwater model? 3.2 Piezometric pressures within and around the slide? 3.3 Relationship of piezometric pressures to rainfall, snowfall and snowmelt, temperature, stream flows, reservoir levels, both seasonally and annually? 3.4 Effect of natural or human activity? 3.5 Groundwater chemistry and sources 3.6 Annual exceedance probability (AEP) of groundwater pressures
4. History of Movement?	4.1 Velocity, total displacement and vectors of surface movement? 4.2 Any current movements and relation to hydrogeology and other natural or human activity? 4.3 Evidence of historic movement and incidence of sliding e.g. lacustrine deposits formed behind a landslide dam, shallow natural slides or failures of cuts and fills 4.4 Geomorphic or historic evidence of movement of slope or adjacent slopes
5. Geotechnical characterisation of the slide or potential slide?	Stage of movement (pre-failure, post failure, re-activated, active) Classification of movement (e.g. slide, flow) Materials factors (classification, fabric, volume change, degree of saturation)
6. Mechanisms and dimensions of the slide or potential slide?	Configuration of basal, other bounding and internal rupture surfaces? Is the slide part of an existing or larger slide? Slide dimensions, volume? Is a slide mechanism feasible?
7. Mechanics of shearing and strength of the rupture surface?	Relationship to stratigraphy, fabric, pre-existing rupture surfaces Drained or undrained shear? First time or re-activated shear? Contractant or dilatant? Saturated or partially saturated? Strength pre- and post-failure and stress-strain characteristics
8. Assessment of Stability?	Current and likely factors of safety, allowing for hydrological, seismic and human influences? AEP of failure (factor of safety ≤ 1)?
9. Assessment of deformations and travel distance?	Likely pre-failure deformations? Post-failure travel distance and velocity? Likelihood of rapid sliding?

6.0 DATA ANALYSIS

6.1 Landslide Source Susceptibility

Landslide susceptibility is a quantitative or qualitative assessment of the volume (or area) and spatial distribution of landslides, which exist or may potentially occur in an area. Susceptibility may also include a description of the velocity and intensity of the existing or potential landslide (Corominas et al. 2015). Landslide susceptibility does not represent a hazard map, as there is no indication within a susceptibility map of frequency (annual probability) that a landslide might occur. However, they are a fundamental input to hazard analysis as they determine the most probable source areas of landslides.

Susceptibility maps are determined using information from the landslide inventory and pre-disposing factors and can be developed for a specific triggering event. The data are analysed using one of three methods:

1. **Heuristic techniques**, where expert knowledge and relative ranking scales are used to assign a rank of susceptibility from low to high for a particular mapping unit.
2. **Statistical techniques**, where combinations of pre-disposing factors and their contributions to explaining previous landslides in an area are evaluated statistically, with susceptibility expressed in terms of probability.
3. **Deterministic techniques**, where physics-based models are applied to site-specific slopes to determine their susceptibility to failure.

Comprehensive reviews of landslide susceptibility mapping include Corominas et al. (2014), Guzzetti et al. (2006), Reichenbach et al. (2018) and van Westen et al. (2008).

For basic-level risk analysis, heuristic methods are recommended, given the limited data inputs, time and resources, while, for advanced-level analysis, more data-driven, statistical methods should be used. Deterministic methods would only be used for advanced-level, point source, site-specific risk analysis, not regional or local risk analysis of linear sites. Similarly, for both basic-level and advanced-level analysis at a point site and a site-specific scale, susceptibility to rockfalls can be determined from the engineering geomorphological maps and the rockfall inventory, plus topographic and kinematic analysis. An example of a statistical landslide susceptibility model based on the EIL inventory of the 2016 Kaikōura earthquake, applicable for advanced analysis, is presented in Massey et al. (2018b).

Sources of error and uncertainty surrounding susceptibility mapping (Guzzetti et al. 2006; Corominas et al. 2014; Reichenbach et al. 2018) include:

- Input data quality, both in terms of incomplete landslide inventories and incomplete and/or incorrect pre-disposing factors or the weightings applied to them.
- Using data of pre-disposing factors that is not consistent with when the landslide occurred, for example, using a current land-use map when the land use may have been different when the landslide occurred.
- Combining all landslide types or triggering events into one map, though the occurrence of certain landslide types may be controlled by certain causal factors.
- Inappropriate selection of mapping unit and scale, which is not representative of, or linked to, landslides within the study area.

6.2 Landslide Size

6.2.1 Topographic Controls on Landslide Size

Only large slopes can generate large landslides; therefore, topography presents a control on the size of landslides that can be generated. Topography should therefore be used as a tool to screen landslide size. Additionally, for shallow landslides in colluvium and highly to completely weathered rock, the depth of such deposits will limit the amount of material and therefore size of the landslides that can occur, as well as reducing the potential for future landslides from the same area, especially if the susceptible material had been removed by the previous landslide.

Massey et al. (2020b) provides an example of analysis of the Kaikōura EIL inventory, where the coincidence of landslides was assessed against local slope relief (LSR), which represents the local height of the slope. In general, the trend shows that smaller landslides occur for lower LSR values, while larger landslides occur only for bigger LSR values (see Figure 6.2). In some circumstances, the structural geology of the slope can generate landslide sizes that exceed what any LSR value would suggest, such as the Green Lake Landslide in Fiordland.

The landslides shown in Figure 6.2 comprise multiple types, adopting the classification scheme of Hungr et al. (2014), but most are debris avalanches in rock (regolith). For small landslides (<1000 m³ in volume), the dominant landslide types are soil and rock falls and avalanches, where their depth is dictated by the depth of the soil and regolith. For medium landslides (with volumes >1000 to 100,000 m³), the dominant landslide types are soil and rock avalanches. For medium and large landslides (with volumes >100,000 to 1,000,000 m³), the dominant landslide types are rock avalanches and translational and rotational rock coherent (after Keefer [1984]) slides. Large landslides (with volumes >1,000,000 m³) typically comprise translational and rotational coherent rock slides and a few rock avalanches.

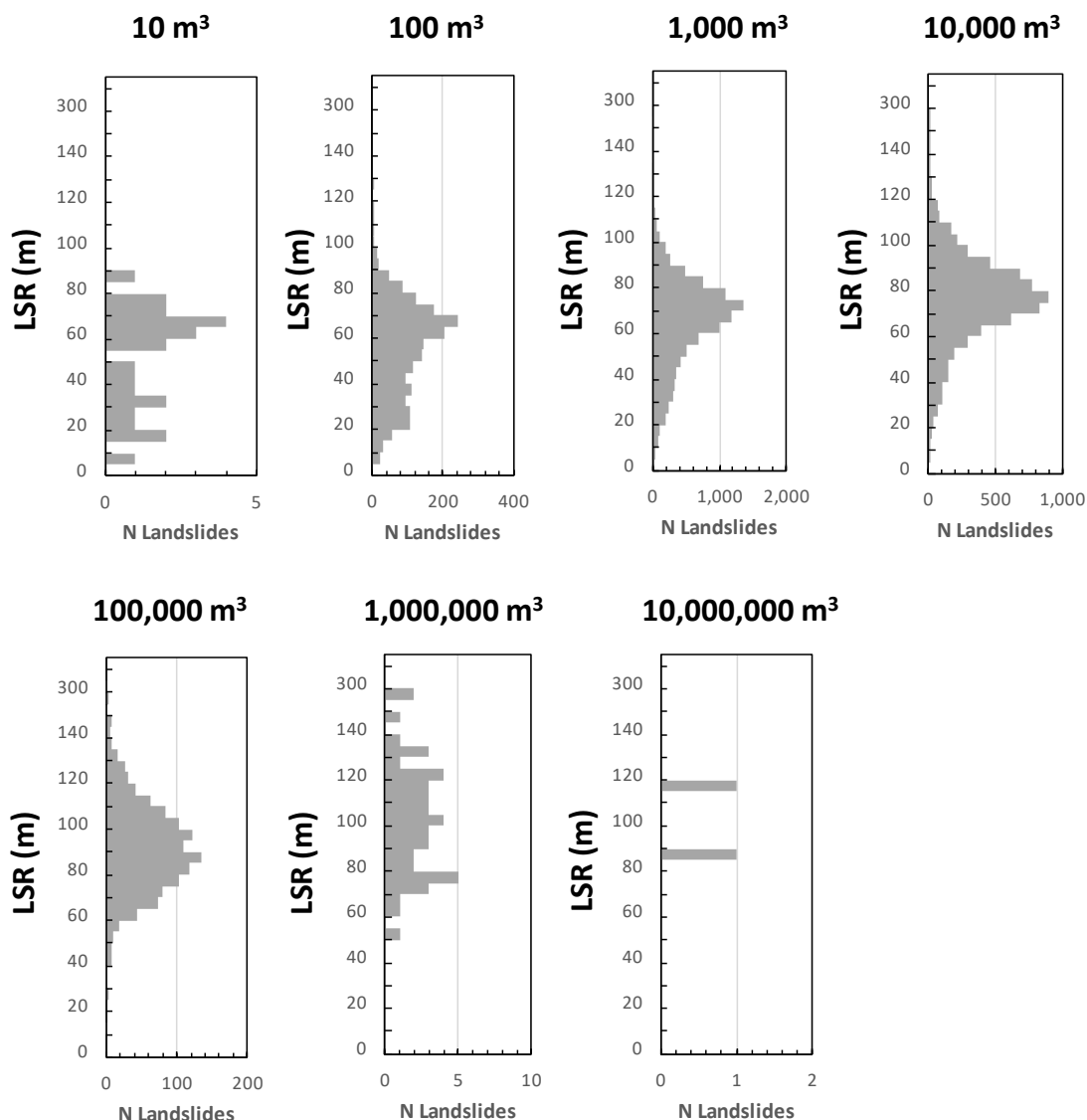


Figure 6.1 Histograms of the occurrence of landslide for local slope relief (LSR) categories. Landslides are divided into landslide volume categories (Massey et al. 2020b). Landslides with volumes <1000 m³ were not all mapped, due to the scale of the mapping and size of the area affected.

6.2.2 Area to Volume Scaling Relationships

Landslide volume is an important characteristic of landslides that impacts frequency, runoff and regression. For point sites at a site-specific scale of analysis, it may be practicable to determine landslide depths for the different types of landslides present within the study area. However, as the spatial scale increases from site-specific to regional, it may become impractical to accurately determine landslide depths and associated volumes. For large study areas, it is impractical to measure the depth of every landslide scar in order to calculate landslide volumes. Therefore, a scaling relationship (Equation 6.1) between landslide area (A) and landslide volume (V) is used to estimate landslide volumes, where:

$$\text{Landslide Volume } (V) = a \cdot A^y \quad \text{Equation 6.1}$$

If area – volume-scaling relationships exist for similar areas and landslide types, these can be used, provided that they are validated with the inspection of past landslides in the study area and by consideration of the depth of colluvium/soil/regolith on the slopes. Figure 6.3 displays the relationship between landslide volume and area for the 2016 Kaikōura EIL dataset and the power law fitted to the data. Many studies have documented power-law scaling for landslide

area volume distributions (Hovius et al. 1997; Korup 2005; Guzzetti et al. 2009; Larsen et al. 2010; Parker et al. 2011). As the scatter in Figure 6.3 displays, these relationships should be applied appropriately to reflect the landslide geology and mechanism. For example, deep-seated block landslides in Tertiary sedimentary units will have a different area to volume scaling exponent compared to shallow greywacke debris avalanches, as demonstrated by Massey et al. (2020a). Defining the possible range of exponents (γ) is important because even small variations can result in substantial over- or under-estimates in landslide volume (Larsen et al. 2010).

Table 6.1 represents a published version of area to volume scaling relationships. Massey et al. (2020a) contains a more comprehensive overview and updated area to volume scaling relationships for the different landslide types generated during the 2016 Kaikōura earthquake.

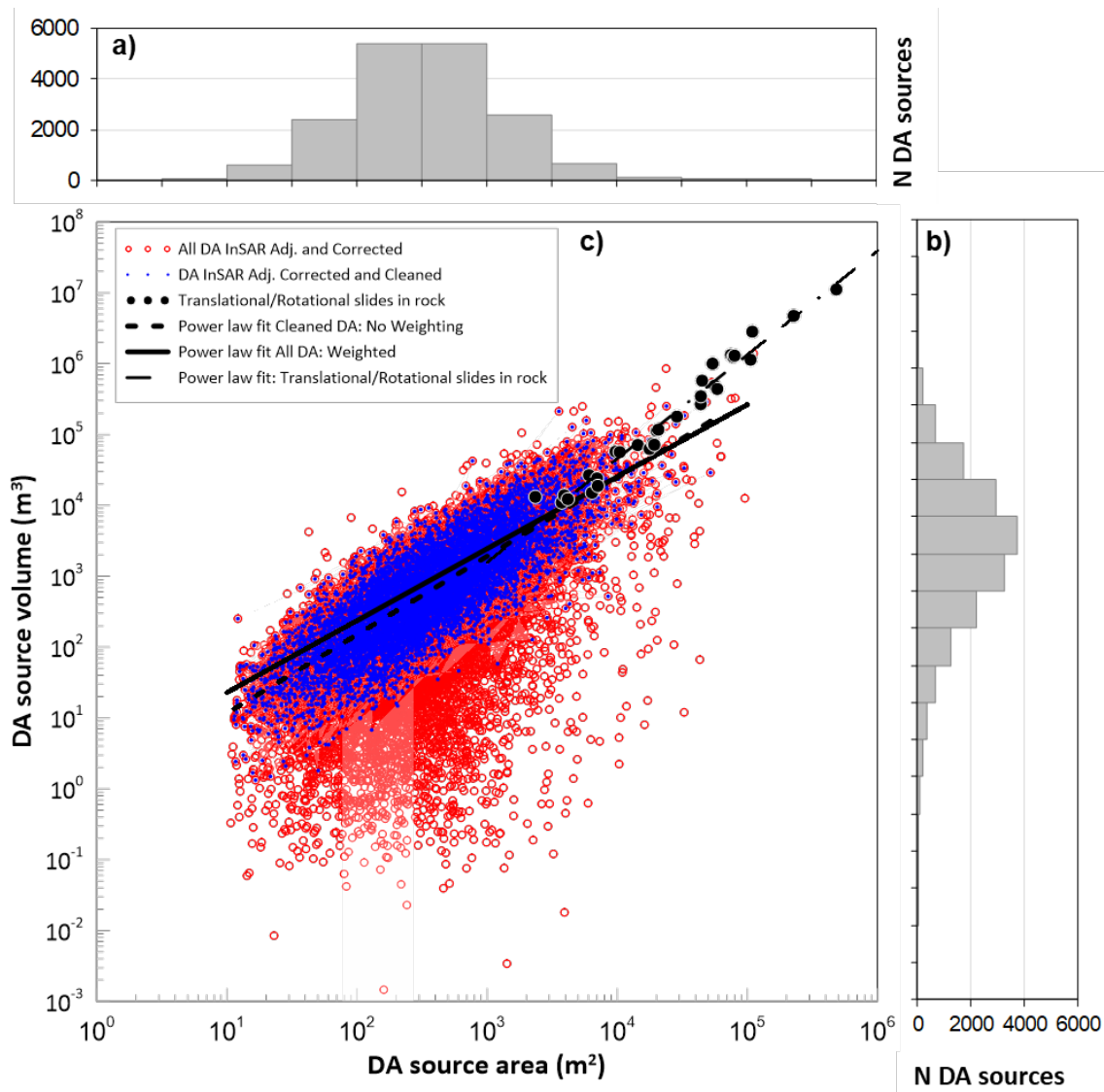


Figure 6.2 Landslide source areas and volumes. (a) Histogram showing the number of landslides in each source area bin. (b) Histogram showing the number of landslides in each source volume bin. (c) Landslide volume versus landslide plan area for all 17,256 debris avalanches in soil and rock, where volumes were calculated from a difference model (red hollow circles) derived by subtracting a post-earthquake digital surface model from a pre-earthquake digital surface model. The blue solid dots represent the 8442 'cleaned' landslides representing those for which the authors had a high confidence on the volume measurements. The lines shown are power laws fitted to the data, with and without weighting. The black dots are 50 translational, rotational or compound slides in Upper Cretaceous to Neogene limestones, siltstones and sandstones, where the volumes were calculated manually as debris remained relatively intact and within the source area (Massey et al. 2020a).

Table 6.1 Compilation of scaling relationships between landslide area and volume from Massey et al. (2020a).

Dataset	γ^*	$\log \alpha^*$	R^2	N	Landslide Type	Source
Global	1.332 ± 0.005	-0.836 ± 0.015	0.95	4231	No distinction	Larsen et al. (2010)
Global Bedrock	1.35 ± 0.01	-0.73 ± 0.06	0.96	604	No distinction	Larsen et al. (2010)
Global Soil	1.145 ± 0.008	-0.44 ± 0.02	0.90	2136	No distinction	Larsen et al. (2010)
New Zealand	1.36 ± 0.01	-0.86 ± 0.05	0.97	389	No distinction	Larsen et al. (2010)
New Zealand Soil	113 ± 0.03	-0.37 ± 0.06	0.86	237	No distinction	Larsen et al. (2010)
New Zealand Bedrock	1.49 ± 0.03	-1.60 ± 0.19	0.93	140	No distinction	Larsen et al. (2010)
Global	1.45 ± 0.009	-1.131	0.97	677	Slides	Guzzetti et al. (2009)
New Zealand, Inangahua Earthquake	1.1 to 1.15	-1.0	N/A	6000	No distinction	Hancox et al. (2014)
New Zealand, Murchison Earthquake	1.1 to 1.23	-1.0	N/A	6000	No distinction	Hancox et al. (2016)
New Zealand, Kaikōura earthquake	1.109 ± 0.008	-0.05 ± 0.02	0.68	8442	Debris avalanches	Massey et al. (2020a)
	1.06 ± 0.017	0.12 ± 0.04	0.69	1842	Debris avalanches in soil	
	1.461 ± 0.059	-1.32 ± 0.26	0.96	50	Translational/rotational/compound slides in weathered rock	
	1.059 ± 0.03	0.07 ± 0.07	0.69	569	Debris avalanches in soil: sand, silts and gravel	
	1.091 ± 0.032	0.1 ± 0.06	0.68	531	Debris avalanches in soil: completely to highly weathered sandstones and siltstone and residual soils	
	1.07 ± 0.026	0.1 ± 0.06	0.7	724	Debris avalanches in soil: completely to highly weathered limestones, sandstones and siltstones and residual soils	
	1.138 ± 0.01	-0.13 ± 0.03	0.67	6618	Debris avalanches in rock: high to moderately weathered sandstones and argillite	

6.3 Landslide Frequency

The factors of how big (volume) and how often a landslide of a given size occurs (frequency) form an integral part of the quantitative risk analysis. Landslide magnitude-frequency relationships are often expressed as the expected annual frequency of landslide events of a given magnitude (e.g. landslides per km² per year or, for rockfall, number of rockfalls per square metre of slope surface area per year).

Landslide frequency is determined from the assessment of recurrence interval (average time between events of the same magnitude) of the landslides (AGS 2007c). This can be determined using similar techniques used to generate a landslide inventory map, as outlined in detail in AGS (2007c), Fell et al. (2008b), Corominas et al. (2014) and Guzzetti et al. (2012).

For advanced-level analysis, for each triggering event, separate magnitude-frequency relationships can be developed or obtained. This can include: EIL magnitude-frequency relationships, rainfall-induced landslide magnitude-frequency relationships and 'background' annual magnitude-frequency relationships.

For some environments (e.g. alpine) where it may not be possible to link any of the past landslides in the study area to rainfall events, there can be just an earthquake-induced and non-earthquake-induced magnitude-frequency relationship. Sub-sets of magnitude-frequency relationships can also be established for different landslide types.

Constructing magnitude-frequency relationships and their associated interpretation is discussed in the following studies: Brardinoni and Church (2004), Brunetti et al. (2009), Dussauge-Peisser et al. (2002), Guthrie et al. (2008), Guzzetti et al. (2002), Hungr et al. (1999), Malamud et al. (2004a) and Moon et al. (2005). Corominas et al. (2014) is a good place to start, as it provides an overview of the process.

It is recommended to follow the Moon et al. (2005) methodology for determining the frequency of landslides for a given volume by constructing a log-log histogram. The histogram shows the number of landslides in a given volume range (often in order of magnitude categories). The histogram can also be shown as a curve or fitted line (Figure 6.4). The average annual volume of landslides is determined by calculating the area under the curve in the histogram, with the calculated volumes needing to be consistent with the overall landslide process or erosion rate (e.g. the predicted number and volume of landslides from magnitude-frequency relationships reflects the geomorphological setting and history of the study area). An example of this calculation route is in Section 6.3.1. It is important here to distinguish between discrete and cumulative frequencies, as the return period is the inverse of the cumulative frequency or the AEP, not the incremental probability (Lee and Jones 2014; Strouth et al. 2022). If hazard curves are used to define the frequency of exceeding a hazard of a given size, the frequency of events within a given band of landslide size is:

$$F(\textit{exceedence of lower band}) - F(\textit{exceedance of upper band})$$

Sources of error and uncertainty surrounding the determination of magnitude-frequency relationships (Corominas et al. 2014; Lee and Jones 2014) include:

- Incomplete datasets. Due to the nature of requiring multiple datasets distributed through time, the data are often incomplete both spatially and temporally.
- Statistical validity of magnitude-frequency relationships, with statistics often used as a black box approach that may not be representative of the types and mechanics of landslides that occur.
- Changes in environmental conditions, so that the past rate and size of landsliding does not reflect possible future landslide events.

- Under-sampling of low-magnitude events due to a detection cut-off threshold or mis-identification of multi-event deposits as single event deposits.
- Extrapolation of data on smaller landslides to predict possible larger landslides and vice versa.

For larger individual landslides, the frequency should be determined by expert judgement taking account of the class of slide, the slope geometry, topographic relief, rock structural controls, performance of similar slopes in the area under rainfall and seismic loads, databases of landsliding resulting from seismic loading elsewhere and signs of instability of the slope. The procedure is often done by seeking expert judgement to ask, 'what is the probability this slope will fail if a 1-in-100 annual return interval (ARI) rainfall occurred?', followed by seeking estimates for 1-in-1000 ARI, etc. and, for seismic loading, 'what is the probability the slope will fail given a 1-in-1000 AEP PGA and lower AEP (larger PGA) events', and combining the result with the ARI/AEP of the loading. These should be summed over the range of ARI/AEP used.

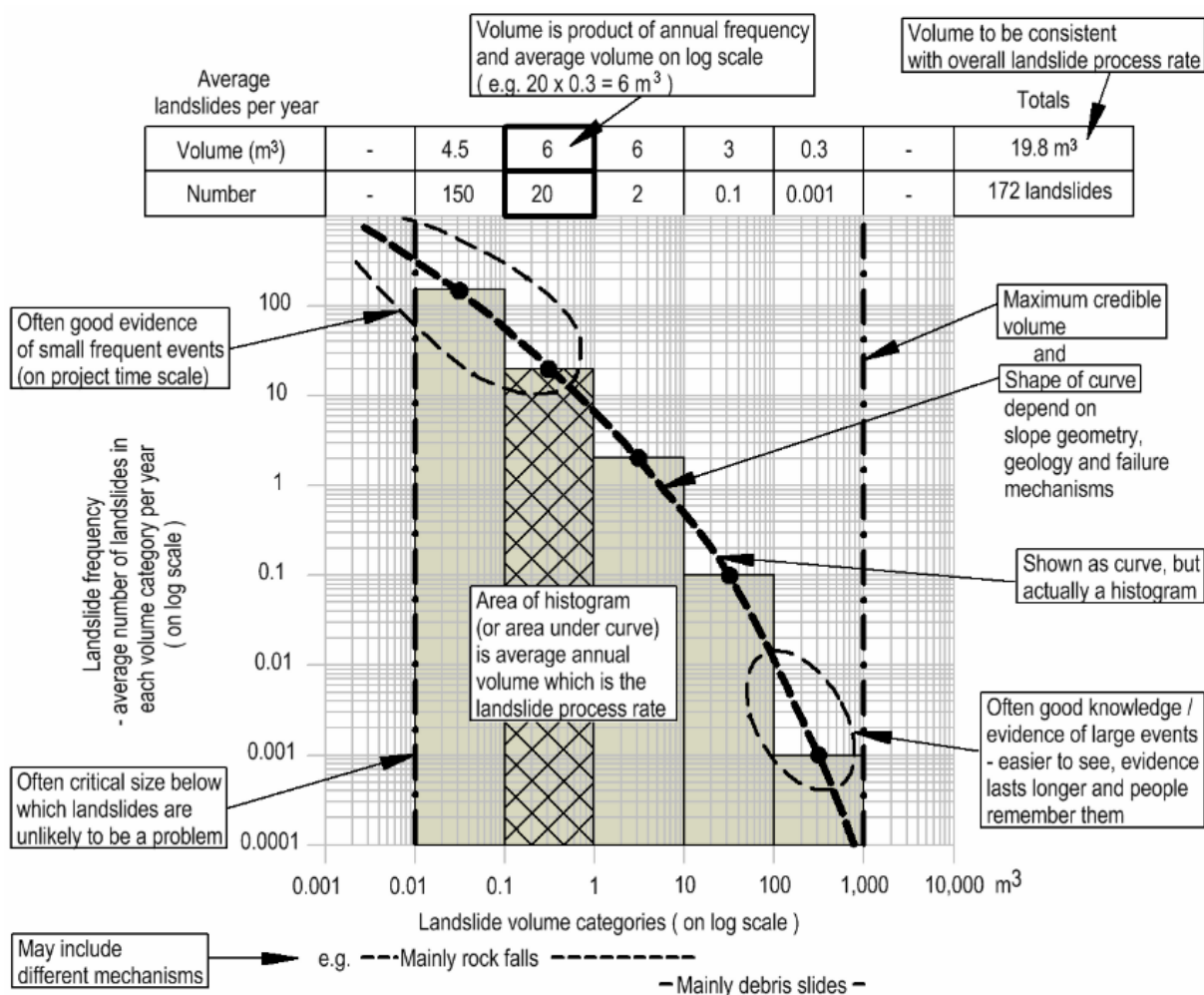


Figure 6.3 Explanation of the graphical presentation of a landslide size frequency model (Moon et al. 2005).

6.3.1 Earthquake-Induced Landsliding: Compiling Magnitude-Frequency Relationships for Different Levels of Earthquake Shaking for Advanced-Level Analysis

For EIL for advanced-level analysis and/or where event inventories are not readily available for a study area, the following framework may be followed. An example of how this framework is worked through and calculated is included here. This framework involves the following steps:

1. **Identify representative earthquake event inventories from elsewhere that may be of relevance to the geomorphic, geological and land-use conditions of the study area.**
2. **Determine area to volume scaling relationships for the event inventories.**
3. **Determine frequency to area landslide relationships for each of the earthquake events** (e.g. Hovius et al. 1997; Malamud et al. 2004a, 2004b; Marc and Hovius 2015; Massey et al. 2018b).

The purpose of this Step 3 is to determine how many landslides of a certain area are generated in a particular earthquake event (band of PGA). Landslide frequency / source area distributions have a typical form, whereby the number of landslides decays as an inverse power of the landslide area, indicating that smaller landslides (source areas) occur more frequently than larger landslides. For medium and large landslides, the landslide frequency / source area distribution tends to be linear in log-log space. For smaller landslides, the distributions tend to 'roll-over' (defined as the point on a log-log graph where the trend of the landslide frequency / source area distribution deviates from a linear one), which is thought to be related to factors such as sample bias, as not all small landslides are routinely mapped or are amalgamated into a larger mapped landslide (Tanyaş et al. 2019). One important implication of this distribution is that the average area of landslides that occur in a landslide event, such as an earthquake, will be the same for every 'complete' inventory (Malamud et al. 2004a). Furthermore, if only medium to large landslides are considered, defined as those with source areas greater than ten times the area at which the rollover occurs ($>5000\text{--}10,000\text{ m}^2$), then the specific functional forms (gradients of the power-law trend lines) do not have to be prescribed and power-law exponents can be used to assess differences between distributions (Marc and Hovius 2015).

Landslide frequency / source area relationships derived from historical EIL inventories can be used to forecast the frequency and area of landslides in future earthquakes by using a power-law exponent for scaling. This scaling behaviour was used to assess how representative the landslide – in particular, debris avalanche – datasets of the 2016 Kaikōura, 1968 Inangahua and 1929 Murchison earthquakes are of EIL more generally. This is done by comparing the frequency / source area distributions for these events with those of three nominally complete landslide inventories from global earthquakes (see Figure 6.5). The results show that, for the Inangahua and Murchison landslide datasets, the frequency / source area power-law scaling exponents are $-2.6 (\pm 0.2)$ and $-2.4 (\pm 0.1)$, respectively (errors at one standard deviation). These are comparable to those from the three complete landslide inventories, which range from -2.2 to -2.7 (Table 6.1). However, the Kaikōura exponent is at the lower end of the range (-1.9 ± 0.1) but fits within the overall spread of the six datasets. Inconsistencies aside, the 2016 Kaikōura, 1968 Inangahua and 1929 Murchison EIL datasets are ostensibly complete for medium to large landslides, and the datasets are suitable for establishing relationships between PGA and landslide frequency for New Zealand earthquakes that are broadly representative of other global EIL inventories. It may be still important to verify that these are fit for purpose for the study area.

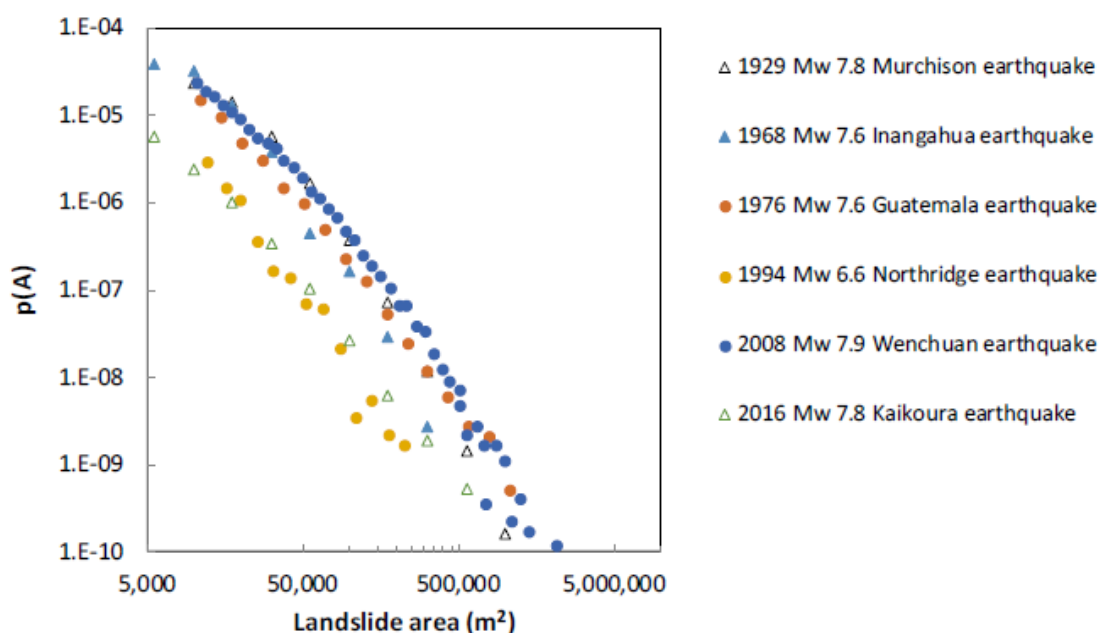


Figure 6.4 Landslide area-probability distributions and power-law scaling for medium to large landslides induced by the 1968 M_w 7.6 Inangahua earthquake, 1929 M_w 7.8 Murchison earthquake and for nominally complete landslide inventories for the 1976 M_w 7.6 Guatemala, M_w 6.6 1994 Northridge and 2008 M_w 7.9 Wenchuan earthquakes. $p(A)$ is the landslide probability density, p (m^{-2}). Calculated from Malamud et al. (2004a, 2004b) where: $p(A) = (1/NLT) * (NLC/Ac)$, where NLT is the total number of landslides, NLC is the number of landslides in a given area class and Ac is the area.

4. **Combine estimates of annual frequency of the representative earthquake events and the number of landslides of a given volume class produced.**

For earthquake events, the annual frequency of occurrence of a given number of landslides of a given volume can be estimated using an empirical relationship between the number and volume of landslides generated per unit area of slope (within a given slope angle range) at different levels of PGA. In this example, these were estimated from the mapped landslides induced by the 2016 Kaikōura, 1968 Inangahua and 1929 Murchison earthquakes for slopes with angles greater than 30° (Figure 6.6). Five PGA bands were used (Band 1: 0.1–0.2 g, Band 2: 0.2–0.35 g, Band 3: 0.35–0.65 g, Band 4: 0.65–1.2 g and Band 5 >1.2 g). To estimate the number of landslides within the different volume class bins for each band, use the following steps:

5. **Calculate the cumulative number of landslides for each area bin.** The area bin widths increase with increasing landslide source area so that bin widths are equal in logarithmic space.
6. **Estimate a representative volume for each area bin using the appropriate source area to volume scaling exponent.** For this example, the mean of the source area to volume scaling exponent of γ (Equation 6.1) from the three landslide inventories of Kaikōura, Inangahua and Murchison were used. This mean value was 1.122.
7. **Divide the number of landslides in each area bin by the total area of the slope (with a slope angle $\geq 30^\circ$) that had experienced the representative PGA values.** In this example, only slopes with angles greater than or equal to 30° were considered to be susceptible to landsliding.
8. **Fit a power-law relationship between the values of Step 2 (landslide volume m^3) and Step 3 (cumulative number of landslides per km^2), where:**

$$\text{Cumulative } N \text{ Landslides } \geq a \text{ given Vol}/km^2/PGA \text{ Band}(x) = a \cdot X^b \quad \text{Equation 6.2}$$

9. **To undertake this in Excel, input the data from Step 2 and 3 converted into log data and then fit a least squares relationship.** To fit the power-law models in this example, a minimum landslide volume bin of 10,000 m³ was used to define the smallest landslide bin for Bands 3 and 4, and a minimum landslide volume bin of 17,800 m³ was used for Band 5, as the data for landslides less than these deviate from the straight-line fit of the power laws and display a 'roll-over', indicating that not all of the smaller landslides had been mapped for the given inventories (Figure 6.5). These power laws were then used to forecast the cumulative numbers of landslides \geq a given volume class/km². The parameter (a) and scaling exponent (b) were varied for each PGA Band (based off NSHM 2012), based on the power law fits to the PGA Band data.
10. **From the power – law relationship defined in Step 4, calculate the number of landslides \geq a given volume class for the study area** by determining the number of landslides for each landslide volume bin (e.g. 1000–10,000 m³). This is done by iteratively subtracting the cumulative number of landslides for each volume and then multiplying the output from the power-law relationship by the study area (km²).
11. **Determine the annual frequency of the number of landslides \geq a given volume class for the study area** by multiplying the values from Step 5 by the annual frequency of the PGA band values occurring (as determined in Section 4.4.2) for each PGA Band.

To account for the variability in the data, the standard error (SE) of the exponent can be added to the mean (to create a mean + SE exponent value) and used to calculate the upper bound of the data (Table 6.2). The mean + SE value statistically represents the 68th percentile of all the values within the dataset, assuming a normal distribution. This upper bound value results in an increase in the number and volume of landslides occurring for a PGA Band.

No landslides were mapped by Hancox et al. (2014, 2016) or Massey et al. (2018b) in the lower PGA Band 1 (<0.2 g). Given the lack of data to generate a meaningful relationship for Band 2 landslides, the number of landslides in each volume bin for PGA Band 2 were interpolated from the power-law forms derived for PGA Bands 3 to 5 (Table 6.2 and Figure 6.6).

Table 6.2 Details of the power-law trends fitted to the cumulative number of landslides \geq a given volume per km² per PGA Band.

PGA Band	Parameter (a) Mean Fit	Scaling Exponent (b) Mean Fit	Scaling Exponent Mean + SE
Band 2 (0.2–0.35 g)	3.91×10^6	-1.88	-1.66
Band 3 (0.35–0.65 g)	5.8×10^6	-1.76	-1.63
Band 4 (0.65–1.2 g)	2.2×10^7	-1.67	-1.59
Band 5 (>1.2 g)	4.4×10^7	-1.62	-1.43

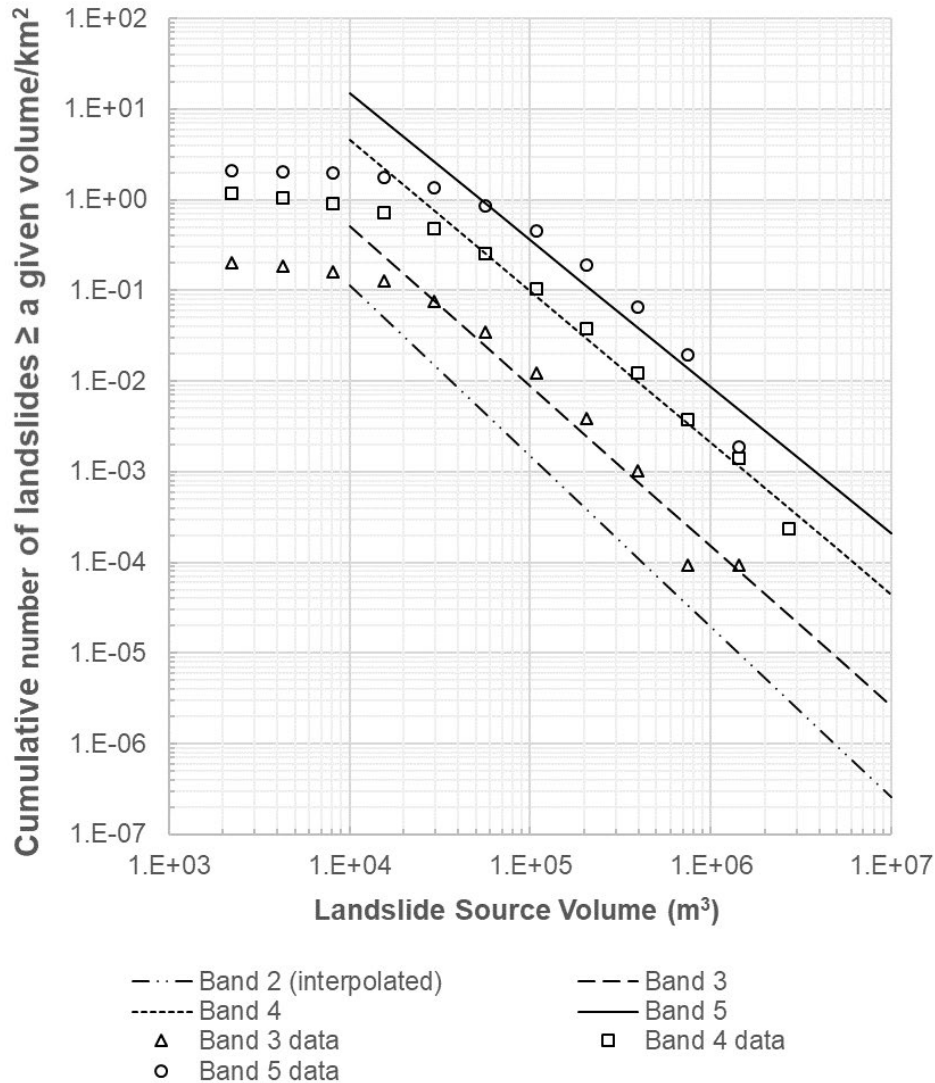


Figure 6.5 The cumulative number of landslides \geq a given volume per km² per PGA Band for slopes $\geq 30^\circ$. The trend lines for Bands 3 to 5 represent power laws fitted to this data (shown as points). Trend lines for Band 2 are interpolated from the power-law forms derived for PGA Bands 3 to 5.

6.4 Landslide Impact Area

6.4.1 Landslide Runout

The landslide runout probability is the probability that a specified landslide will reach a certain distance downslope or affect a specified area (Corominas et al. 2015). The intensity and runout of a landslide will determine its impact on the elements at risk. Elements at risk located in a potential landslide source area need to also be considered as part of the probability of a landslide impacting an element at risk.

Comprehensive reviews of landslide runout analysis include AGS (2007d), Corominas et al. (2014), Dai et al. (2002), Fell et al. (2008a) and McDougall (2017), which include a selection of techniques that are used to analyse landslide runout (Table 6.3).

Table 6.3 Techniques to analyse landslide runout (Corominas et al. 2014; Fell et al. 2008a; McDougall 2017).

Analysis Type		Analysis Level and Scale	Description	Examples
Geomorphological		All levels and scales	Mapped field evidence of landslide runout.	<ol style="list-style-type: none"> 1. Hazard footprints drawn around, for example, boulder, talus and/or colluvial deposits 2. Fan deposits and characteristics
Empirical		Preliminary screening at basic level and at all scales	Simple geometrical correlations between slope height or area and travel distance from back-analysed landslides or other geometrical and topographic variables.	<ol style="list-style-type: none"> 3. Shadow angles (for rockfalls) 4. Angle of reach / Fahrböschung angle (for landslides) 5. Melton ratio 6. Volume change method
Analytical	Numerical continuum models	Advanced level, at local and site-specific scales	Based on continuum mechanics, with many using hydrodynamic modelling methods. Used for debris/rock avalanches, debris flows, mudflows, lahars, etc.	<ol style="list-style-type: none"> 7. Infinite landslide models and sliding consolidation models 8. Multi-sliding block models 9. Depth-integrated models 10. 3D models
	Numerical dis-continuum models	Advanced level, at local and site-specific scales	Elements are modelled as discrete blocks, which can interact with each other.	<ol style="list-style-type: none"> 11. Lumped rockfall models 12. Hybrid / rigid body models 13. Discrete-element-based models

For each analysis type, there are the following sources of error and uncertainty:

- For **geomorphological evidence**, relict and/or ancient landslides may have been reworked and therefore do not represent the true runout extent (AGS 2007c).
- For **empirical methods**, the scatter in the data results in high uncertainty in runout predictions (Finlay et al. 1999). However, this uncertainty can be expressed probabilistically in quantitative statistical terms (McDougall 2017).
- For **numerical methods**, uncertainty surrounds model calibration and derived model input parameters. The simulations are also not perfect replicas of reality and therefore have difficulty simulating flow splitting, obstructions and avulsions. Numerical methods are also sensitive to the resolution and quality of the input topography (McDougall 2017).

6.4.2 Empirical Landslide Runout Datasets

Heim (1932) proposed that the distance a landslide travelled was proportional to its volume. The tangent of the ratio of the fall height (H) to horizontal runout distance (L) between the crest of the source zone and toe of the deposit, known as the 'Fahrböschung' (α), is correlated with landslide volume (Figure 6.7a). Measurement of the slope crest and deposit toe can be measured for many different landslide types and locations. From this, a relationship can be derived with respect to landslide volume (Figure 6.7b).

The scatter in the data also allows for the probability of runout exceedance, or limits of confidence for prediction, to be calculated for each landslide volume (e.g. Hungr et al. 2005; Berti and Simoni 2014). For example, the best-fit line in Figure 6.8 represents an exceedance probability of 50%, where half of the landslides of a specified size and type will travel farther than this line, while the 10% line represents a 10% chance that a similar landslide will travel farther (McDougall 2017).

GNS Science (Brideau et al. 2021a) has recently compiled an empirical landslide dataset from New Zealand and overseas for different landslide types and volumes. The dataset presented in Sections 6.4.2.1–6.4.2.4, and Figures 6.9 through to 6.12, is from Brideau et al. (2021b) and can be accessed through the Design Safe⁴ website.

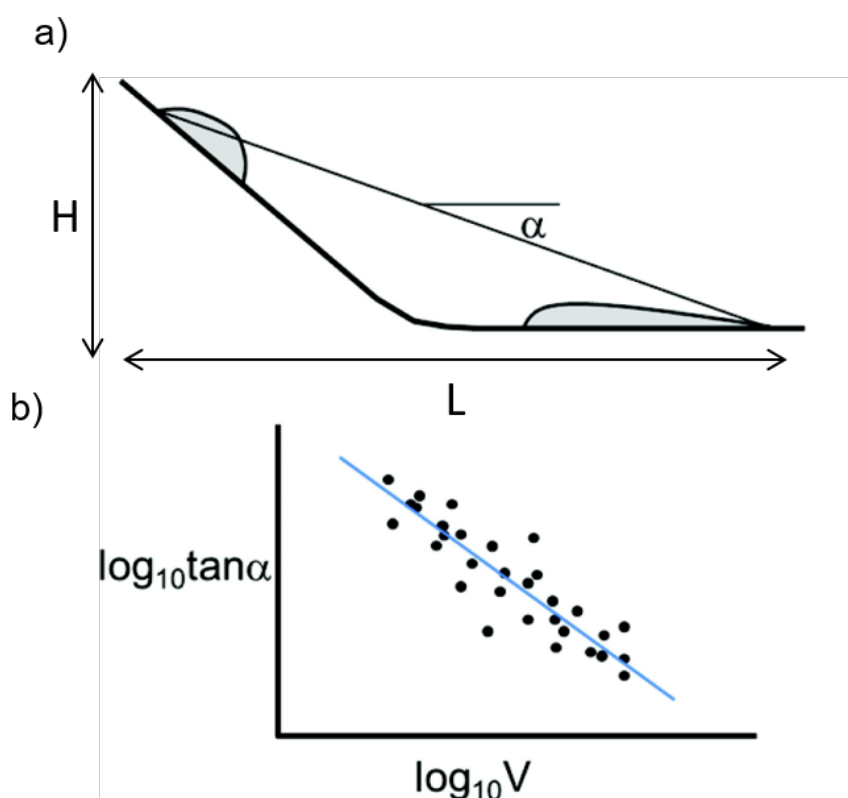


Figure 6.6 Fahrböschung correlated to landslide volume. (a) Calculation of the Fahrböschung, which is the tangent of the fall height (H) and horizontal runout distance (L). (b) Conceptual log-scale scatter plot displaying the H/L ratio (e.g. $\tan \alpha$) versus volume (V) (figure from McDougall [2017]).

4 <https://doi.org/10.17603/ds2-9qbx-n796>

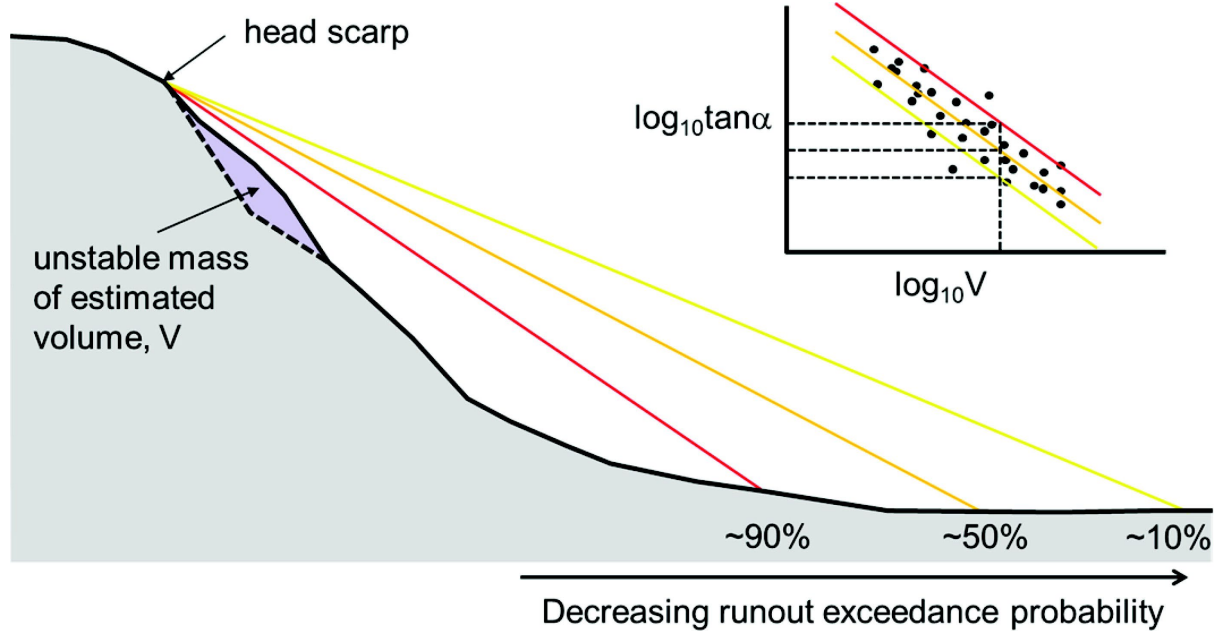


Figure 6.7 Calculation of the probability of runout exceedance based on the scatter in the empirical data (figure from McDougall [2017]).

6.4.2.1 Earthquake-Induced Debris Avalanches and Rock Avalanches

A selection of debris avalanches induced during the 2016 Kaikōura earthquake ($n = 67$) and 2011/12 Canterbury Earthquake Sequence ($n = 47$) were back-analysed to determine their H/L ratios for different volume classes (Brideau et al. 2021b; Figure 6.9). Additionally, two recent Wellington debris avalanches at the Ngaio and Ngauranga gorges in July 2017 were also included in the analysis. These debris avalanches were included with earthquake-induced debris avalanches, as they occurred under dry slope conditions and occurred within the Wellington region. In total, 116 debris avalanches were back-analysed. Figure 6.9 presents a compilation of previously published international rock avalanche (not all earthquake-induced) case studies and mostly unpublished New Zealand examples.

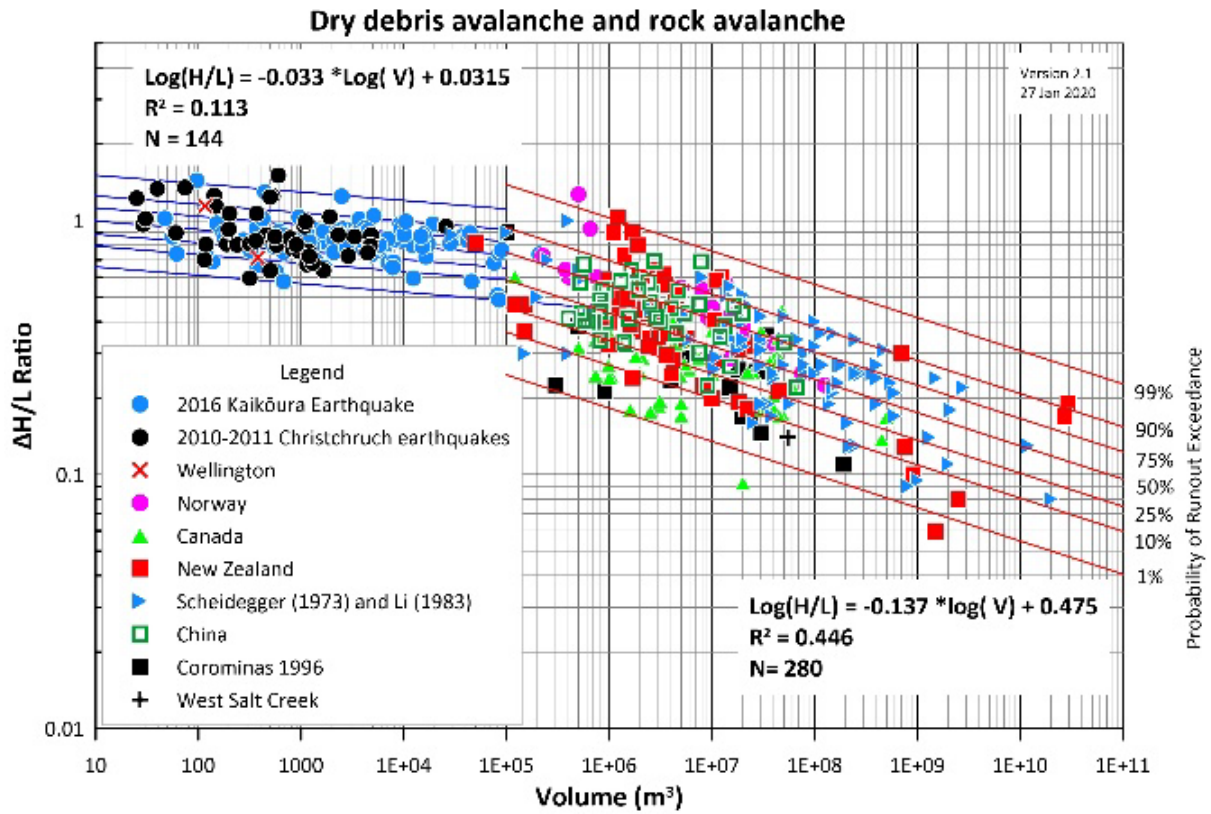


Figure 6.8 Empirical relationship between $\Delta H/L$ ratio and volume of dry (i.e. earthquake-induced) debris avalanches (<100,000 m³) and rock avalanches (>100,000 m³). The data are available from Brideau et al. (2021b).

6.4.2.2 Rainfall-Induced Debris Avalanches

A selection of debris avalanches induced during rainfall events in Hong Kong (Hunter and Fell 2003; Wong et al. 1998, 2006) and British Columbia, Canada (Brideau et al. 2019) were back-analysed to determine the H/L ratios of ‘wet’ debris avalanches for different volume classes (Figure 6.10). In total, 146 debris avalanches were back-analysed.

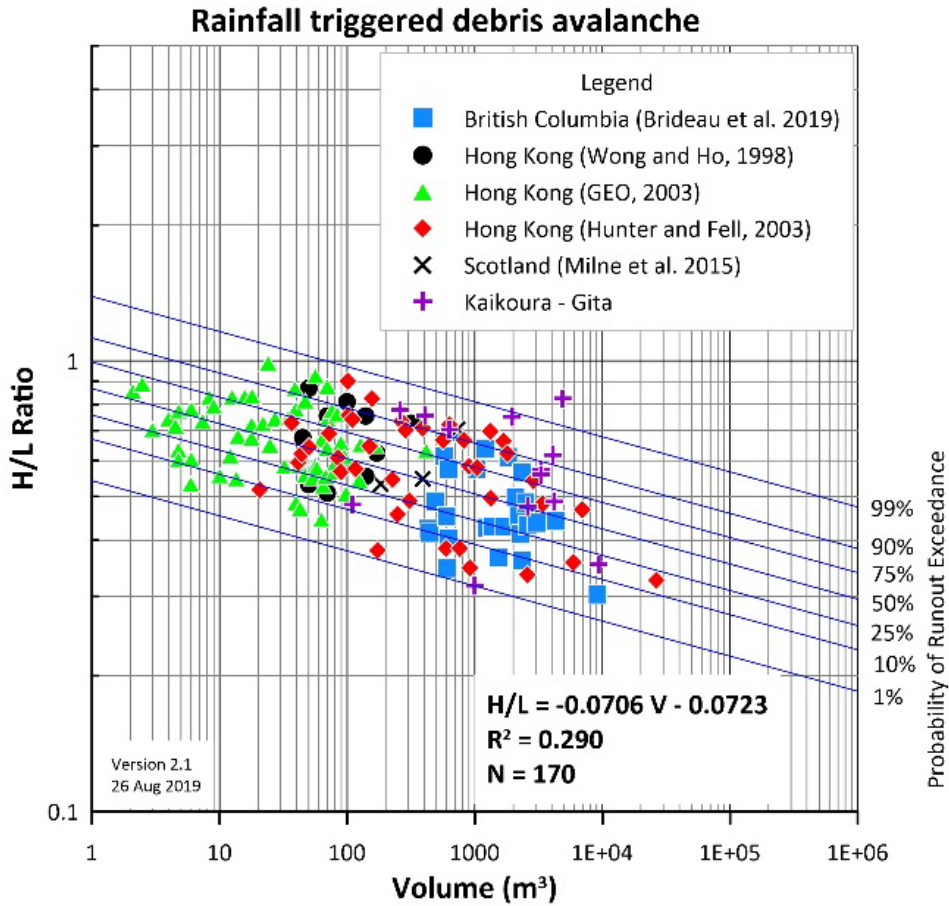


Figure 6.9 H/L ratio versus volume for rainfall-induced debris avalanches from international case studies. The data are available from Brideau et al. (2021b).

6.4.2.3 Rainfall-Induced Debris Flows

A selection of debris flows from both New Zealand and overseas were back-analysed to determine their H/L ratios (Figure 6.11). These included 408 debris flows from Tauranga (Bell et al. 2003), four debris flows from the Coromandel (Harvey 2011), nine debris flows from the Port Hills, 13 from various locations in New Zealand (Kailey 2013) and 23 from Hong Kong (GEO 2003).

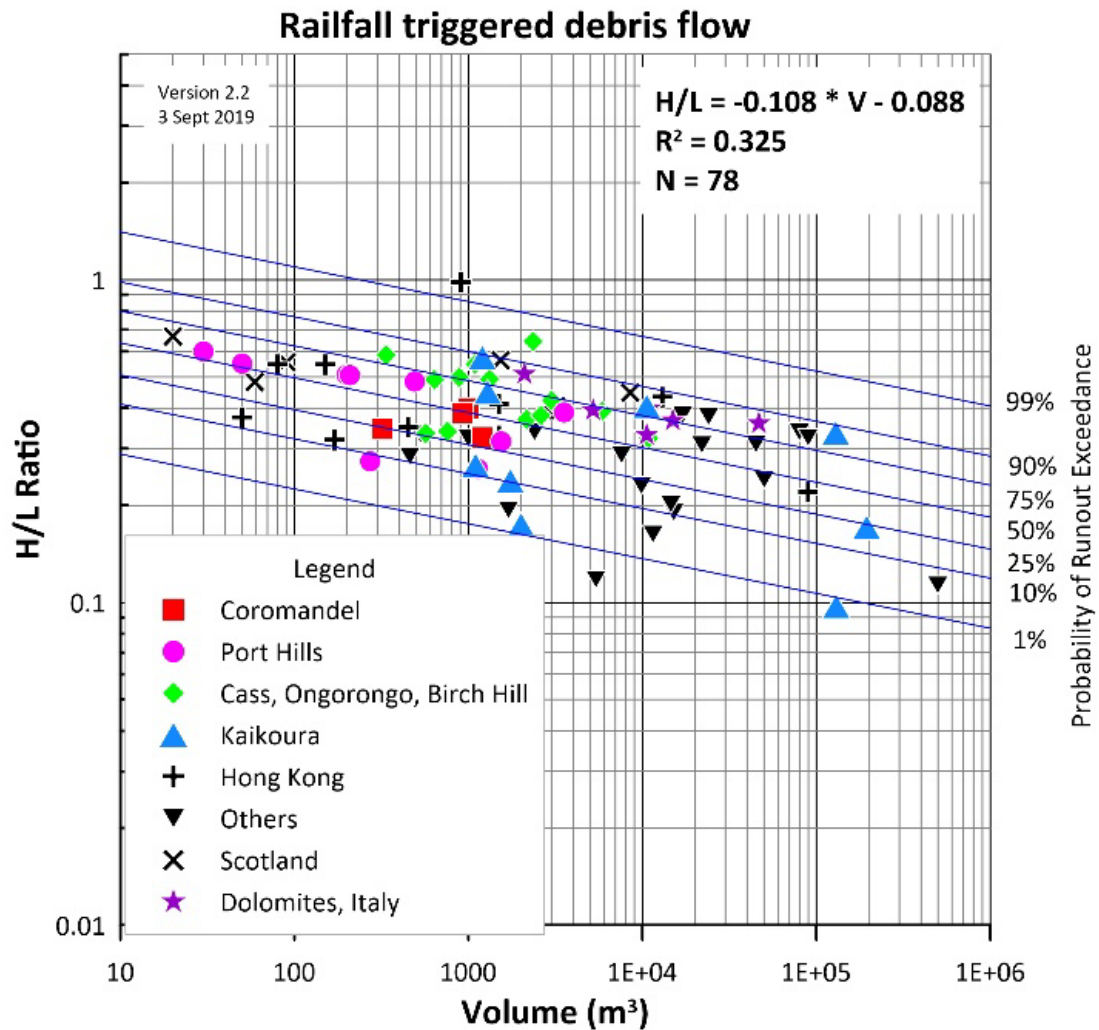


Figure 6.10 H/L ratio versus volume for rainfall-induced debris flows in New Zealand and Hong Kong. The data are available from Brideau et al. (2021b).

6.4.2.4 Fill Slope Failures

A selection of fill slope failures that occurred as debris flows were back-analysed to determine their H/L ratios (Figure 6.12). These included 72 examples from Hong Kong (Finlay et al. 1999; Hunter and Fell 2002, 2003) and two examples of recent fill slope failures in Wellington at Halifax Crescent in 2017 and Priscilla Crescent in 2013.

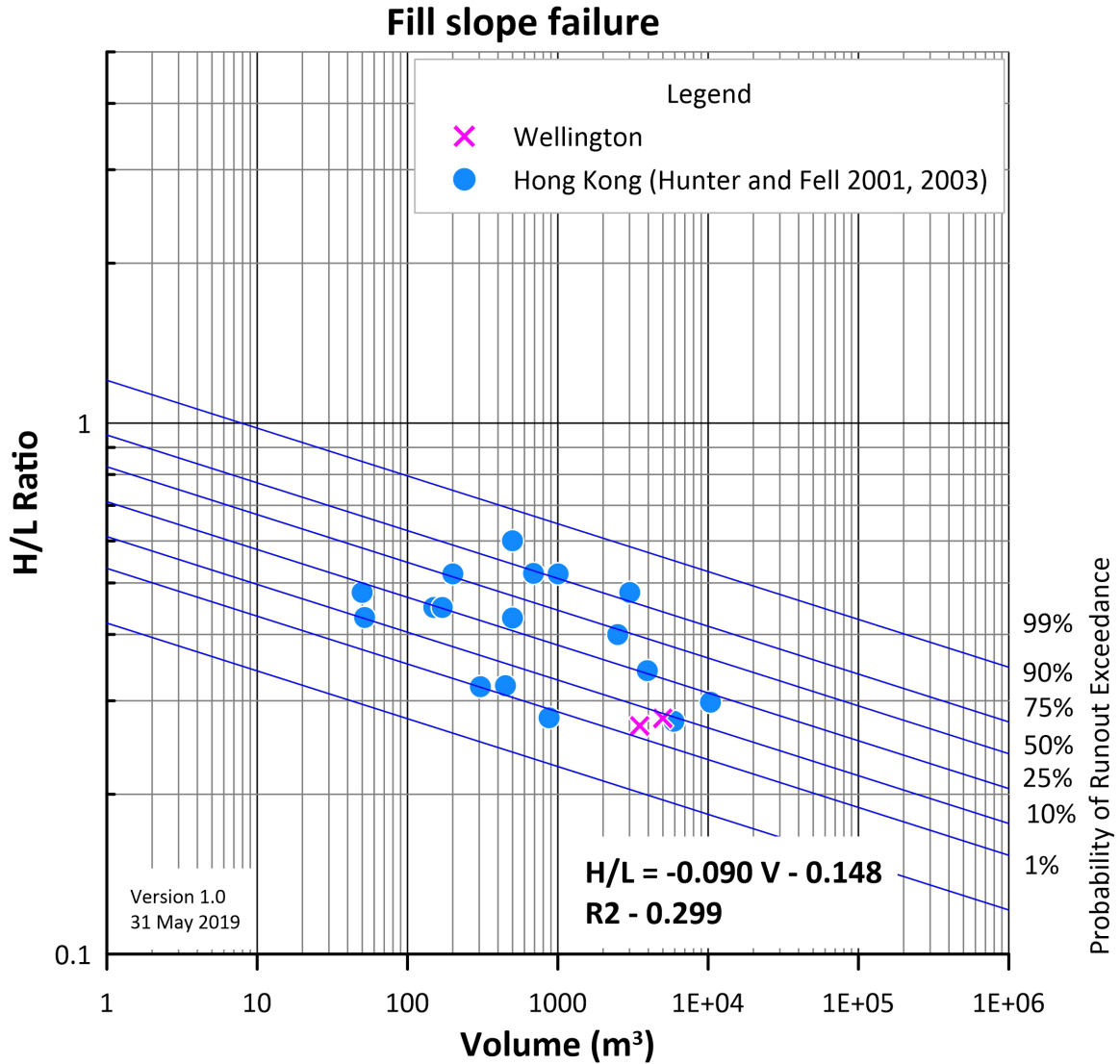


Figure 6.11 H/L ratio versus volume for fill slope failures in Wellington and Hong Kong. The data are available from Brideau et al. (2021b).

6.4.3 Debris Flow Runout Estimation

Debris flows are defined by Hungr et al. (2014) as a:

“very rapid to extremely rapid surging flow of saturated debris in a steep channel. Strong entrainment of material and water from the flow path can occur along the runout path. Debris flows often occur simultaneously with floods. The debris flow may be initiated by a debris slide, debris avalanche or rockfall from a steep bank, or by spontaneous instability of the steep stream bed.”

Following Hungr et al. (2014), a ‘debris flow’ refers exclusively to a channelised landslide, whereas a landslide consisting of flowing debris on an open slope is referred to as a ‘debris avalanche’. It is possible that debris flows become debris avalanches if the channel they flow down becomes less confined, and, conversely, a debris avalanche may become debris flows if the debris enters a channel.

The sediment concentration of debris flows exceeds 40% (typically 50–70%), and their volume can be up to 1,000,000,000 m³ (Iverson et al. 2011). Figure 6.13 shows the source and travel paths of mobile debris flows that resulted in destruction of residential dwellings.

Once saturated debris material begins to move in a steep channel, the volume of a debris flow can change due to entrainment (Iverson et al. 2011). Entrainment results from scour of channel bed sediment or collapse of stream banks. The majority of the total material involved in a debris flow can originate from entrainment.

To estimate the potential travel path and hazard footprint of a debris flow, the ‘Fahrböschung’ angle (e.g. Section 6.4.2.3) should be used in conjunction with geomorphic evidence (e.g. debris or alluvial fans) to determine the extent of debris flow hazard footprint.



Figure 6.12 Debris flows induced by rain in Eastbourne, Wellington, in November 2006. The source areas of the debris flows are in the left of the photograph. The debris travelled down-slope several hundreds of metres, where it impacted the dwellings shown in the right of the photograph, resulting in removal/replacement of the dwellings. Photograph by G Hancox, GNS Science.

6.4.3.1 Fan

Fans are cone-shaped landforms that are generated when confined watercourses (e.g. gullies, creeks, rivers) become wider and the water course becomes less confined, for example, when watercourses enter valleys, plains or lakes. The resulting decrease in flow velocity promotes sediment deposition. Mapping the extent of fans is important because they are dynamic landforms that result from cyclic avulsion of channels radiating from the fan apex, therefore the fan extent demarks an area likely to be affected by debris inundation in the future (Figure 6.14). The dynamic nature of such landforms poses a hazard to people and infrastructure located on them, as areas that were considered inactive (and have since been built on) can re-activate and start actively eroding or receiving sediments. Davies and McSaveney (2008) discussed some of the considerations for sustainable development on fans, suggesting that fans can be divided into two end-member types: (1) alluvial fan – dominated by deposition of sediment from fluvial processes; and (2) debris-flow fan – dominated by deposition of sediment from debris flows and debris floods (Figure 6.15). As debris-flow fans are typically associated with comparatively small and steep catchments, morphometric (i.e. measurements of the landscape shape) parameters, such as the Melton Ratio, can be used to estimate the dominant fan-building process (fluvial versus debris flow).

Fans can be delineated where topographic contours show a reversal of curvature – defined by a concave break in slope – where the watercourse (channel) changes from being confined to less confined (Figure 6.16). Floods, debris floods and debris flows could travel farther than mapped fan extents, as the fans may have been modified by anthropogenic (e.g. road) and natural (river erosion) processes or due to an extreme landslide event.

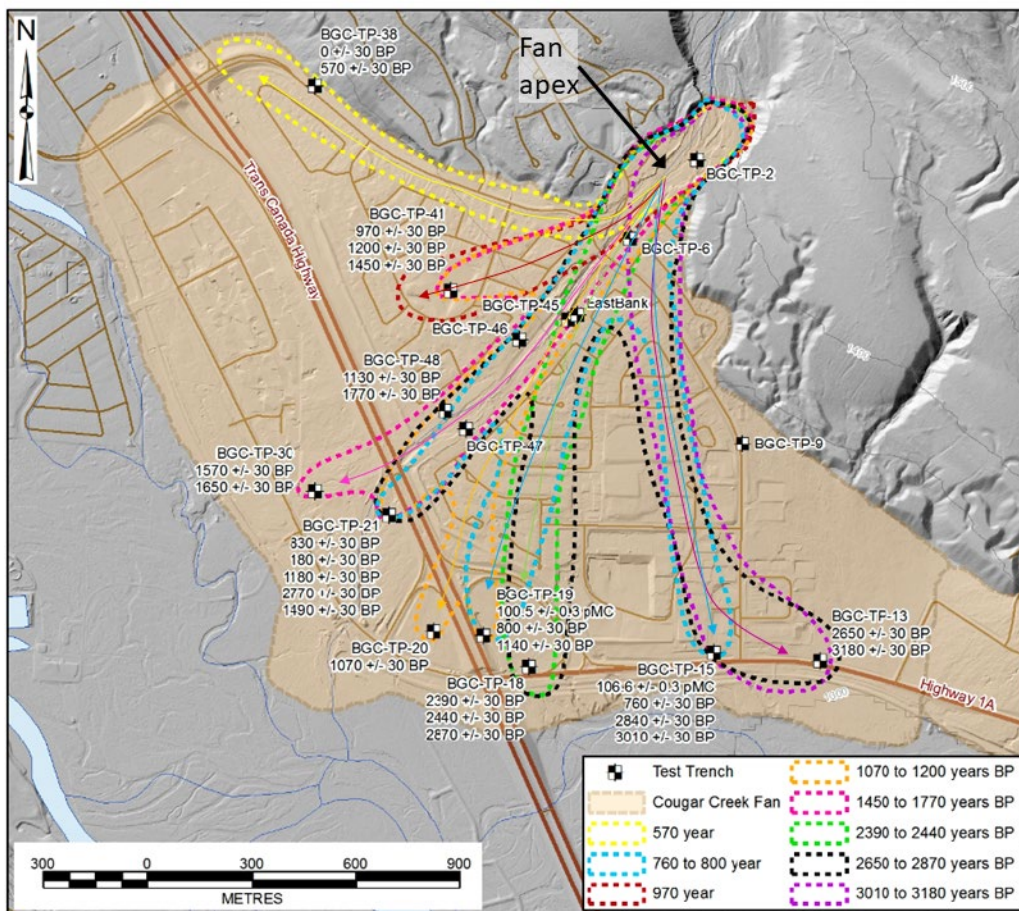


Figure 6.13 Example from Cougar Creek, Alberta, Canada, of the different sections of a fan receiving sediment during the last ~3200 years (modified from Jakob et al. [2017]).



Figure 6.14 Oblique aerial view of debris-flow fans in the Makarora valley. Photograph by L Homer, 1996, GNS Science.

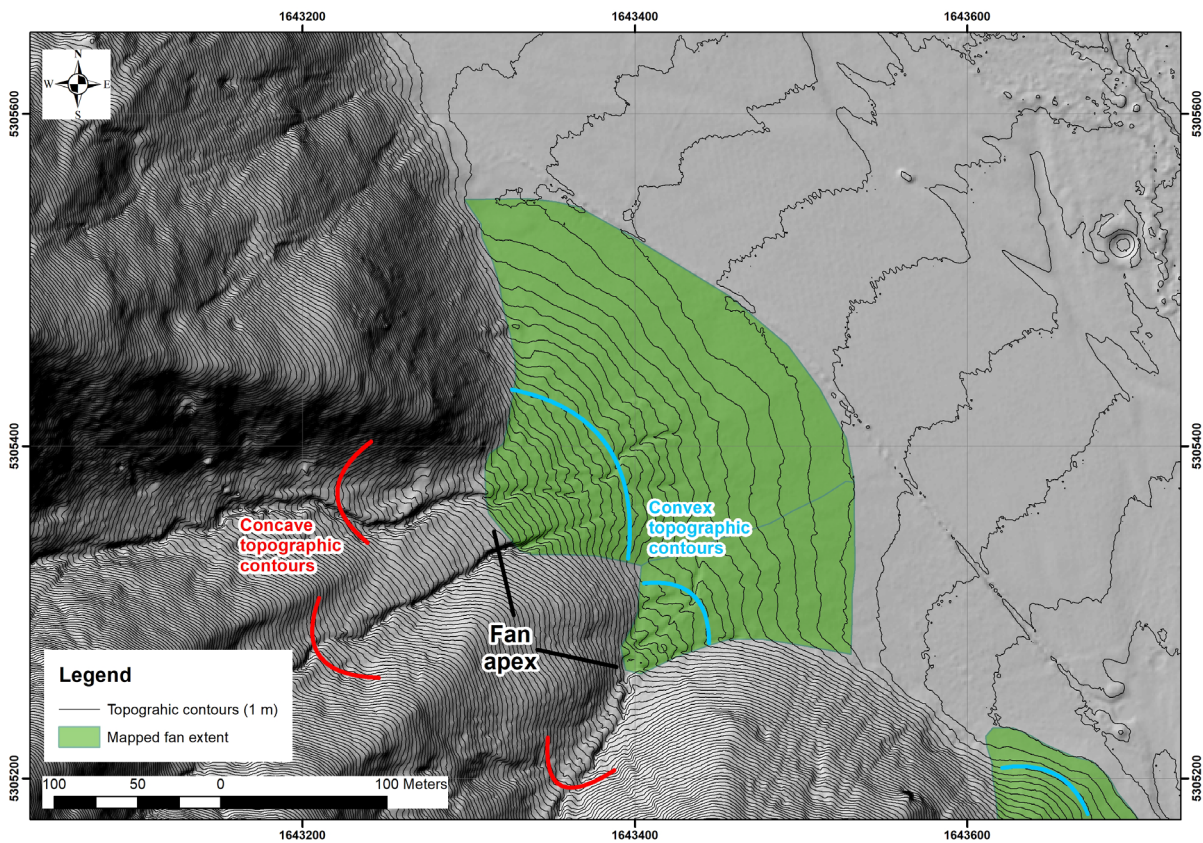


Figure 6.15 Example of fan delineation based on topographic contours.

6.4.3.2 Debris Floods

A debris flood is defined by Hungr et al. (2014) as a landslide consisting of:

“very rapid flow of water, heavily charged with debris, in a steep channel, whose peak discharge is comparable to that of a water flood.”

Pierson (2005) referred to debris floods as hyper-concentrated flows that are transitional between debris flows and water floods. Catchments more limited to sustaining debris floods all the way to a fan are distinguished from those more capable of sustaining debris flows to the fan by using the Melton Ratio and catchment-length thresholds described below.

6.4.3.3 Melton Ratio

The Melton Ratio was first defined by Melton (1965) as the topographic relief of the catchment ($\Delta H_{\text{catchment}}$, which is highest elevation minus lowest elevation in the catchment) divided by the square root of its area ($A_{\text{catchment}}$).

$$\text{Melton Ratio} = \frac{\Delta H_{\text{catchment}}}{\sqrt{A_{\text{catchment}}}}$$

The Melton Ratio has been used to identify debris-flow-dominated fans in New Zealand; for example, in the Southern Alps (de Scally and Owen 2004; Kritikos and Davies 2015) and the Coromandel and the Kaimai ranges (Welsh 2007), along with the Bay of Plenty and Westland (Welsh and Davies 2011) regions. Wilford et al. (2004) conducted a study in west central British Columbia, Canada, that investigated what morphometric parameters are the most useful to estimate which hazard (flood, debris flood, debris flow) is the dominant one contributing sediment to fan at the end of its catchment. They found that the ‘Melton Ratio’ and catchment length were the best indicators of the dominant process/hazard. It should be emphasised that using the Melton Ratio and catchment length for estimating the dominant hazard is an empirical approach and that hazards other than the dominant one are also possible on a fan, based on site-specific and meteorological event-specific conditions. For example, Welsh and Davies (2011) noted that, in two cases from their study, fans with documented debris-flow activity (Awatarariki and Waiteperu) were not identified as such based on the criteria outlined in Table 6.4.

Table 6.4 Summary of the Melton Ratio and catchment length used to estimate the dominant hazard type at each fan (Brideau et al. 2021b).

Dominant Hazard Type	Melton Ratio	Catchment Length (km)
Flood	<0.3	-
Debris flood	0.3–0.5	>2.7
Debris flow	>0.5	<2.7

6.4.3.4 Stream Order

A commonly used classification to characterise the hydrology and ecology of a stream is the stream order. Stream order can be used to quantify the stream size and complexity. Larger stream orders typically indicate larger catchments with a lower overall channel gradient, which leads to fluvial processes dominating the resulting fan.

Based on the classification system outlined in the River Environment Classification (REC) by the Ministry for the Environment (Snelder et al. 2010), a stream order represents the numerical position of a tributary within a catchment. When two tributaries of the same stream order join, the segment downstream of their confluence is given a higher stream order (Figure 6.17).

Numerous researchers (e.g. Bigelow et al. 2007) noted that debris flows typically initiate in first- and second-order streams.

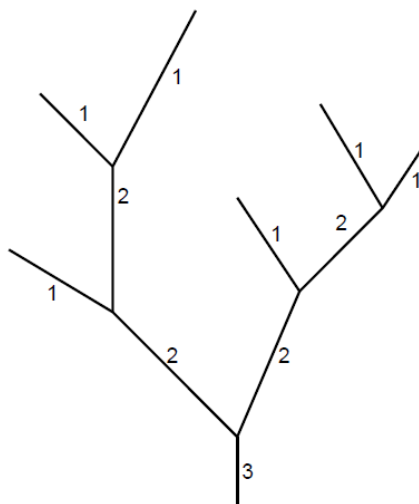


Figure 6.16 Schematic representation of how the order of a stream is defined in the River Environment Classification (REC) by the Ministry for the Environment (Snelder et al. 2010). This is the stream order definition used in this project.

6.4.4 Example Calculation Route of $P_{(T:L)}$

After estimating the extent and characteristics of landslide runout and slippage, the probability of debris reaching an element at risk at a given location needs to be calculated (i.e. the spatial probability of impact). This section provides an example of the calculation of probability that an element at risk is in the path of the debris at a given location ($P_{(T:L)}$). This example is from rockfall and landslide events for people walking along the beach below Cape Kidnapper Cliffs for the following volume categories: 1 m³, 10 m³, 100 m³, 1000 m³, 10,000 m³, 25,000 m³ and 50,000 m³. An empirical relationship between landslide volume and the 'Fahrböschung' angle for debris avalanches (>10 m³) was used and 3D rockfall trajectory modelling using RAMMS software (2016) for rockfalls (1 m³). Using the outputs from this empirical relationship and the rockfall modelling, $P_{(T:L)}$ was calculated as follows:

1. A square for a source area was assumed (based on the volume to area scaling relationship data, from which a source width can be determined [S_w]). See Figure 6.18 and Table 6.5 for more details.
2. To account for the effect of debris spreading as it travels from the source area, the width of debris at the cliff toe ($W_{\text{cliff bottom}}$) and at the runout extent was calculated as estimated from the empirical data ($D_{F\text{-angle}}$). A factor was applied to calculate how the debris spreads is based on observations from fieldwork (see equation in Table 6.5).
3. To translate this into $P_{(S:H)}$, the following equation was used:

$$\text{Cumulative } N \text{ Landslides } \geq a \text{ given Vol/km}^2/\text{PGA Band}(x) = a \cdot X^b \quad \text{Equation 6.3}$$

Where d is the diameter of a person (assumed to be 1 m), D is the width of the debris (either at the cliff toe or at the runout extent) and L is total length of either the cliff toe or runout extent. In Table 6.4, the length of the cliff toe and runout extent changes for

different volume classes. This change in length reflects that, along the cliffs, there are only certain locations where the cliff is high enough or big enough to generate large landslides. Therefore, the length of the cliff toe and runout extent by the extent is filtered of the source areas that could generate such a volume.

4. The $L_{F\text{-angle}}$ line is a conservative approach, whereby it is assumed that all landslide sources occur and fail from the top of the cliff and therefore travel the farthest. However, in reality, landslides occur from the whole area of the cliff. To account for this in the calculation of $P_{(T:L)}$, the $P_{(T:L)}$ value at $L_{F\text{-angle}}$ is multiplied by a scaling factor of 0.5.

Section 8.1.1 will detail how the two different $P_{(S:H)}$ values are used to calculate local personal risk.

Table 6.5 Example calculation route and input data required to calculate the $P_{(S:H)}$ at the cliff bottom and F-angle extent.

Volume Class (m ³)	Sw Source (m)	W Cliff Bottom: (m)	L Cliff Bottom: (m)	W F-angle: (m)	W F-angle (m)	$P_{(T:L)}$: Cliff Bottom	$P_{(T:L)}$: F-angle
Equation	Input Data	= (Sw / 2) + Sw	Input Data	= (Sw / 1.5) + Sw	Input Data	= (d + $D_{\text{cliff bottom}}$) / $L_{\text{cliff bottom}}$	= [(d + $D_{F\text{-angle}}$) / $L_{F\text{-angle}}$] x 0.5
1	2	3	2179	4	2340	2.0E-03	2.1E-03
10	5	8	2202	9	2266	3.9E-03	4.4E-03
100	12	17	2198	21	2282	8.3E-03	9.6E-03
1,000	27	40	2200	48	2268	1.9E-02	2.2E-02
10,000	61	92	2211	110	2274	4.2E-02	4.9E-02
25,000	85	128	1680	153	1793	7.7E-02	8.6E-02
50,000	109	164	1439	197	1585	1.1E-01	1.2E-02
100,000	141	211	1439	253	1586	1.5E-01	1.6E-01

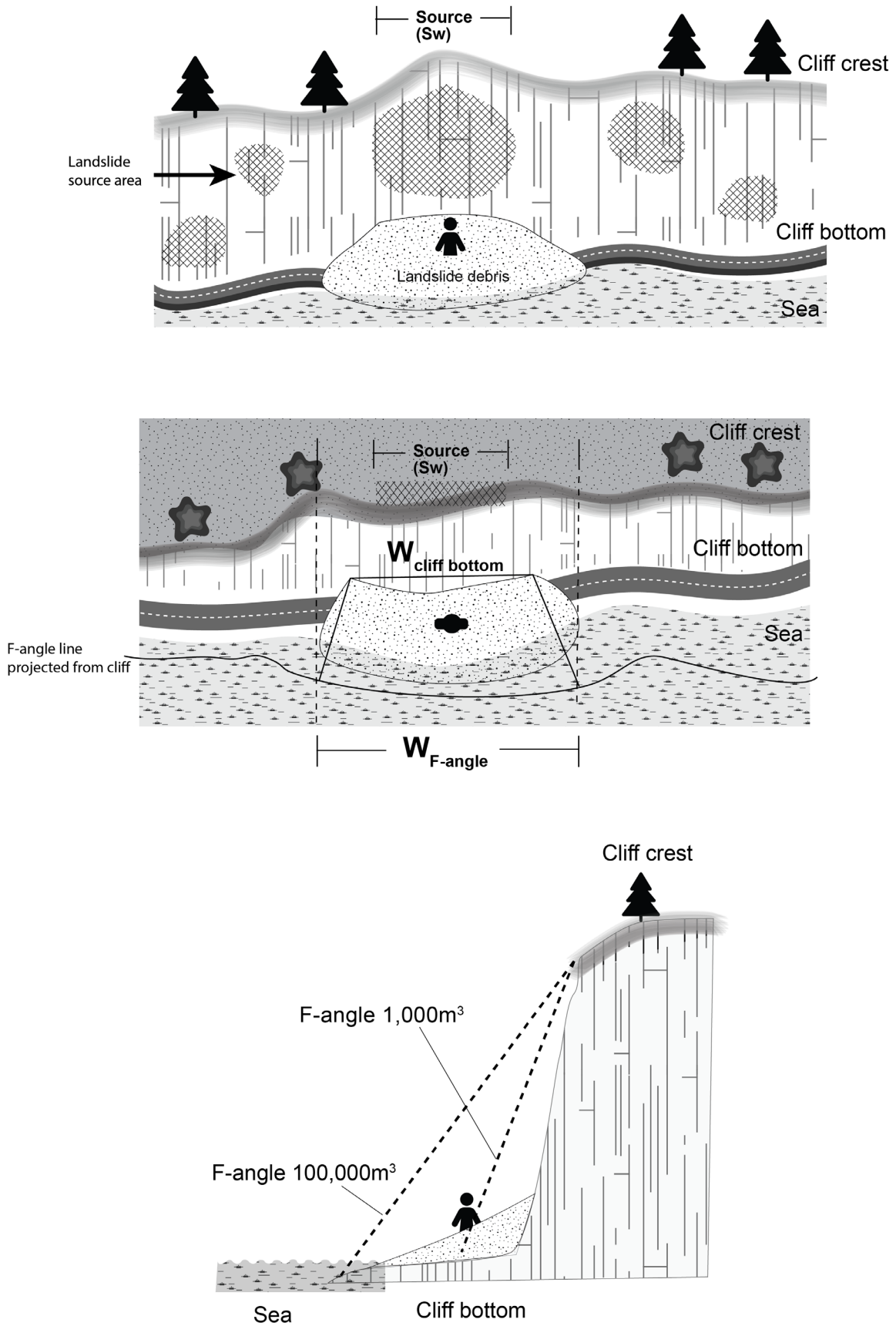


Figure 6.17 Schematic of the input data and variables required to calculate $P_{(T:L)}$.

6.4.5 Slippage

Slippage, as defined in the guideline, includes the movement or loss (including partial loss) of land from a slope when it occurs beneath it, e.g. a structure, path, road, car park, etc.

Slippage is often associated with slides (as shown schematically in Figure 6.19), which are defined as movement of an intact mass by sliding along a basal rupture surface. These types of hazard are generally slower moving (1.6 m/year to 16 mm/year) and have deeper rupture (slip) surfaces than the type of shallow slides that lead to flow-type landslides. The displaced material tends to move along the surface of rupture as a series of discrete intact blocks (these types of landslide are often referred to as translational block-slides). Retrogressive failure (eroding backwards) of the landslide main scarp or movement of the intact mass can result in slippage.

Slippage may often be associated with pre-existing slides. Such slides may display changes in activity and the rate of movement due to fluctuations in pore pressure associated with long periods of wet weather, strong earthquakes, loading at the crest of the slope and unloading at the toe of the slope (via fluvial erosion, excavation, etc.). Changes in the rate of movement results in displacement. More references on controls on the rates of movement for New Zealand slides can be found in Massey et al. (2013).

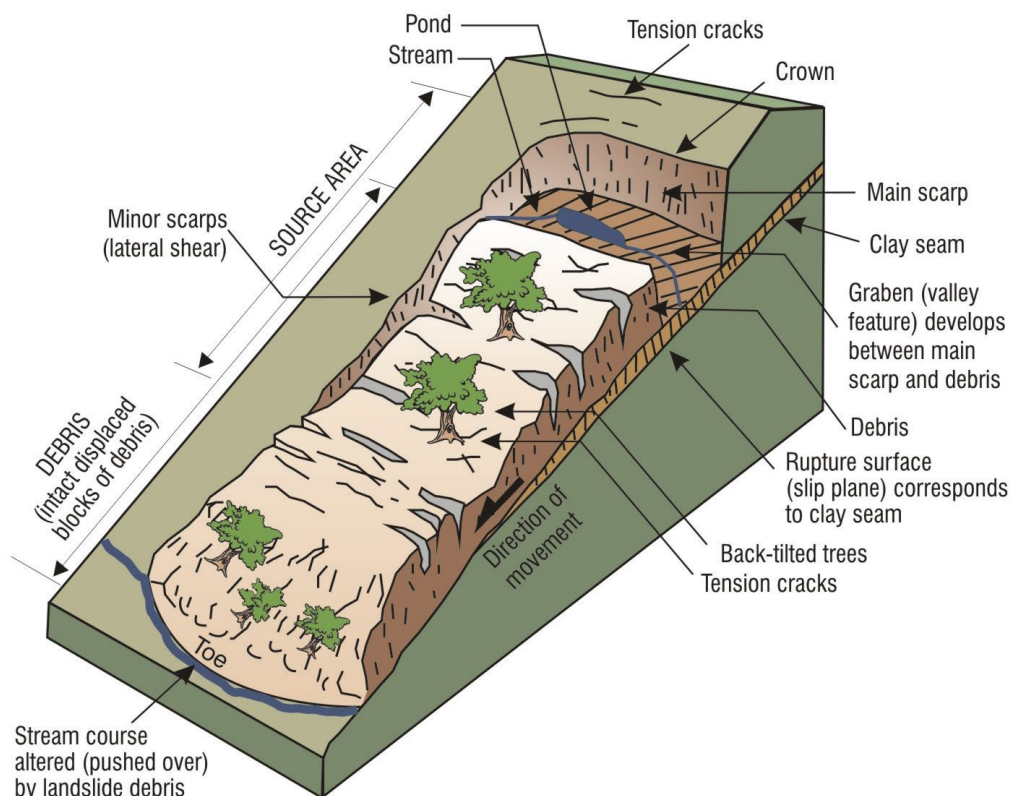


Figure 6.18 Schematic of a slide.

7.0 CONSEQUENCE ANALYSIS

7.1 Elements at Risk

As part of the scope of the study, there should be discussions between DOC staff and the consultant conducting the landslide quantitative risk analysis about the information available for visitor numbers, workers, asset locations, etc. for each section of track or different tracks within the study area. This might identify areas where DOC may have to collect more information during the risk analysis or areas where the confidence in estimated risk for the track is lower (due to this lack of knowledge of the elements at risk).

7.2 Exposure

No additional comment.

7.3 Vulnerability

The vulnerability (V) is the probability of a person being killed, if present and in the path of a landslide, considering both: (a) the likelihood of being killed if struck and (b) the possibility of being able to take evasive action and avoid being struck. It can also apply to a person in a building or in a vehicle travelling on a road who may be killed if the vehicle is hit by debris or rockfall (debris inundation) or falls into a void (caused by, for example, slippage).

Physical vulnerability depends on the landslide intensity and characteristics of the elements at risk (e.g. Du et al. 2013). This probability is expressed as vulnerability, the term used to describe the amount of damage that results from a particular degree of hazard. Vulnerability ranges between 0 and 1 and, for fatality risk, combines the likelihood of an injury sustained by the individual (if struck) being fatal (1) and the possibility of getting out of the way to avoid being struck.

The assessment of vulnerability is subjective, with little published information, and is therefore often based on expert opinion. Some of the available data, and assumed values of vulnerability for the following elements at risk, include data for:

1. People
2. Property
3. People in property
4. People in vehicles.

Information on vulnerability to property is also included. As stated in the AGS (2007b) guidelines, the data should be applied with common sense, taking into account the circumstance of the landslides being studied. Judgement may indicate that values other than the recommended values are appropriate for a particular case. This must be well-documented and well-justified.

The AGS guidelines also include some general points of note:

- For persons below the landslide, the velocity of the landslide has a major effect on the vulnerability. Persons who are near the toe of a landslide that will travel a long distance are likely to experience a high-velocity impact and will have a high vulnerability, and persons who are near the limit of the travel (or runout) of the landslide will experience low-velocity impact by only part of the landslide mass and will have a lower vulnerability.
- Persons who are in buildings that collapse totally have high vulnerability.

- Persons who are in buildings are less vulnerable than those in the open, unless the building collapses.
- Persons in vehicles are less vulnerable than those in the open. Their vulnerability depends on the volume and velocity of the landslide. Experience in Hong Kong (Finlay et al. 1999) indicates that rapid landslides with volumes of only a few hundred cubic metres are likely to result in death of the occupants of the vehicle.

7.3.1 Vulnerability for Persons (Physical Vulnerability)

There are limited data concerning the vulnerability of people in open areas to landslide impacts, with the vulnerability values used often estimated by expert opinion. Finlay et al. (1999) presents data from 27 fatal landslides in Hong Kong (Table 7.1), while expert opinion and literature reviews have been used to determine the vulnerability values of Corominas et al. (2005) (Table 7.2).

Table 7.1 Summary of Hong Kong vulnerability ranges for persons and recommended values for loss of life for landsliding in similar situations (Finlay et al. 1999).

Location	Description	Population Vulnerability (Individuals)		
		Data Range	Recommended	Comments
Open Space	Struck by rockfall	0.1–0.7	0.5	May be injured but unlikely to cause death
	Buried by debris	0.8–0.1	1	Death by asphyxia
	Not buried but hit by debris	0.1–0.5	0.1	High chance of survival
Vehicle	Vehicle is buried/crushed	0.9–1	1	Death almost certain
	Vehicle is damaged only	0.0–0.3	0.3	High chance of survival
Building	Building collapse	0.9–1	1	Death almost certain
	Building inundated with debris	0.8–1	1	Death is highly likely
	Building inundated with debris, but person is not buried	0.0–0.5	0.2	High chances of survival
	Debris strikes building only	0.0–0.1	0.05	Virtually no danger

Table 7.2 Vulnerability values for different elements at risk and size of impact block as determined by expert judgement (Corominas et al. 2005).

Element	Vulnerability
Buildings	
Impact block $\leq 1 \text{ m}^3$	0.1
Impact block $1\text{--}5 \text{ m}^3$	0.2
Impact block $>5 \text{ m}^3$	0.3
People	
Inside buildings	0.8
Outside buildings	1.0

7.3.2 Vulnerability for Property

More data exist for building damage related to landsliding, including the recent New-Zealand-specific study showing vulnerability of dwellings to landslides (Massey et al. 2019b), than data for vulnerability of persons within a property. As such, the vulnerability of a person in a property can firstly be assessed as the vulnerability of the dwelling to damage from landslides and then the data outlined in Section 7.3.3 used along with expert judgement to assess the vulnerability of a person in a property if the property is damaged by a landslide.

The Massey et al. (2019b) report outlines damage functions for New Zealand timber-framed dwellings to landsliding. The study collated information on landslide impacts on 57 dwellings from the NHC Toka Tū Ake claims database, with the dataset compared to overseas landslide datasets. The vulnerability to dwellings was assessed in terms of damage from debris flows, debris avalanches and rockfalls. We recommend using these New-Zealand-specific vulnerability values for building damage (Sections 7.3.2.1 and 7.3.2.2) where possible, rather than the values of Finlay et al. (1999) (Table 7.1) and Corominas et al. (2005) (Table 7.2).

7.3.2.1 Debris Flow and Debris Avalanche Impacts

For debris flows and debris avalanches, Massey et al. (2019b) found that the landslide intensity metric that statistically best fits the New Zealand (NHC Toka Tū Ake) data is debris height. In general, building structure type does appear to affect the relationship between damage state and landslide intensity (debris height). A sigmoid logistic and simple linear damage function were fitted to the damage ratio versus debris height data, combining both the literature and New Zealand datasets (Figure 7.1 and Table 7.3). It should be noted that the debris flows and debris avalanches included in the Massey et al. (2019b) research were all induced by rainfall.

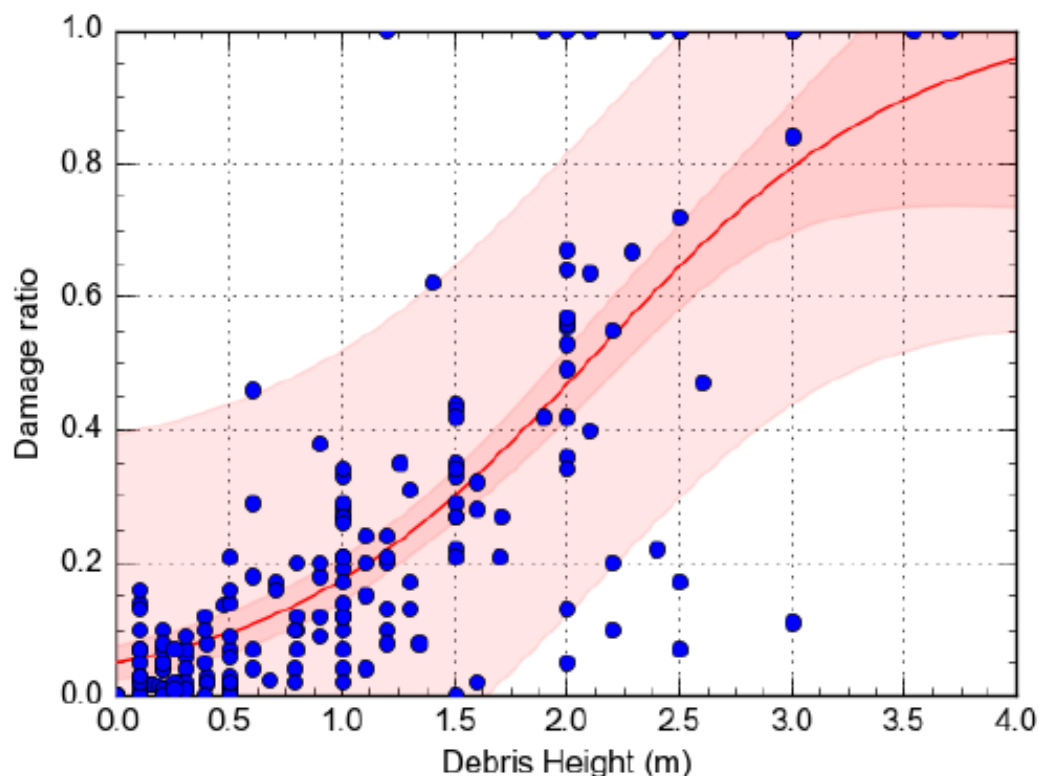


Figure 7.1 Damage ratio versus debris height for falling debris: debris flows, combining both the literature and New Zealand (NHC Toka Tū Ake) datasets, N = 168, for all building types. The damage ratio represents economic loss and is the repair cost divided by the replacement value. A sigmoid logistic damage function is fitted to the data. The darker red and lighter red shaded areas represent the 1 σ and 95% confidence ranges, respectively (Massey et al. 2019b).

Table 7.3 Damage functions and statistics for falling debris: all data for debris flows and debris avalanches (Massey et al. 2019b).

Vulnerability Metric	Landslide Intensity Metric (x)	Damage Function (Fitted and Coefficients)	Mathematical Notation	R ²	Standard Deviation (σ')
Damage Ratio	Debris Height (m)	Sigmoid logistic: a = 1.024, b = 20.051, c = 1.409	$V = \frac{a}{(1 + b \cdot e^{-v \cdot x})}$ Equation 7.1	0.6	0.23
Damage Ratio	Debris Height (m)	Linear: a = 0, b = 0.231	$V = a + bx$ Equation 7.2	0.58	0.21

7.3.2.2 Rockfall

For rockfall, the landslide intensity metric that statistically best fits the New Zealand data is kinetic energy, although penetration distance was also a good indicator of damage ratio (Massey et al. 2019b). Most of the literature reports kinetic energy but not penetration distance. For a slight increase in either the penetration distance of the boulder into the dwelling, or the kinetic energy of the boulder on impacting the dwelling, there is a rapid increase in both the damage ratio and state at the lower end of the intensity ranges (Massey et al. 2019b; Figure 7.2). At the upper end of the ranges, the damage ratio and state increase much less. This means that even low-intensity rockfalls can result in high damage ratios and states, which is consistent with the literature reviewed. A sigmoid logistic damage function was fitted to the damage ratio versus kinetic energy data, combining both the global literature and New Zealand datasets (Massey et al. 2019b; Figure 7.2 and Table 7.4).

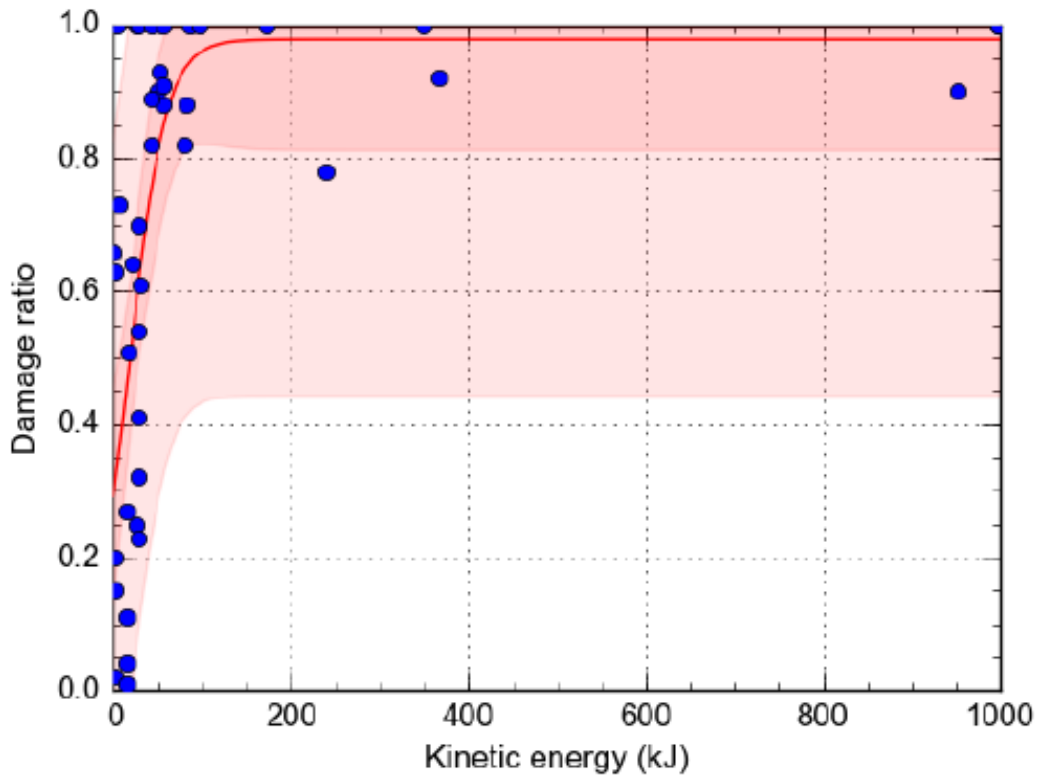


Figure 7.2 Damage ratio versus the kinetic energy for falling debris: rockfalls, combining both the literature and New Zealand (NHC Toka Tū Ake) datasets, n = 41, for all building types. A sigmoid logistic damage function is fitted to the data. The darker red and lighter red shaded areas represent the 1σ and 95% confidence ranges, respectively (Massey et al. 2019b).

Table 7.4 Damage functions and statistics for falling debris: all data for rockfalls (Massey et al. 2019b).

Vulnerability Metric	Landslide Intensity Metric (x)	Damage Function (Fitted and Coefficients)	Mathematical Notation	R ²	Standard Deviation (σ')	N Data Points
Damage Ratio	Kinetic Energy (kJ)	Sigmoid logistic: a = 0.978, b = 2.35, c = 0.049	$V = \frac{a}{(1 + b \cdot e^{-c \cdot x})}$ Equation 7.3	0.47	0.18	41

7.3.3 Vulnerability for Persons in Property

Vulnerability values for people in property represent the probability of loss of life if present within a building and inundated (buried) by debris. From Massey et al. (2019b), for debris flow events, there are only three cases in New Zealand of human losses in property on which to assess vulnerability. These three fatalities occurred when the debris heights exceeded the window height (about 1.0 to 1.4 m) and/or when the load from the debris exceeded the lateral load capacity of a typical light timber-framed wall, which occurs when the debris reaches a height of 1.4 to 1.6 m. In these circumstances, debris can enter a dwelling and bury a person. Such debris heights are associated with damage ratios of typically >0.8. Coroner reports relating to debris flow fatalities (within dwellings) indicate that the victims died due to asphyxiation. For rockfall, fatalities can occur when boulders can penetrate a dwelling and if a person is present in the dwelling at the time. Coroner reports relating to rockfall fatalities (within and outside of dwellings) indicate that the victims died due to trauma.

Pollock and Wartman (2020) have compiled a fatality dataset (n = 96) from international data, where they have been able to relate the probability of death within a building to landslide inundation depth (Figure 7.3). Their analysis suggests that, between 0.9 m and 5.9 m inundation depth, human behaviour is a key factor that drives vulnerability.

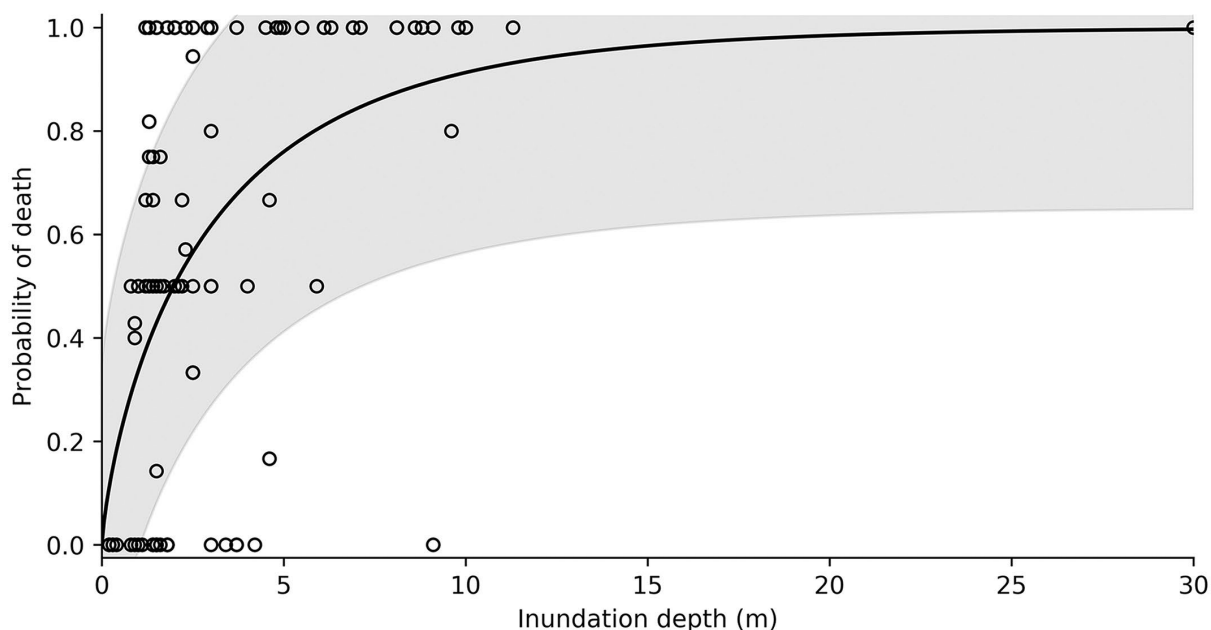


Figure 7.3 Human vulnerability to landslides over a range of common landslide inundation depths (n = 96). Gray shading represents ± one standard deviation.

Finlay et al. (1999) also present vulnerability values for people in buildings (Table 7.1) related to rainfall-induced flows and slides of soil. It is important to note that the building types in Hong Kong are different to those of New Zealand; Corominas et al. (2005) present expert opinion values for people in buildings (Table 7.2). The location of people within a building is also important (Pollock and Wartman 2020). For huts, where persons congregate and/or are likely to be present relative to where the debris/rockfall may impact, the building should be taken into account, e.g. if the bedroom/bunkroom is on the uphill side, it will be worse than if it is on the downhill side. However, rockfalls can come through a roof, as observed during the 2010/11 Canterbury Earthquake Sequence.

7.3.4 Vulnerability for People in Vehicles

Risk to people in vehicles can result in two different scenarios, as illustrated by the event tree in Figure 7.4. There are two distinct types of hazard to road users. The first (Hazard 1) is that they will be hit by debris while travelling along or stationary upon an at-risk section of road. The second (Hazard 2) is that rock(s) will fall onto the road or a road fill fails in front of them and, if they are unable to brake in time, they may drive or ride into the debris or void formed by the fill failure (or into something else while swerving to try and avoid the debris). For the first hazard, the level of vulnerability and risk depends on the velocity, volume and number of boulders passing/reaching the road, should an event occur, and a road user being present in the path of the boulders. In the second, the risk level depends on the velocity of the road user and their ability to stop or avoid the object safely.

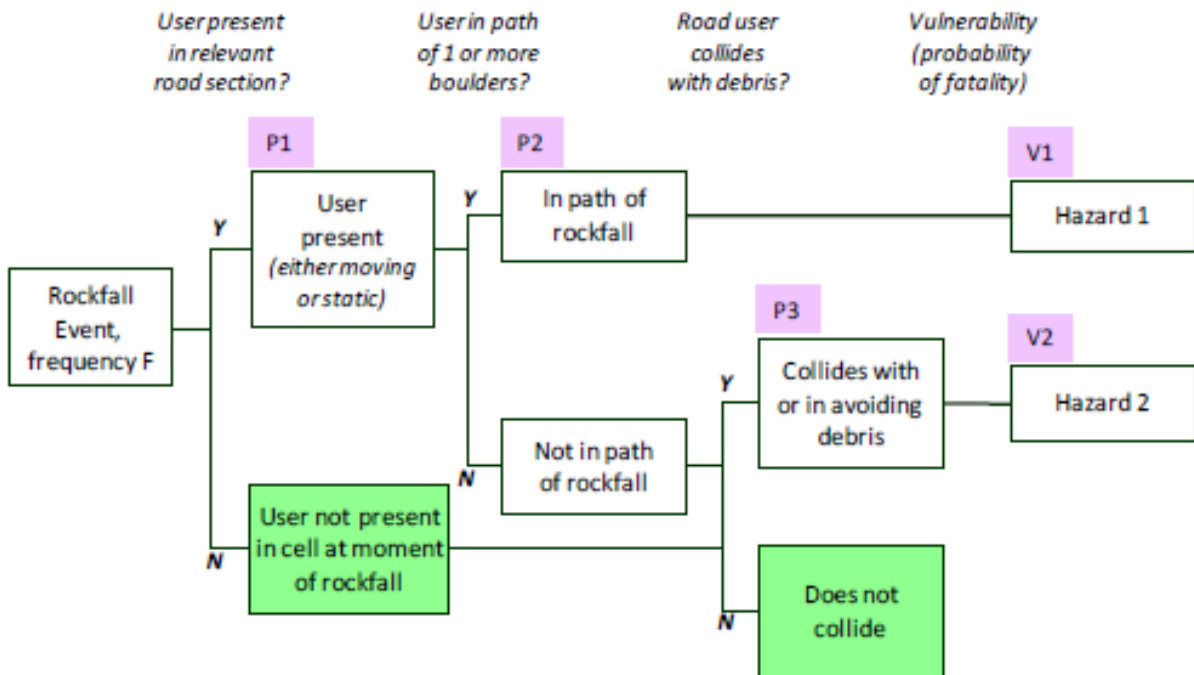


Figure 7.4 Example event-tree model for road-user risk assessment for rockfalls on Wakefield Avenue, Christchurch (Taig and Massey 2014).

Vulnerability values for people in vehicles are presented in the following tables (Table 7.5 to Table 7.6). Table 7.5 represents the vulnerability of people in the path of a rockfall from the Taig and Massey (2014) Port Hills rockfall analysis report, while Table 7.6 represents the vulnerability of people in vehicles who collide with debris. The vulnerability values in Table 7.6 have been estimated using New Zealand Ministry of Transport statistics for 2012 (for cars) on the number of crashes and fatal crashes involving collision with a wider variety of road objects and (for motorcycles) the number of crashes and fatal crashes involved in a smaller

range of different incident types – the much lower volume of motorcycle traffic means there is insufficient data to compile statistics at the detail available for cars. The vulnerability for pedal cycles has been estimated as 20% of the corresponding probability for motorcycles, reflecting the generally much lower speeds likely to be involved. The mean vulnerability values are shown in Table 7.6.

Table 7.5 Effective diameters perpendicular to the main trajectory of debris and the assumed vulnerability of road users per travel mode (Taig and Massey 2014).

Travel Mode	Effective Collision Diameter (m)		Vulnerability (If Present and Hit by Boulder)	
	Lower Estimate	Higher Estimate	Lower Estimate	Higher Estimate
Car Occupant	1	2	0.5	0.9
Motorcyclist	1	2	0.75	0.95
Pedal Cyclist	1	2	0.5	0.75
Pedestrian	0.5	1	0.5	0.75

Table 7.6 Vulnerabilities (V) of road users in collision with / trying to avoid boulders on the road ahead (Taig and Massey 2014).

Travel Mode	V (Lower)	V (Higher)
Car Occupant	0.013	0.052
Motorcycle	0.032	0.065
Pedal Cycle	0.006	0.013

8.0 RISK ESTIMATION

8.1 Local Personal Risk (if Requested by DOC)

8.1.1 Example Risk Calculation of Local Personal Risk

We present an example of calculation local personal risk from Cape Kidnapper Cliffs, Hawke's Bay, New Zealand. In Section 6.4.3, we presented an example of the calculation of $P_{(T:L)}$ for Cape Kidnappers, which was calculated at the cliff toe and at the maximum extent of the runout for each volume class. The following steps, as outlined below and in Table 8.1 are used to estimate the local personal risk:

1. Calculate the $P_{(L)}$ term, which is the annual probability of a landslide of a particular volume occurring. This is estimated from magnitude–frequency relationships, as outlined in Section 6.3. This $P_{(L)}$ term is dependent on trigger type and therefore will differ for EIL or background landslides.
2. Calculate the $P_{(T:L)}$ term, as outlined in Section 6.4.3.
3. Determine the vulnerability values to be used for the different landslide volume classes and type at both the cliff toe and runout extent.
4. Calculate the Local Personal Risk (LPR) at the cliff toe and at the runout extent for each volume class, as:

$$LPR_{(vol\ class)} = P_{(H)} \times P_{(S:H)} \times V \quad \text{Equation 8.1}$$

5. Within a GIS system, create a series of points along the cliff-toe line and the runout extent for each volume class and attach the representative LPR values to these points.
6. Within a GIS system, interpolate the LPR values between the cliff-toe line and runout extent line to create an LPR map for each volume class.
7. Add the raster values of the LPR maps of each volume class together to derive an LPR map of the risk of all background landslides.
8. Repeat Steps 1 to 7, using a $P_{(H)}$ term for annual probability of EIL to derive an LPR map of the risk from all EIL.
9. Add together the raster values of the LPR background map and LPR earthquake-induced map to determine the total LPR map for all landslides.

Table 8.1 Example calculation route and input data required to calculate local personal risk for the cliff toe.

Volume Class (m ³)	$P_{(L)}$	$P_{(T:L)}$ – Cliff Toe	$P_{(T:L)}$ – Runout Extent	V Cliff Toe	V: Runout Extent	LPR (Cliff Toe)	LPR (Runout Extent)
1	1000	2.5E-04	2.4E-04	0.5	0.2	1.25E-01	4.71E-02
10	800	7.2E-04	7.0E-04	0.5	0.2	2.87E-01	1.11E-01
100	200	2.0E-03	1.9E-03	0.5	0.2	2.00E-01	7.44E-02
1000	50	1.2E-02	9.8E-03	0.8	0.5	4.84E-01	2.44E-01
10,000	12	5.0E-02	2.8E-02	0.8	0.5	4.83E-01	1.68E-01
25,000	3	1.2E-01	4.8E-02	1	0.8	3.57E-01	1.15E-01
50,000	1	2.2E-01	7.5E-02	1	0.8	2.24E-01	5.98E-02

8.2 Risk Per Trip

An example of the calculation of risk from rockfall events for people in vehicles along a road can be found in Taig and Massey (2014). Section 8.2.1. describes an example risk per trip calculation for a walker.

8.2.1 Example Basic Analysis Calculation Route

We present an example of a visitor walking along a fictional track that is subject to rockfall and debris avalanche hazard from both non-event and event triggers. We calculate the risk of the most likely landslide volume and maximum credible landslide volume occurring for both trigger types separately, and then sum them.

For landslides that do not occur during an event (e.g. rainfall or earthquake) where multiple landslides can be induced, we calculate the risk as follows:

1. Estimate the annual frequency of the most likely volume occurring, as set out in Table 8.2.

Table 8.2 Calculation route for annual frequency of non-event-induced landslides.

	Type	Size (m ³)	Source	Return Period	Source	No. of Landslides/Year/km ²
Most Likely	Rockfall	1	Field measurements of boulders	10 per year	DOC ranger observations	1
Maximum Credible	Debris avalanche	10,000	GIS measurements of area and field measurements of depth of a pre-existing failure in next valley, e.g. a measured depth of 4 m and source area of 250 m ²	1 every 50 years	Aerial photography analysis	0.0066

2. Calculate the annual frequency of the maximum credible landslide occurring within the study area in Table 8.2 using the following calculation route:
 - a. Determine the amount of the study area that has ground with greater than >20° slope angle; we assumed that landslides do not occur on slopes with a slope angle less than 20°. In this example, this is 10 km².
 - b. Determine the extent of the aerial imagery analysed where slope angles are greater than 20°. In this example, this is 30 km², which is greater than the study area to capture this larger landslide that may occur there (i.e. what is the largest possible landslide that is feasible to occur?).
 - c. The AEP of the maximum credible landslide occurring in the area of aerial imagery is calculated from the ARI using the formula:

$$AEP = 1 - \exp\left(\frac{-1}{ARI}\right)$$

- d. This gives an AEP of 0.02/year. To determine the annual frequency of the landslide occurring in the study area, we:
 - i. Divide the annual frequency by the aerial imagery area (0.02/30 km²) to determine the number of maximum credible landslides/year/km² (0.00066).

- ii. Scale this number to the study area: multiply it by the study area in km² to give an annual frequency estimate of 0.0066.
3. Calculate the annual frequency of the most likely landslide occurring within the study area in Table 8.2 using the following calculation route:
 - a. Divide the annual frequency by the study area to determine the number of most likely landslides/year/km² (1).
4. Estimate the spatial probability of impact of the most likely and maximum credible landslide volume ($P_{(T:L)}$), as set out in Table 8.3.

Table 8.3 Calculation route for spatial probability of impact $P_{(T:L)}$.

	Type	<i>LSw</i> Width of Impact Area (m)	Source	Length of Track (m)	<i>LStrack</i> Length of track along which a landslide impact could occur (m)	Source	<i>d</i> Diameter of a Person (If Present) (m)	$P_{(T:L)}$ General Equation	$P_{(T:L)}$
Most Likely	Rockfall	1	Field measurements of boulders	2000	2000	Field observations suggest that rockfall hazards are present along the entire extent of the track	1	$\frac{LSw + d}{LStrack}$	0.001
Maximum Credible	Debris avalanche	50	GIS and field measurements of width of pre-existing landslide(s) in the next valley, along with F-Angle empirical runout areas	2000	1500	Field observations suggest that there are areas of slope that are not big enough to generate a large debris avalanche. The length of track that could be impacted by the maximum credible volume is determined by using empirical F-Angle data.	1		0.034

5. Estimate the spatio-temporal exposure of the person at risk ($P_{(S:T)}$).
 - a. Calculate the total length of time that a person is exposed to the most likely landslide volume. In this example, this is 1.5 hours, which represents 0.00017% per year.
 - b. Calculate the total length of time that a person is exposed to the maximum credible landslide volume. In this example, this is 1 hour, which represents 0.00011% per year.

6. Estimate the vulnerability ($V_{(D:T)}$) of the person to each landslide volume. For most likely landslide volume, this estimate is 0.8, while, for the maximum credible landslide, this estimate is 1.

7. Calculate the risk for both most likely and maximum credible landslide volume using the general risk equation:

$$P_{(L)} \times P_{(T:L)} \times P_{(S:T)} \times V_{(D:T)}$$

In this example, the risk from the most likely landslide volume is 1.37×10^{-6} while, for the maximum credible landslide volume, it is 2.56×10^{-8}

8. Sum the risk from most likely and maximum credible landslide volume to calculate the total non-event landslide risk. In this example, this is 1.4×10^{-6} .

For landslides that occur during an event (e.g. rainfall or earthquake) where multiple landslides can be induced, we calculate the risk as follows (using an earthquake event as an example):

1. Determine the representative earthquake event. In this example, this is a 1-in-500-year event. The estimated ground shaking is 0.5 g, using the NSHM figures in the Part 3 report. This indicates that, if the representative earthquake event were to occur, it would result in widespread small-scale landsliding and few moderate to very large landslides (using Table 4.8 in the Part 3 report).
2. Estimate the frequency of the most likely landslide volume and maximum credible landslide volume occurring during the earthquake event, as set out in Table 8.4.

Table 8.4 Estimate of the size and number of most likely and maximum credible landslides that could occur during a 1-in-500-year earthquake event.

	Type	Size (m ³)	Source	Frequency	Source	Number of Landslides that Could Occur
Most Likely	Rockfall	1 m ³	Field measurements of boulders	10 per event	Table 4.8 (Part 3 report)	10
Maximum Credible	Debris avalanche	50,000 m ³	Based off a geomorphic assessment of the largest volume that the slope could produce, using a similar depth of 4 m to the observed pre-existing debris avalanche in the next valley	1 per event	Table 4.8 (Part 3 report)	1

3. Estimate the spatial probability of impact of the most likely landslide volume and maximum credible landslide volume ($P_{(T:L)}$), as set out in Table 8.5.

Table 8.5 Calculation route for spatial probability of impact.

	Type	LS_w Width of Impact Area (m)	Source	Length of Track (m)	L_{Strack} Length of Track along which a Landslide impact Could Occur (m)	Source	d : Diameter of a Person (If Present) (m)	$P_{(T:L)}$ General Equation	P_{hit} from One Landslide (P_{hit1})	P_{hit} from all Landslides in Volume Category (to ensure you cannot be hit multiple times and therefore killed more than once)	P_{hit} from All Landslides in Volume Category
Most Likely	Rockfall	1	Field measurements of boulders.	2000	2000	Field observations suggest that rockfall hazards are present along the entire extent of the track.	1		0.001		0.0099
Maximum Credible	Debris avalanche	100	Based off a geomorphic assessment of the width of the largest volume that the slope could produce.	2000	1000	Field observations suggest that there are areas of slope that are not big enough to generate a large debris avalanche. The length of track that could be impacted by the maximum credible volume is determined by using empirical F-Angle data.	1	$\frac{LS_w + d}{L_{Strack}}$	0.101	$= 1 - (1 - P_{hit1})^n$	0.101

4. Estimate the spatio-temporal exposure of the person at risk ($P_{(S:T)}$): the total length of time that a person is exposed to the most likely landslide volume. In this example, this is 1.5 hours, which represents 0.017% per year.
5. Estimate the vulnerability ($V_{(D:T)}$) of the person to each landslide volume. For the most likely volume, this estimate is 0.8 while, for the maximum credible volume, this estimate is 1. Calculate the probability of death (P_{death}) for the event using the following equation for each landslide volume:

$$P_{death} = P_{(hit)} \times V_{(D:T)}$$

In this example, the P_{death} value for the most likely landslide volume is 7.93×10^{-3} and, for the maximum credible landslide volume, 1.01×10^{-1} .

6. Sum the P_{death} for each landslide volume to calculate the total probability of death using the following equation:

$$P_{death\ all} = 1 - (1 - P_{death}(most\ likely))(1 - P_{death}(max\ credible))$$

In this example, the total P_{death} value is 1.08×10^{-1} .

7. Calculate the EIL event by multiplying P_{death} by the annual frequency of the event occurring (here, 0.002 AEP based off a 1-in-500 ARI) and $P_{(S:T)}$. In this example, the risk is 3.7×10^{-8}

To calculate the total landslide risk, sum the non-earthquake and EIL risk. In this example, the total risk is 1.43×10^{-6} .

8.3 Annual Individual Fatality Trip

No additional comment.

8.4 Multiple Fatality Risk (if Requested by DOC)

Multiple fatality risk is scenario-based and can be expressed using fN pairs, an FN curve and annual probable life loss metrics (APPL). Table 8.6 presents a worked example to show how the multiple fatality risk for a given landslide scenario could be estimated for a hut.

Table 8.6 Worked example to calculate an F/N pair for multiple fatality risk.

Landslide Scenario	Volume (m ³)	Annual Exceedance Probability	Approximate Annual Return Interval	Comments
Maximum credible volume	100,000	0.0001	10,000	The largest landslide that could feasibly impact the site irrespective of time (use slope height and slope-facet area to define landslide area and then volume using A-V relationship – uses site geometry, noting that the geomorphic indicators might not be a useful indicator, as landslide scars could have been removed)
Most likely	1000	0.001	1000	Defined using, for example, geomorphic indicators, such as past landslide sources or block sizes (rock), but mainly based on site observations and evidence of past landslides

Example Landslide Scenario	Maximum Credible		Comments
Point site	Hut		-
Total occupants per year	10,000		-
Season	High (e.g. Nov to Feb)	Low (e.g. Mar to Oct)	For preliminary and basic analysis, use only the High season estimates
Months	4	8	-
Total N people using hut/season/year	6000	3000	-
Days hut occupied	122	244	-
Hrs per day hut occupied	8		-
Temporal spatial probability: percent of year point/linear feature occupied	0.11	0.22	-
Number of people in hut	49	12	-
Vulnerability of a person in the hut	1	-	This could be varied for changes in landslide intensity
Spatial probability of impact: the proportion of the point/linear feature within the hazard footprint (this is the proportion of people within the footprint)	1	-	This could be varied based on the likely proportion of the location that could be impacted by the given Landslide event – adopting the conservative hazard footprint
N Deaths (per season) if location impacted by the given event (N)	5	3	-
Landslide event	Maximum credible landslide volume		-
Annual frequency of landslide/event (f)	0.0001	0.0001	For events that could induce multiple landslides, the N people killed would need to be summed for all landslides assumed to be induced by the same event, which may impact point or linear features

8.5 Asset Impact

No additional comment.

8.6 Risk-Sensitivity Analysis

There are multiple ways to undertake risk-sensitivity analysis, including Monte-Carlo Simulations, Bayesian Statistics and Factor Analysis (Corominas et al. 2014). We present an example of Factor Analysis from the Port Hills rockfall risk analysis (Massey et al. 2012) as a pragmatic approach to understand the sensitivity of the risk results to the variance (and uncertainty) associated with the input parameters of the risk calculation.

For the Port Hills rockfall risk analysis, the following input parameters were varied:

1. Rockfall scale factors, including both seismically induced rockfall and non-seismically induced rockfall.
2. Probability that a person is present in a home at the time of an event.
3. Probability of the person being killed if hit by a boulder.

Each of these parameters was varied incrementally, and for each sensitivity test the average reduction (or gain) in risk is calculated from comparison with the reference test (Test 1: Table 8.7). For sensitivity tests 2 to 5, only one parameter per test was changed.

Table 8.7 Input parameters used in the Port Hills rockfall model for each assessment and the impact of their variance on average risk. Parameter varied is shown in bold (Massey et al. 2012).

Sensitivity Test Number	Non-Seismic Rockfall Scale Factor	Seismic Rockfall Scale Factor	Probability Person Present	Vulnerability of a Person if Hit	Reduction in Rockfall Risk (All Areas) from Test 1	Factor by which the Average Risk Reduces from Test 1**
1*	2	1.5	100%	0.5	-	-
2	1.2	1.5	100%	0.5	6%	1.1
3	2	1.2	100%	0.5	14%	1.2
4	2	1.5	67%	0.5	33%	1.5
5	1.2	1.2	67%	0.5	47%	1.9

* Sensitivity Test 1 represents the original parameters used for rockfall risk Scenario C in Massey et al. (2012).

** A factor of 10 is one order of magnitude change.

9.0 RISK MITIGATION

The principal aim of the risk-mitigation measures should be to reduce risk, engineer out uncertainty in the risk and provide a level of risk that satisfies community expectations through the regulator's criteria once properly implemented. These risk mitigations must be discussed with DOC staff and in-line with or appropriate to DOC policy. Risk-mitigation measures are likely to require ongoing maintenance in most, if not all, instances.

Specific mitigation options for rockfall hazards are specified in the MBIE guidance document: 'Rockfall: Design Considerations for Passive Protection Structures'.⁵

5 <https://www.building.govt.nz/assets/Uploads/building-code-compliance/b-stability/b1-structure/rockfall-design-consideration/rockfall-design-passive-protection-structures.pdf>

10.0 REPORTING REQUIREMENTS

The reporting requirements for the three different levels of risk analysis will vary. However, all reports should at a minimum document the data, assumptions and thought process used for the given level of analysis. Such documentation facilitates subsequent review and revision. The reports should be written at a level aimed at both technical consultants and non-technical DOC staff.

The report should fully document the sources of data, extent of investigations completed, assumptions made and associated limitations. The report is to be clear and unambiguous, stating outcomes from the investigations and analysis and making clear recommendations. If there is uncertainty, then such doubt needs to be stated in the report together with what can be done to clear up the doubt.

For an advanced-level analysis, a good principle to adopt for such reporting is to assume that the report may be tendered as an expert report to a subsequent court case. This may be more applicable for advanced-level analysis, while for basic-level analysis it is crucial to detail the uncertainty and information gaps in the analysis. Such documentation is necessary to justify the expert's conclusions if it is not to be rejected on the basis of being an unsubstantiated opinion rather than based on facts, calculations or precedents. The report should document the best-estimate results for the risk analysis, based on data available at that stage.

10.1 Peer-Review Requirements

No additional comment.

11.0 ACKNOWLEDGEMENTS

This report has been internally reviewed by Sam McColl. Previous versions have been peer-reviewed by Marc-Andre Brideau (formerly GNS Science), Regine Morgenstern (GNS Science), Emeritus Professor Robin Fell (University New South Wales, Sydney) and Mr Don Macfarlane (AECOM New Zealand, Christchurch). GNS Science appreciates the assistance provided by the independent reviewers through their comments on the draft guidelines. All comments have received careful consideration and many improvements have been made to the guidelines as a result. However, GNS Science acknowledges that any comments made by the reviewers were non-binding. Ultimately, the final decisions with regards to any diversity of views between co-authors and internal reviewers and external reviewers were made by the lead author of each document in consultation with the co-authors.

12.0 REFERENCES

- [AGS] Australian Geomechanics Society. 2007a. Commentary on guideline for landslide susceptibility, hazard and risk zoning for land use management. *Australian Geomechanics*. 42(1):37–62.
- [AGS] Australian Geomechanics Society. 2007b. Commentary on practice note guidelines for landslide risk management. *Australian Geomechanics*. 42(1): 115–158.
- [AGS] Australian Geomechanics Society. 2007c. Guideline for landslide susceptibility, hazard and risk zoning for land use management. *Australian Geomechanics*. 42(1):13–36.
- [AGS] Australian Geomechanics Society. 2007d. Practice note guidelines for landslide risk management. *Australian Geomechanics*. 42(1):63–114.
- Ashford SA, Sitar N. 2002. Simplified method for evaluating seismic stability of steep slopes. *Journal of Geotechnical and Geoenvironmental Engineering*. 128(2):119–128. [https://doi.org/10.1061/\(ASCE\)1090-0241\(2002\)128:2\(119\)](https://doi.org/10.1061/(ASCE)1090-0241(2002)128:2(119))
- Athanasopoulos-Zekkos A, Seed RB. 2013. Simplified methodology for consideration of two-dimensional dynamic response of levees in liquefaction-triggering evaluation. *Journal of Geotechnical and Geoenvironmental Engineering*. 139(11):1911–1922. [https://doi.org/10.1061/\(ASCE\)GT.1943-5606.0000913](https://doi.org/10.1061/(ASCE)GT.1943-5606.0000913)
- Bell H, Richards L, Thomson R. 2003. Relic slip verification study – Tauranga District. In: Crawford S, Baunton P, Hargraves S. *Geotechnics on the volcanic edge: Tauranga, March 2003, New Zealand Geotechnical Society Symposium*. Wellington (NZ): Institution of Professional Engineers New Zealand. p. 281–289. (Proceedings of Technical Groups; 30(1 GM)).
- Berti M, Simoni A. 2014. DFLOWZ: A free program to evaluate the area potentially inundated by a debris flow. *Computers & Geosciences*. 67:14–23. <https://doi.org/10.1016/j.cageo.2014.02.002>
- Bigelow PE, Benda LE, Miller DJ, Burnett KM. 2007. On debris flows, river networks, and the spatial structure of channel morphology. *Forest Science*. 53(2):220–238. <https://doi.org/10.1093/forestscience/53.2.220>
- Brardinoni F, Church M. 2004. Representing the landslide magnitude–frequency relation: Capilano River basin, British Columbia. *Earth Surface Processes and Landforms*. 29(1):115–124. <https://doi.org/10.1002/esp.1029>
- Bray JD, Travararou T. 2007. Simplified procedure for estimating earthquake-induced deviatoric slope displacements. *Journal of Geotechnical and Geoenvironmental Engineering*. 133(4):381–392. [https://doi.org/10.1061/\(ASCE\)1090-0241\(2007\)133:4\(381\)](https://doi.org/10.1061/(ASCE)1090-0241(2007)133:4(381))

- Brideau M-A, Stead D, Millard T, Ward B. 2019. Field characterisation and numerical modelling of debris avalanche runout on Vancouver Island, British Columbia, Canada. *Landslides*. 16:875–891. <https://doi.org/10.1007/s10346-019-01141-7>
- Brideau M-A, de Vilder S, Massey C, Mitchell A, McDougall S, Aaron J. 2021a. Empirical relationships to estimate the probability of runout exceedance for various landslide types. In: Guzzetti F, Mihalić Arbanas S, Reichenbach P, Sassa K, Bobrowsky PT, Takara K, editors. *Understanding and reducing landslide disaster risk Volume 2: from mapping to hazard and risk zonation*. Cham (CH): Springer International Publishing. p. 321–327. https://doi.org/10.1007/978-3-030-60227-7_36
- Brideau M, de Vilder S, Massey C, Mitchell A, McDougall S, Aaron J. 2021b. V1.0 Empirical landslide runout relationships, compiled from international examples, for various landslide types. [Place unknown]: DesignSafe-Cl. <https://doi.org/10.17603/ds2-9qbx-n796>
- Brunetti MT, Guzzetti F, Rossi M. 2009. Probability distributions of landslide volumes. *Nonlinear Processes in Geophysics*. 16(2):179–188. <https://doi.org/10.5194/npg-16-179-2009>
- Corominas J, Copons R, Moya J, Vilaplana JM, Altimir J, Amigó J. 2005. Quantitative assessment of the residual risk in a rockfall protected area. *Landslides*. 2(4):343–357. <https://doi.org/10.1007/s10346-005-0022-z>
- Corominas J, van Westen C, Frattini P, Cascini L, Malet JP, Fotopoulou S, Catani F, Van Den Eeckhaut M, Mavrouli O, Agliardi F, et al. 2014. Recommendations for the quantitative analysis of landslide risk. *Bulletin of Engineering Geology and the Environment*. 73(2):209–263. <https://doi.org/10.1007/s10064-013-0538-8>
- Corominas J, Einstein H, Davis T, Strom A, Zuccaro G, Nadim F, Verdel T. 2015. Glossary of terms on landslide hazard and risk. In: Lollino G, Giordan D, Crosta GB, Corominas J, Azzam R, Wasowski J, Sciarra N, editors. *Engineering Geology for Society and Territory – Volume 2*. Cham (CH): Springer International Publishing. p. 1775–1779. https://doi.org/10.1007/978-3-319-09057-3_314
- Crosta GB, Agliardi F, Frattini P, Lari S. 2015. Key issues in rock fall modeling, hazard and risk assessment for rockfall protection. In: Lollino G, Giordan D, Crosta GB, Corominas J, Azzam R, Wasowski J, Sciarra N, editors. *Engineering Geology for Society and Territory – Volume 2*. Cham (CH): Springer International Publishing. p. 43–58. https://doi.org/10.1007/978-3-319-09057-3_4
- Crozier MJ. 2010. Deciphering the effect of climate change on landslide activity: a review. *Geomorphology*. 124(3–4):260–267. <https://doi.org/10.1016/j.geomorph.2010.04.009>
- Cruden DM, Varnes DJ. 1996. Landslide types and processes. In: Turner AK, Schuster RL, editors. *Landslides: investigation and mitigation*. Washington (DC): Transportation Research Board. p. 36–75. (Special Report; 247).
- Dai FC, Lee CF, Ngai YY. 2002. Landslide risk assessment and management: an overview. *Engineering Geology*. 64(1):65–87. [https://doi.org/10.1016/S0013-7952\(01\)00093-X](https://doi.org/10.1016/S0013-7952(01)00093-X)
- Davies TR, McSaveney MJ. 2008. Principles of sustainable development on fans. *Journal of Hydrology (New Zealand)*. 47(1):43–65.
- de Scally FA, Owens IF. 2004. Morphometric controls and geomorphic responses on fans in the Southern Alps, New Zealand. *Earth Surface Processes and Landforms*. 29(3):311–322. <https://doi.org/10.1002/esp.1022>

- de Vilder SJ, Massey CI. 2024a. Guidelines for natural hazard risk analysis on public conservation lands and waters – Part 2: preliminary hazard and exposure analysis for landslides. Lower Hutt (NZ): GNS Science. 35 p. Consultancy Report 2024/36. Prepared for the Department of Conservation.
- de Vilder SJ, Massey CI. 2024b. Guidelines for natural hazard risk analysis on public conservation lands and waters – Part 3: analysing landslide risk to point and linear sites. Lower Hutt (NZ): GNS Science. 61 p. Consultancy Report 2024/37. Prepared for the Department of Conservation.
- de Vilder SJ, Massey CI, Power WL, Burbidge DR, Deligne NI, Leonard GS. 2020. Guideline for natural hazard risk analysis on public conservation lands and waters – Part 1: risk analysis framework. Lower Hutt (NZ): GNS Science. 27 p. Consultancy Report 2024/35. Prepared for the Department of Conservation.
- Dowrick DJ, Hancox GT, Perrin ND, Dellow GD. 2008. The Modified Mercalli intensity scale: revisions arising from New Zealand experience. *Bulletin of the New Zealand Society for Earthquake Engineering*. 41(3):193–205. <https://doi.org/10.5459/bnzsee.41.3.193-205>
- Du J, Yin K, Nadim F, Lacasse S. 2013. Quantitative vulnerability estimation for individual landslides. In: Delage P, Desrues P, Frank R, Puech A, Schlosser F, editors. *Proceedings of the 18th International Conference on Soil Mechanics and Geotechnical Engineering, Paris 2013: challenges and innovations in geotechnics*. Paris (FR): Presses de Ponts. p. 2181–2184.
- Dussauge-Peisser C, Helmstetter A, Grasso JR, Hantz D, Desvarreux P, Jeannin M, Giraud A. 2002. Probabilistic approach to rock fall hazard assessment: potential of historical data analysis. *Natural Hazards and Earth System Sciences*. 2(1–2):15–26. <https://doi.org/10.5194/nhess-2-15-2002>
- Fan X, Scaringi G, Korup O, West AJ, van Westen CJ, Tanyas H, Hovius N, Hales TC, Jibson RW, Allstadt KE, et al. 2019. Earthquake-induced chains of geologic hazards: patterns, mechanisms, and impacts. *Reviews of Geophysics*. 57(2):421–503. <https://doi.org/10.1029/2018rg000626>
- Fell R, Hungr O, Leroueil S, Reimer, W. 2000. Keynote Lecture: Geotechnical Engineering of the stability of natural slopes, and cuts and fills in soils. In: *ISRM International Symposium; 2000 Nov 19–24; Melbourne Australia*. [place unknown]: International Society for Rock Mechanics and Rock Engineering. ISRM-IS-2000-002.
- Fell R, Corominas J, Bonnard C, Cascini L, Leroi E, Savage WZ. 2008a. Commentary: guidelines for landslide susceptibility, hazard and risk zoning for land use planning. *Engineering Geology*. 102(3–4):99–111. <https://doi.org/10.1016/j.enggeo.2008.03.014>
- Fell R, Corominas J, Bonnard C, Cascini L, Leroi E, Savage WZ. 2008b. Guidelines for landslide susceptibility, hazard and risk zoning for land use planning. *Engineering Geology*. 102(3–4):85–98. <https://doi.org/10.1016/j.enggeo.2008.03.022>
- Finlay PJ, Mostyn GR, Fell R. 1999. Landslides: prediction of travel distance and guidelines for vulnerability of persons. In: Vitharana ND, Colman R, editors. *Proceedings 8th Australia New Zealand Conference on Geomechanics: Consolidating Knowledge; 1999 Feb 15–17; Hobart, Australia*. Barton (AU): Australian Geomechanics Society. p. 105–113.
- Gariano SL, Guzzetti F. 2016. Landslides in a changing climate. *Earth-Science Reviews*. 162:227–252. <https://doi.org/10.1016/j.earscirev.2016.08.011>
- Gischig VS, Eberhardt E, Moore JR, Hungr O. 2015. On the seismic response of deep-seated rock slope instabilities – insights from numerical modeling. *Engineering Geology*. 193:1–18. <https://doi.org/10.1016/j.enggeo.2015.04.003>

- Gunzburger Y, Merrien-Soukatchoff V, Guglielmi Y. 2005. Influence of daily surface temperature fluctuations on rock slope stability: case study of the Rochers de Valabres slope (France). *International Journal of Rock Mechanics and Mining Sciences*. 42(3):331–349. <https://doi.org/10.1016/j.ijrmms.2004.11.003>
- Guthrie RH, Deadman PJ, Cabrera AR, Evans SG. 2008. Exploring the magnitude–frequency distribution: a cellular automata model for landslides. *Landslides*. 5(1):151–159. <https://doi.org/10.1007/s10346-007-0104-1>
- Guzzetti F, Malamud BD, Turcotte DL, Reichenbach P. 2002. Power-law correlations of landslide areas in central Italy. *Earth and Planetary Science Letters*. 195(3):169–183. [https://doi.org/10.1016/S0012-821X\(01\)00589-1](https://doi.org/10.1016/S0012-821X(01)00589-1)
- Guzzetti F, Reichenbach P, Ardizzone F, Cardinali M, Galli M. 2006. Estimating the quality of landslide susceptibility models. *Geomorphology*. 81(1):166–184. <https://doi.org/10.1016/j.geomorph.2006.04.007>
- Guzzetti F, Ardizzone F, Cardinali M, Rossi M, Valigi D. 2009. Landslide volumes and landslide mobilization rates in Umbria, central Italy. *Earth and Planetary Science Letters*. 279(3):222–229. <https://doi.org/10.1016/j.epsl.2009.01.005>
- Guzzetti F, Mondini AC, Cardinali M, Fiorucci F, Santangelo M, Chang K-T. 2012. Landslide inventory maps: new tools for an old problem. *Earth-Science Reviews*. 112(1–2):42–66. <https://doi.org/10.1016/j.earscirev.2012.02.001>
- Hancox GT, Perrin ND, Dellow GD. 2002. Recent studies of historical earthquake-induced landsliding, ground damage, and MM intensity in New Zealand. *Bulletin of the New Zealand Society for Earthquake Engineering*. 35(2):59–95. <https://doi.org/10.5459/bnzsee.35.2.59-95>
- Hancox GT, Ries WF, Lukovic B, Parker RN. 2014. Landslides and ground damage caused by the Mw 7.1 Inangahua earthquake of May 1968 in northwest South Island, New Zealand. Lower Hutt (NZ): GNS Science. 89 p. + folded map. (GNS Science report; 2014/06).
- Hancox GT, Ries WF, Parker RN, Rosser BJ. 2016. Landslides caused by the MS 7.8 Murchison earthquake of 17 June 1929 in northwest South Island, New Zealand. Lower Hutt (NZ): GNS Science. 131 p. + 4 maps. (GNS Science report; 2015/42).
- Harvey J. 2011. An investigation of the runout paths, sediment budget and material behaviour of four debris flow-like landslides in the Coromandel Peninsula, New Zealand [BSc Hons thesis]. Auckland (NZ): University of Auckland.
- Heim A. 1932. Landslides & human lives. Skermer N, translator. Vancouver (CA): BiTech Publishers. 195 p.
- Ho K, Leroi E, Roberds B. 2000. Quantitative risk assessment: application, myths and future direction. In: *GeoEng2000: an International Conference on Geotechnical & Geological Engineering*; 2000 Nov 19–24; Melbourne, Australia. Lancaster (PA): Technomic. p. 269–312.
- Hovius N, Stark CP, Allen PA. 1997. Sediment flux from a mountain belt derived by landslide mapping. *Geology*. 25(3):231–234. [https://doi.org/10.1130/0091-7613\(1997\)025<0231:Sffamb>2.3.Co:2](https://doi.org/10.1130/0091-7613(1997)025<0231:Sffamb>2.3.Co:2)
- Hungr O, Evans SG, Hazzard J. 1999. Magnitude and frequency of rock falls and rock slides along the main transportation corridors of southwestern British Columbia. *Canadian Geotechnical Journal*. 36(2):224–238. <https://doi.org/10.1139/t98-106>
- Hungr O, McDougall S, Bovis M. 2005. Entrainment of material by debris flows. In: Jakob M, Hungr O, editors. *Debris-flow Hazards and Related Phenomena*. Berlin (DE): Springer. p. 135–158. https://doi.org/10.1007/3-540-27129-5_7

- Hungr O, Leroueil S, Picarelli L. 2014. The Varnes classification of landslide types, an update. *Landslides*. 11(2):167–194. <https://doi.org/10.1007/s10346-013-0436-y>
- Hunter G, Fell R. 2002. The deformation behaviour of rockfill. Sydney (AU): University of New South Wales. 58 p. (Studies from School of Civil and Environmental Engineering).
- Hunter G, Fell R. 2003. Travel distance angle for “rapid” landslides in constructed and natural soil slopes. *Canadian Geotechnical Journal*. 40(6):1123–1141. <https://doi.org/10.1139/t03-061>
- Iverson RM, Reid ME, Logan M, LaHusen RG, Godt JW, Griswold JP. 2011. Positive feedback and momentum growth during debris-flow entrainment of wet bed sediment. *Nature Geoscience*. 4(2):116–121. <https://doi.org/10.1038/ngeo1040>
- Jakob M. 2022. Landslides in a changing climate. In: Davies T, Rosser N, Shroder JF, editors. *Landslide hazards, risks, and disasters*. 2nd ed. Amsterdam (NL): Elsevier. p. 505–579. <https://doi.org/10.1016/B978-0-12-818464-6.00003-2>
- Jakob M, Weatherly H, Bale S, Perkins A, MacDonald B. 2017. A multi-faceted debris-flood hazard assessment for Cougar Creek, Alberta, Canada. *Hydrology*. 4(1):7. <https://doi.org/10.3390/hydrology4010007>
- Jibson RW. 2011. Methods for assessing the stability of slopes during earthquakes – a retrospective. *Engineering Geology*. 122(1):43–50. <https://doi.org/10.1016/j.enggeo.2010.09.017>
- Kailey P. 2013. Debris flows in New Zealand alpine catchments [PhD thesis]. Christchurch (NZ): University of Canterbury. 295 p.
- Kaiser AE, Holden C, Massey CI. 2014. Site amplification, polarity and topographic effects in the Port Hills during the Canterbury earthquake sequence. Lower Hutt (NZ): GNS Science. 33 p. Consultancy Report 2014/121. Prepared for the Earthquake Commission.
- Kean JW, Staley DM, Lancaster JT, Rengers FK, Swanson BJ, Coe JA, Hernandez JL, Sigman AJ, Allstadt KE, Lindsay DN. 2019. Inundation, flow dynamics, and damage in the 9 January 2018 Montecito debris-flow event, California, USA: opportunities and challenges for post-wildfire risk assessment. *Geosphere*. 15(4):1140–1163. <https://doi.org/10.1130/GES02048.1>
- Keefer DK. 1984. Landslides caused by earthquakes. *Geological Society of America Bulletin*. 95(4):406–421. [https://doi.org/10.1130/0016-7606\(1984\)95<406:LCBE>2.0.CO;2](https://doi.org/10.1130/0016-7606(1984)95<406:LCBE>2.0.CO;2)
- Korup O. 2005. Distribution of landslides in southwest New Zealand. *Landslides*. 2(1):43–51. <https://doi.org/10.1007/s10346-004-0042-0>
- Kramer SL. 1996. Geotechnical earthquake engineering. Upper Saddle River (NJ): Prentice Hall. 653 p.
- Kritikos T, Davies T. 2015. Assessment of rainfall-generated shallow landslide/debris-flow susceptibility and runout using a GIS-based approach: application to western Southern Alps of New Zealand. *Landslides*. 12(6):1051–1075. <https://doi.org/10.1007/s10346-014-0533-6>
- Larsen IJ, Montgomery DR, Korup O. 2010. Landslide erosion controlled by hillslope material. *Nature Geoscience*. 3(4):247–251. <https://doi.org/10.1038/ngeo776>
- Lee EM, Jones DKC. 2014. Landslide risk assessment. 2nd ed. London (UK): ICE Publishing. 509 p.
- Makdisi FI, Bolton Seed H. 1979. Simplified procedure for evaluating embankment response. *Journal of the Geotechnical Engineering Division*. 105(12):1427–1434. <https://doi.org/10.1061/AJGEB6.0000898>
- Malamud BD, Turcotte DL, Guzzetti F, Reichenbach P. 2004a. Landslide inventories and their statistical properties. *Earth Surface Processes and Landforms*. 29(6):687–711. <https://doi.org/10.1002/esp.1064>

- Malamud BD, Turcotte DL, Guzzetti F, Reichenbach P. 2004b. Landslides, earthquakes, and erosion. *Earth and Planetary Science Letters*. 229(1):45–59. <https://doi.org/10.1016/j.epsl.2004.10.018>
- Marc O, Hovius N. 2015. Amalgamation in landslide maps: effects and automatic detection. *Natural Hazards and Earth System Sciences*. 15(4):723–733. <https://doi.org/10.5194/nhess-15-723-2015>
- Massey CI, Gerstenberger MC, McVerry GH, Litchfield NJ. 2012. Canterbury earthquakes 2010/11 Port Hills slope stability: additional assessment of the life-safety risk from rockfalls (boulder rolls). Lower Hutt (NZ): GNS Science. 18 p. Consultancy Report 2012/214. Prepared for Christchurch City Council.
- Massey CI, Petley DN, McSaveney MJ. 2013. Patterns of movement in reactivated landslides. *Engineering Geology*. 159:1–19. <https://doi.org/10.1016/j.enggeo.2013.03.011>
- Massey CI, Hancox GT, Page MJ. 2018a. TXT-tool 1.064-1.1 field guide for the identification and assessment of landslide and erosion features and related hazards affecting pipelines. In: Sassa K, Guzzetti F, Yamagishi H, Arbanas Z, Casagli N, McSaveney MJ, Dang K, editors. *Landslide dynamics: ISDR-ICL Landslide Interactive Teaching Tools. Volume 1: Fundamentals, mapping and monitoring*. Cham (CH): Springer International Publishing. p. 209–232. https://doi.org/10.1007/978-3-319-57774-6_16
- Massey CI, Townsend DB, Rathje E, Allstadt KE, Lukovic B, Kaneko Y, Bradley B, Wartman J, Jibson RW, Petley DM, et al. 2018b. Landslides triggered by the 14 November 2016 Mw 7.8 Kaikoura earthquake, New Zealand. *Bulletin of the Seismological Society of America*. 108(3B):1630–1648. <https://doi.org/10.1785/0120170305>
- Massey CI, de Vilder SJ, Taig T, Lukovic B, Archibald GC, Morgenstern R. 2019a. Landslide hazard and risk assessment for the Fox and Franz Josef Glacier valleys. Lower Hutt (NZ): GNS Science. 79 p. + appendices. Consultancy Report 2018/206. Prepared for the Department of Conservation.
- Massey CI, Thomas K-L, King AB, Singeisen C, Taig T, Horspool NA. 2019b. SLIDE (Wellington): vulnerability of dwellings to landslides (Project No. 16/SP740). Lower Hutt (NZ): GNS Science. 76 p. (GNS Science report; 2018/27). <https://doi.org/10.21420/G2DD2Q>
- Massey CI, Townsend D, Jones K, Lukovic B, Rhoades D, Morgenstern R, Rosser B, Ries W, Howarth J, Hamling I, et al. 2020a. Volume characteristics of landslides triggered by the Mw7.8 2016 Kaikōura earthquake, New Zealand, derived from digital surface difference modeling. *Journal of Geophysical Research: Earth Surface*. 125(7):e2019JF005163. <https://doi.org/10.1029/2019jf005163>
- Massey CI, Townsend D, Lukovic B, Morgenstern R, Jones K, Rosser B, de Vilder S. 2020b. Landslides triggered by the Mw7.8 14 November 2016 Kaikōura earthquake: an update. *Landslides*. 17(2401–2408). <https://doi.org/10.1007/s10346-020-01439-x>
- Massey CI, Lukovic B, Huso R, Buxton R, Potter SH. 2021. Earthquake-induced landslide forecast tool for New Zealand: version 2.0. Lower Hutt (NZ): GNS Science. 77 p. (GNS Science report; 2018/08). <https://doi.org/10.21420/G2TP9V>
- McDougall S. 2017. 2014 Canadian Geotechnical Colloquium: landslide runout analysis – current practice and challenges. *Canadian Geotechnical Journal*. 54(5):605–620. <https://doi.org/10.1139/cgj-2016-0104>
- Melton MA. 1965. The geomorphic and paleoclimatic significance of alluvial deposits in Southern Arizona. *The Journal of Geology*. 73(1):1–38. <https://doi.org/10.1086/627044>

- Moon AT, Wilson RA. 2004. In: Farquhar G, Kelsey P, Marsh J, Fellows D, editors. *To the eNZ of the Earth: proceedings of the 9th Australia New Zealand Conference on Geomechanics*; 2004 Feb 8–11; Auckland, New Zealand. Auckland (NZ): New Zealand Geotechnical Society. p. 754–760.
- Moon AT, Wilson RA, Flentje PN. 2005. Developing and using landslide size frequency models. In: Hungr O, Fell R, Couture R, Eberhardt E, editors. *Proceedings of the International Conference on Landslide Risk Management, 18th Annual Vancouver Geotechnical Society Symposium*; 2005 May 31 – Jun 4; Vancouver, Canada. London (GB): Taylor and Francis Group. p. 589–598.
- Moratalla J, Goded T, Gerstenberger M, Canessa S. 2021. New ground motion to intensity conversion equations (GMCIEs) for New Zealand. In: *17th World Conference on Earthquake Engineering*; 2021 Sep 27 – Oct 2; Sendai, Japan. Tokyo (JP): International Association for Earthquake Engineering.
- Newmark NM. 1965. Effects of earthquakes on dams and embankments. *Géotechnique*. 15(2):139–160. <https://doi.org/10.1680/geot.1965.15.2.139>
- [NZGS] New Zealand Geotechnical Society. 2005. Field guide sheet description of soil and rock. Wellington (NZ): NZ Geotechnical Society Inc.; [accessed 2024 Jun]. <https://fi-nzgs-media.s3.amazonaws.com/uploads/2016/06/Field-guide-sheet-description-of-soil-and-rock-2005.pdf>
- Parker RN, Densmore AL, Rosser NJ, de Michele M, Li Y, Huang R, Whadcoat S, Petley DN. 2011. Mass wasting triggered by the 2008 Wenchuan earthquake is greater than orogenic growth. *Nature Geoscience*. 4(7):449–452. <https://doi.org/10.1038/ngeo1154>
- Parker RN, Hancox GT, Petley DN, Massey CI, Densmore AL, Rosser NJ. 2015. Spatial distributions of earthquake-induced landslides and hillslope preconditioning in the northwest South Island, New Zealand. *Earth Surface Dynamics*. 3(4):501–525. <https://doi.org/10.5194/esurf-3-501-2015>
- Pierson TC. 2005. Hyperconcentrated flow – transitional process between water flow and debris flow. In: Jakob M, Hungr O, editors. *Debris-flow hazards and related phenomena*. Berlin (DE): Springer. p. 159–202. https://doi.org/10.1007/3-540-27129-5_8
- Pollock W, Wartman J. 2020. Human vulnerability to landslides. *GeoHealth*. 4(10):e2020GH000287. <https://doi.org/10.1029/2020GH000287>
- RAMMS. 2016. A numerical model for rockfall in research and practice, user manual v1.6 rockfall. Davos Dorf (CH): WSL Institute for Snow and Avalanche Research SLF. 102 p.
- Ravanel L, Magnin F, Deline P. 2017. Impacts of the 2003 and 2015 summer heatwaves on permafrost-affected rock-walls in the Mont Blanc massif. *Science of The Total Environment*. 609:132–143. <https://doi.org/10.1016/j.scitotenv.2017.07.055>
- Reichenbach P, Rossi M, Malamud BD, Mihir M, Guzzetti F. 2018. A review of statistically-based landslide susceptibility models. *Earth-Science Reviews*. 180:60–91. <https://doi.org/10.1016/j.earscirev.2018.03.001>
- Rizzitano S, Biondi G, Cascone E. 2010. Effect of simple topographic irregularities on site seismic response. In: Islam MS, Yasin SJM, Abedin MZ, Siddique A, editors. *Proceedings of Bangladesh Geotechnical Conference 2010: natural hazards and countermeasures in geotechnical engineering*; 2010 Nov 4–5; Dhaka, Bangladesh. Dhaka (BD): Bangladesh Society for Geotechnical Engineering. p. 295–302.

- Roberds WJ. 1990. Methods for developing defensible subjective probability assessments. In: *Geotechnical engineering 1990 – soils, geology and foundations*. Washington (DC): Transportation Research Board. p. 183–190. (Transportation research record; 1288).
- Sepúlveda SA, Murphy W, Petley DN. 2005. Topographic controls on coseismic rock slides during the 1999 Chi-Chi earthquake, Taiwan. *Quarterly Journal of Engineering Geology and Hydrogeology*. 38(2):189–196. <https://doi.org/10.1144/1470-9236/04-062>
- Snelder T, Biggs B, Weatherhead M. 2010. New Zealand river environment classification user guide. Wellington (NZ): Ministry for the Environment, National Institute of Water & Atmospheric Research. 144 p. ME 1026.
- Stirling MW, McVerry GH, Gerstenberger MC, Litchfield NJ, Van Dissen RJ, Berryman KR, Barnes P, Wallace LM, Villamor P, Langridge RM, et al. 2012. National seismic hazard model for New Zealand: 2010 update. *Bulletin of the Seismological Society of America*. 102(4):1514–1542. <https://doi.org/10.1785/0120110170>
- Strenk PM, Wartman J. 2011. Uncertainty in seismic slope deformation model predictions. *Engineering Geology*. 122(1):61–72. <https://doi.org/10.1016/j.enggeo.2011.03.003>
- Strouth A, McDougall S. 2022. Individual risk evaluation for landslides: key details. *Landslides*. 19(4):977–991. <https://doi.org/10.1007/s10346-021-01838-8>
- Taig T, Massey CI. 2014. Canterbury Earthquakes 2010/11 Port Hills slope stability: estimating rockfall (boulder roll) risk for the road user along part of Wakefield Avenue. Lower Hutt (NZ): GNS Science. 35 p. Consultancy Report 2013/30. Prepared for Christchurch City Council.
- Tanyaş H, van Westen CJ, Allstadt KE, Anna Nowicki Jessee M, Görüm T, Jibson RW, Godt JW, Sato HP, Schmitt RG, Marc O, et al. 2017. Presentation and analysis of a worldwide database of earthquake-induced landslide inventories. *Journal of Geophysical Research: Earth Surface*. 122(10):1991–2015. <https://doi.org/10.1002/2017jf004236>
- Tanyaş H, van Westen CJ, Allstadt KE, Jibson RW. 2019. Factors controlling landslide frequency–area distributions. *Earth Surface Processes and Landforms*. 44(4):900–917. <https://doi.org/10.1002/esp.4543>
- Townsend DB, Rosser BJ. 2012. Canterbury earthquakes 2010/2011 Port Hills slope stability: geomorphology mapping for rockfall risk assessment. Lower Hutt (NZ): GNS Science. 21 p. Consultancy Report 2012/15. Prepared for Christchurch City Council.
- Townsend DB, Massey CI, Lukovic B, Rosser BJ, de Vilder SJ, Ries W, Morgenstern R, Ashraf S, Jones KE, Carey JM. 2020. SLIDE (Wellington): Geomorphological characterisation of the Wellington urban area. Lower Hutt (NZ): GNS Science. 194 p. (GNS Science report; 2019/28). <https://doi.org/10.21420/CHRR-4G41>
- Varnes DJ. 1978. Slope movement types and processes. In: Schuster RL, Krizek RJ, editors. *Landslides: analysis and control*. Washington (DC): Transportation Research Board. p. 11–33. (Special report; 176).
- Van den Eeckhaut M, Hervás J. 2012. State of the art of national landslide databases in Europe and their potential for assessing landslide susceptibility, hazard and risk. *Geomorphology*. 139–140:545–558. <https://doi.org/10.1016/j.geomorph.2011.12.006>
- van Westen CJ, van Asch TWJ, Soeters R. 2006. Landslide hazard and risk zonation – why is it still so difficult? *Bulletin of Engineering Geology and the Environment*. 65(2):167–184. <https://doi.org/10.1007/s10064-005-0023-0>
- van Westen CJ, Castellanos E, Kuriakose SL. 2008. Spatial data for landslide susceptibility, hazard, and vulnerability assessment: an overview. *Engineering Geology*. 102(3):112–131. <https://doi.org/10.1016/j.enggeo.2008.03.010>

- Vick SG. 2002. Degrees of belief: subjective probability and engineering judgment. Reston (VA): American Society of Civil Engineers. 455 p.
- Wartman J, Bray JD, Seed RB. 2003. Inclined plane studies of the Newmark sliding block procedure. *Journal of Geotechnical and Geoenvironmental Engineering*. 129(8):673–684. [https://doi.org/10.1061/\(ASCE\)1090-0241\(2003\)129:8\(673\)](https://doi.org/10.1061/(ASCE)1090-0241(2003)129:8(673))
- Welsh AJ. 2007. Delineating debris-flow hazards on alluvial fans in the Coromandel and Kaimai regions, New Zealand, using GIS [MSc thesis]. Christchurch (NZ): University of Canterbury. 190 p.
- Welsh A, Davies T. 2011. Identification of alluvial fans susceptible to debris-flow hazards. *Landslides*. 8(2):183–194. <https://doi.org/10.1007/s10346-010-0238-4>
- Wilford DJ, Sakals ME, Innes JL, Sidle RC, Bergerud WA. 2004. Recognition of debris flow, debris flood and flood hazard through watershed morphometrics. *Landslides*. 1(1):61–66. <https://doi.org/10.1007/s10346-003-0002-0>
- Wong HN, Lam KC, Ho KKS. 1998. Diagnostic report on the November 1993 natural terrain landslides on Lantau Island. Hong Kong: Geotechnical Engineering Office. GEO Report 69.
- Wong HN, Ko FWY, Hui THH. 2006. Assessment of landslide risk of natural hillsides in Hong Kong. Hong Kong: Geotechnical Engineering Office. GEO Report 191.



www.gns.cri.nz

Principal Location

1 Fairway Drive, Avalon
Lower Hutt 5010
PO Box 30368
Lower Hutt 5040
New Zealand
T +64-4-570 1444
F +64-4-570 4600

Other Locations

Dunedin Research Centre
764 Cumberland Street
Private Bag 1930
Dunedin 9054
New Zealand
T +64-3-477 4050
F +64-3-477 5232

Wairakei Research Centre
114 Karetoto Road
Private Bag 2000
Taupo 3352
New Zealand
T +64-7-374 8211
F +64-7-374 8199

National Isotope Centre
30 Gracefield Road
PO Box 30368
Lower Hutt 5040
New Zealand
T +64-4-570 1444
F +64-4-570 4657